DOCTOR OF PHILOSOPHY

Analysis of cylindrical semiconductor metal-clad nano-lasers

Abdul Sattar, Zubaida

Award date:
2014

Awarding institution:
Bangor University

PRIFYSGOL
BANGOR
UNIVERSITY

Analysis of Cylindrical Semiconductor Metal-Clad Nano-Lasers

Submitted by Zubaida Abdul Sattar

for the degree of

Doctor of Philosophy

Bangor University

2014

Acknowledgements

I would like to express my appreciation for my supervisor Prof. K. Alan Shore to whom I am enormously grateful for his encouragement and endless patience with me throughout the research and writing this thesis. He has supported me with research scholarship for PhD studies, without which it would not have been possible for me to study in such a prestigious university. My sincere thanks to Jeremy Benjamin Wright and Dr. Igal Brener from Sandia National Laboratories and Centre for High Technology Materials at the University of New Mexico, USA for providing the data to analyse GaN nanowire lasers with helpful discussions. I am grateful to Dr. Zengbo Wang for his help and support for Finite Element Method Analysis. I am fortunate to have Nada Kamel, my colleague for guiding and helping me with my results during my PhD.

My thanks to Dr. Yanhua Hong for demonstrating the experiments on semiconductor lasers that have provided me with the knowledge of experimental procedures involved in semiconductor lasers. I would like to pay my gratitude to Prof. Paul S. Spencer, Dr. Iestyn Pierce and Dr. Roger Giddings for providing me with the work based experience as a Laboratory demonstrator in School of Electronic Engineering at Bangor University, where I was able to develop my teaching experience and confidence. I would also like to thank the Academic Development Unit of Bangor University for offering me quality trainings and research development workshops in developing and enhancing my academic skills.

My special thanks to my supervisor for supporting me for my future career development such as forming the first IEEE Bangor Student Branch, International Student Ambassador, and Enterprise by Design Project. I would also like to offer my kind regards to my friends and colleagues for providing me with the motivation and moral support. Besides, my thanks and acknowledgements to the authority of Bangor University for providing a good environment and facilities especially the administration staff at school of Electronic Engineering for their assistance.

I would like to thank the Memon Communities (Euro Charity Trust; World Memon Organization; The Jetpur Memon Higher Educational Welfare Trust; Aziz Tabba Foundation and Adamjee Foundation) in Pakistan and UK for the financial support. Finally I would thank my Family especially my parents, for supporting me with my career move.

Abstract

The thesis discusses research on analysis of cylindrical metal clad nano-lasers. Numerical modelling of cylindrical semiconductor nano-lasers has been undertaken accommodating local gain variations in the active region of the device. Analysis is performed using the cylindrical transfer matrix method (cTMM) and the Finite Element Method (FEM). Calculations have thereby been performed of the modal gain and the lasing condition for the device supporting TE guided mode and TM Surface Plasmon Polariton (SPP) modes. For representative structures it is shown that TE and TM mode lasing can be supported in devices having cavity lengths on the order of 1μm and 60μm respectively. The methodology adopted offers means to analyse candidate semiconductor lasers.

Attention is also given on structures having GaN as the material platform and utilising silver for the metal cladding. The lasing characteristics of such structures are explored for wide range of operating wavelengths and metal – cladding thicknesses. It is found that for lower order TE and TM mode lasing can be supported in devices having cavity lengths of the order of 2μm and 18μm respectively.

The response of metal clad nano-lasers to direct current modulation has also been analysed in both the small signal and large signal regimes. Calculations have been performed using rate equations which include the Purcell cavity enhanced spontaneous emission factor, F, and the spontaneous emission coupling factor β. It is observed that in general increased F and β reduce the 3dB direct current modulation bandwidth. Conditions are identified where the peak modulation response occurs at frequencies 40GHz and 30 GHz can be achieved. For both small and large signal regimes modulation bandwidth of approximately 60GHz can be achieved.

Publications

Journal Papers

Z. A. Sattar and K. A. Shore, "Spatial profiling of optical gain for optimizing lasing in plasmonic nano-lasers," *J. Euro. Opt. Soc. Rap. Public*. vol. 8, pp. 13045-1–13045-6, July 2013.

Z. A. Sattar, Z. Wang and K. A. Shore, "Design Optimization of Metallic Sub-Wavelength Nanowire Lasers," IET Optoelectronics, vol. 8, no. 2, pp. 129 – 136, April 2014.

Z. A. Sattar, Z. Wang and K. A. Shore, "Wave-guiding Analysis of Annular Core Geometry Metal-Clad Semiconductor Nano-Lasers," IEEE J. Quantum Elect., vol. 50, no. 1, pp. 15-22, Jan. 2014.

Z. A. Sattar and K. A. Shore, "Analysis of the Direct Modulation Response of Metal-Clad Nano-Lasers," IEEE J. Light Wave Tech., submitted for publication.

Conference Papers

Z. A. Sattar and K. A. Shore, "Lasing Condition in Cylindrical Semiconductor Nano-Lasers," Semiconductor and Integrated Optoelectronics Conference in Cardiff University, UK 2 – 4 April 2012.

Z. A. Sattar and K. A. Shore, "Analysis of Modal Gain in Semiconductor Metal Clad Nano-lasers," Nano-structured Materials and Devices Conference in Aberystwyth University, UK 16 May 2012.

Z. A. Sattar and K. A. Shore, "Multi-layered Core Model for metal-clad nano-resonators," The Celebration of the 50th Anniversary of the Diode Laser, University of Warwick, UK 20- 21 September 2012.

Z. A. Sattar and K. A. Shore, "Investigation of TM Surface Guided Modes in a Cylindrical Metal Clad Nano-Structure Laser," Europion Optical Society (EOS) Annual

Meeting 2012 Aberdeen Exhibition and Conference Centre, Scotland, UK 25 - 28 September 2012.

Z. A. Sattar and K. A. Shore, "Analytical modeling of wave-guiding in semiconductor nano-lasers," META'13, the 4th International Conference on Metamaterials, Photonic Crystals and Plasmonics,University of Sharjah, Sharjah – UAE 18 - 22 March 2013.

Z. A. Sattar and K. A. Shore, "Miniaturization of GaN nanowire lasers," META'13, the 4th International Conference on Metamaterials, Photonic Crystals and Plasmonics ,University of Sharjah, Sharjah – UAE 18 - 22 March 2013.

Z. A. Sattar and K. A. Shore, "Cavity length calculation for lasing in metallic nanowire lasers," Semiconductor and Integrated Optoelectronics Conference in Cardiff University 9 – 11 April 2013.

Z. A. Sattar and K. A. Shore, "Analysis of gain properties in silver-clad nanowire lasers," The European Conference on Lasers and Electro-Optics and the International Quantum Electronics Conference Munich Germany 12 - 16 May 2013.

Z. A. Sattar and K. A. Shore, "Design Analysis of Ultra-Short Cavity Silver-Clad Semiconductor Nano Lasers,"10th Int. Conf. *CLEO-PR&OECC/PS,* Kyoto, Japan, 30 June - 4 July, 2013.

Z. A. Sattar and K. A. Shore, "Direct Current Modulation Properties of Semiconductor Nano-Lasers: Small Signal and Large Signal Regimes," The 16th Photonics North Conf., Montreal, Canada, 28 – 30 May 2014.

Z. A. Sattar and K. A. Shore, "Analysis of the Large and Small Signal Direct Current Modulation Response up to 60GHz of Metal-Clad Nano-Lasers ," The Opto-Electronics and Communications Conf. and Australian Conference on Optical Fibre Technology (OECC/ACOFT), Australia, 6-10 July 2014.

Contents

Chapter1: Introduction **1**

1.1 Semiconductor Lasers 1

1.2 Metal Clad Nano-Lasers 2

1.3 Bound and SPP Modes in Nano-Laser 4

1.4 Dynamical Performance of Nano-Lasers 5

1.5 Thesis Aim and Outline 6

Chapter 2: Analysis of Lasing in Dual Core Cylindrical Metal Clad Nano-Lasers **11**

2.1 Introduction 11

2.2 Dual Core Cylindrical Nano-Laser Structure 11

2.3 Transfer Matrix Method & Analysis Technique 13

2.4 Modal Gain & Device Length Calculation 23

2.4.1 TE Mode Analysis 24

2.4.2 TM SPP Mode Analysis 25

2.5 Conclusion 30

Chapter 3: Annular Core Geometry Analysis of Lasing in Cylindrical Metal Clad Nano-Lasers **32**

3.1 Introduction 32

3.2 Annular Core Cylindrical Nano-Laser Structure 32

3.3 Modal Gain & Device Length Calculation 34

3.3.1 TE and TM Mode Analysis 35

3.4 Conclusion 39

Chapter 4: Spatial Profiling of Optical Gain for Optimising Lasing in Cylindrical Metal Clad Nano-Lasers **41**

4.1 Introduction 41

4.2 Nano-Laser Structure 41

4.3 Gain Profile 42

4.4 TE and TM mode Analysis 44

4.5 Lasing Cavity Length Calculations 49
4.6 Conclusion 51

Chapter 5: Device Length Calculation of Visible Emitting Nano-Lasers 53
5.1 Introduction 53
5.2 Device Length Optimisation 53
5.2.1 Analysis Technique 55
5.2.2 GaN and Silver Index Profile 55
5.3 TE and TM Mode Analysis for Device Length Optimisation 56
5.3.1 Cut-Off Radius vs Wavelength 56
5.3.2 Modal Gain at Wavelength 330 nm – 370 nm 57
5.3.3 Modal Gain at Wavelength 370 nm – 830 nm 58
5.3.4 FEM Analysis at Wavelength 480 nm – 830 nm 60
5.3.5 Effect of Insulating Layer on Modal Gain at Wavelength 480nm – 830nm 60
5.3.6 Confinement Factor at Wavelength 480 nm – 830 nm 61
5.3.7 Device Length Estimation at Wavelength 480 nm – 830 nm 62
5.3.8 3D FEM Simulation of 2μm Device 63
5.4 Conclusion 64

Chapter 6: Analysis of Direct Modulation Response of Nano-Lasers 67
6.1 Introduction 67
6.2 Nano-Laser Dynamics 67
6.3 Small and Large Signal Analysis 68
6.4 Numerical Analysis of Direct Current Modulation 70
6.5 Conclusion 74

Chapter 7: Summary & Future Work 76
7.1 Summary 76
7.2 Future Work 77

Chapter 1

Introduction

LASER (Light Amplification by the Stimulated Emission of Radiation) was first experimentally demonstrated by Theodore Maiman in 1960 [1]. Coherent light emission from semiconductor lasers using a GaAs p-n junction was demonstrated in 1962 [2-4]. Semiconductor lasers have high efficiency, small size, low cost as compared to solid state and gas lasers.

1.1 Semiconductor Lasers

The most important semiconductors for laser application are the so called III-V semiconductors, e.g. GaAs, GaN, InP, etc. A laser consists of a gain medium placed between two mirrors. The device will operate as a laser if the net round trip gain including material and mirror losses is unity. A semiconductor laser diode essentially consists of a forward biased p-n junction made from direct band-gap semiconductor materials. The n doped side has an excess of electrons and the p-doped side has an excess of holes.

When no voltage is applied across the junction, a potential barrier exists between the p doped and n doped side of the junction that prevents recombination of electrons and holes. Under forward bias the barrier is lowered allowing the electrons and holes to be injected into the active region of the p-n junction. A population inversion necessary for lasing action is formed in the active region. The electrons and holes recombine, emitting photons which experience gain by stimulated emission producing more photons. The mirrors at each end of the device reflect some of the photons back into the laser for further stimulated emission to occur.

Semiconductor lasers are widely used commercially in laser scanners, printers, optical sensors, medical equipment and for fibre-optic communication etc. The recent drive in miniaturization of semiconductor laser in the sub-wavelength (diameter of laser less than wavelength of light) regime for applications such as on chip integration of photonic and electronic components etc. requires identification of structures that can enable effective light confinement and thereby enable lasing. One

of the most promising schemes in the sub-wavelength regime seems to be the use of metal cladding for effective light confinement, hence the development of metal clad nano-lasers.

1.2 Metal Clad Nano-Lasers

Metal-clad semiconductor lasers offer significant for realizing the potential of light confinement in nano-scale lasers since light penetrates little into the metal (due to its high reflectivity) layer and can, therefore, be confined in a much tighter space. However, metal has great loss that can be compensated by the gain medium in the semiconductor. A variety of nano-lasers, as shown in Figure 1.1 have been explored in recent years, including: nano-pillar [5], nanowires [6, 7], spaser-based [8], nano-patch [9] and nano-rod lasers [10].

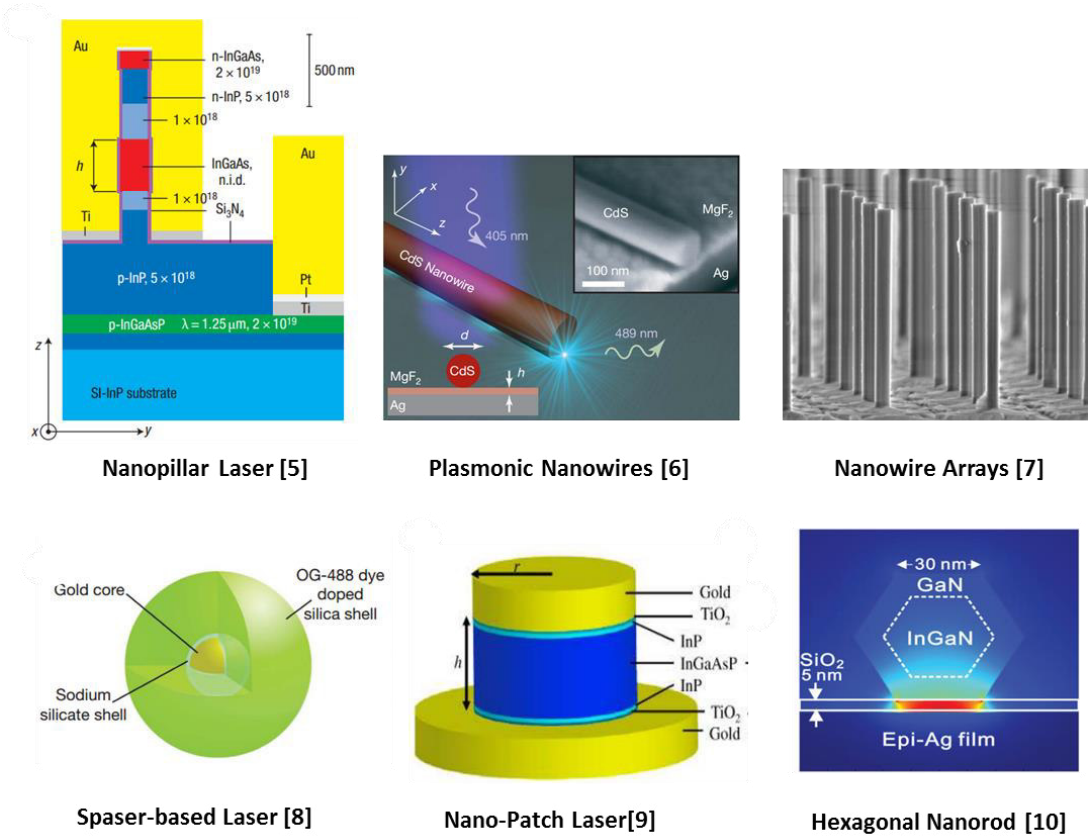

Figure 1.1 Structures of Nano-laser explored in recent years.

A specific class of such devices which has attracted interest is cylindrical metal-clad nano-lasers for which attention has been given due to the low loss transmission and their operation based on the excitation and support of Surface Plasmon Polariton (SPP) modes [11-14]. Surface Plasmon Polaritons (SPPs), are electromagnetic (EM)

waves, which propagate along a metal-dielectric or metal-air interface. The propagation of the EM wave in the metal is known as “Surface Plasmon” and in the air or dielectric is known as “Surface Polariton”. It has been identified that the plasmons in metals are due to the electromagnetic wave propagating and depends on the plasma frequency of individual metals. Equation 1.1 shows the plasma frequency in metals.

$$\omega_p = \sqrt{\frac{Ne^2}{m\varepsilon_o}} \tag{1.1}$$

Where, N is the number of electrons in metal, e is the electron charge, m is the mass of electron and ε_o is the permittivity of free space. Among the metallic elements, silver has higher plasma frequency approximately 9.2eV and is the best-performing choice at optical frequencies. Whereas Gold, which has a lower plasma frequency of the order 8.9eV, is often the metal of choice at lower Near Infrared frequencies. Moreover gold has high losses in the visible spectrum for wavelengths below or about 500 nm [15] and therefore is not considered as material platform in later chapters.

Cylindrical semiconductor metal-clad nano-lasers offer an improvement to the confinement and modal gain. Some improvements can be made through the optimization of the geometry and materials and by reducing structural imperfections. However the lower limit for optical losses is imposed by the physical properties of the metal and can only be balanced by introducing optical gain into the structure. Analysis for metal-clad nano-lasers has been developed where Maslov et al. investigated the optical gain of the guided modes of a GaN nanowire structure in air [16] and also studied the effect of GaAs nanowire surrounded by infinitely thick silver (Ag) cladding as a means to effect size reduction of cylindrical nanowire structures [12].

Vivek et al. investigated the effect of finite metal cladding on the mode confinement and loss characteristics of structure having an InGaAs core surrounded by gold (Au) metal cladding [13]. A recent numerical study by Ikeda et al. gives insight into the gain properties of the nano-laser structure [14], where it is assumed that the active core region could be modelled as a uniform core of prescribed optical properties and specifically of defined optical gain.

1.3 Bound and SPP Modes in Nano-Laser

Metal-clad nano-lasers may support several kinds of waveguide modes and notably bound modes which are largely confined to the active core and surface Plasmon Polariton (SPP) modes which derive from the dielectric-metal interface. The TM_{01} and TE_{01} are the low order modes supported by the nano-laser structure [14]. TE modes are transverse electric modes, where the magnetic field is in the direction of propagation. The TM modes are transverse magnetic modes, where the electric field is in the direction of propagation. The TE_{01} mode is known as the bound mode which is mostly confined in the core because of the metal cladding. The TM_{01} mode is known as the Surface Plasmon Polariton (SPP) modes [11] which are less confined to the core. There are two kinds of TM_{01} SPP modes: core–metal surface guided modes and air–metal surface guided modes [13-14].

The modes guided at the air-metal interface (considered in this thesis) are of much practical interest. On the other hand the core-metal surface guided modes experience high losses and may have reduced applications potential and is therefore not considered in this thesis. In comparison to the TE_{01} mode, the TM_{01} mode is a lossy mode as it is guided mostly in the air-metal interface rather in the core active region, whereas the TE_{01} mode resides mostly in the core. In this thesis attention has been given to both kinds of modes and notably low order TE and TM-SPP modes. The lower order TE and TM modes are evaluated at the mode cut-of radius, where cut-off radius is defined as the minimum radius at which the mode will be supported by the structure. It has been identified that the TM SPP modes show lasing at the cut off and are therefore of importance. In this thesis a comparison has therefore been drawn on the TE and TM SPP mode at their respective cut-off radius.

An intriguing feature of some metal-clad sub-wavelength laser structures is the enhanced modal confinement (due to the high reflective metal cladding, the electric field does not penetrate inside the metal increasing the confinement of the mode), and hence higher modal gain than the bulk material gain [17]. This property is of particular benefit in overcoming metallic losses in order to sustain lasing action in candidate structures.

1.4 Dynamical Performance of Nano-Lasers

Driven by potential applications in photonic integrated circuits, optical information processing and system-on-a-chip technologies considerable efforts has been directed at developing sub-wavelength nano-scale semiconductor lasers. In that context, a number of recent investigations of the dynamical performance of nano-lasers have been made and it is found that direct current modulation of nano-lasers offers a cost-effective option (since an external modulator would not be required for modulation) as an efficient light source for on chip interconnection [18]. The message signal (a signal that contains the information to be transmitted in the form of current) can be impressed on the light output of semiconductor lasers via direct modulation of the bias current without requiring external modulators to enhance signal strength for optical communication systems. Such nano-lasers are anticipated to exhibit enhanced dynamical performance which may arise from a combination of physical factors including mode quality factor, Purcell spontaneous emission enhancement factor F, and spontaneous emission coupling factor, β.

The quality factor Q is a quantity that measures the capability of the optical cavity to store optical field inside the laser cavity. A higher Q factor means that the mode is confined well inside the cavity and has more chance to lase. β is the spontaneous emission coupling rate into the lasing mode divided by the total spontaneous emission rate. The enhancement of the spontaneous emission rate of a lasing mode due to the confinement of the photon energy density inside a laser cavity is known as the Purcell effect. The spontaneous emission enhancement rate of the lasing mode is known as the Purcell factor, or the spontaneous emission enhancement factor, F [19].

In recent work, the impact of Purcell enhanced spontaneous emission on the modulation performance of nano-LEDS and nano-lasers [20] have been examined and it was found that for high device quality factor the Purcell enhancement is saturated limiting the modulation bandwidth to a few tens of GHz. The behaviour of optically pumped nano-lasers has been studied including the role of the spontaneous emission coupling factor, β, in achieving single mode operation of GaN nano-laser [21].

Ding et al. explored the dynamics of electrically pumped nano-lasers where the effects of the Purcell Factor, F, and the spontaneous emission coupling factor, β, on laser performance were studied [22]. It was found that the total spontaneous

emission factor is two to three orders larger than in conventional lasers. Also in recent work the dynamical characteristics of semiconductor nano-lasers have been analysed taking into account the influence of mode quality factor in small and large signal modulation analysis of nano-lasers [23]. It was found that high quality factor is required for high speed operation of micro-cavity lasers.

It has been studied that small cavity sized lasers are capable of fast modulation speeds. Enhancement of nano-laser dynamics have been studied based on the Purcell effect leading to a proposal of modulation bandwidths in excess of 100GHz [24]. However, in complementary work [25] on the dynamical performance of metal-clad nano-lasers it was shown by means of a simple analysis that the direct-current modulation bandwidth of such lasers may suffer deleterious effects due to increased Purcell spontaneous emission enhancement factor F, and spontaneous emission coupling factor, β.

1.5 Thesis Aim and Outline

The aim of the thesis is to explore the opportunities and challenges which arise in the design of metal-clad semiconductor lasers. The approach adopted is to take into account spatial profiling of the optical gain as a means both for optimizing lasing operation and as a step towards a fully self-consistent theoretical model of such structures.

Using a numerical model that emulates a cylindrical metal-clad nano-laser using cTMM (cylindrical transfer matrix method) has been used in this thesis, which is discussed in detail in later chapters and appendix [26-27]. A model utilizing material gain variation in the core, of prescribed optical properties and of specifically defined optical gain is also considered. The advantage of this approach is that it is a simple and straightforward way to analyse waveguide structures. Significant attention has been given to determining the modal gain and optical confinement factor to effect reduction in size of such lasers.

The present thesis consists of seven chapters. In chapter 2 a dual core nano-laser structure is analysed to provide insight into the effect of gain variation in the active

region. Use is made of cTMM to solve the modal properties of TE_{01} and TM_{01} mode in the structure. Calculations on the modal gain and device length of the structure have also been carried out.

In chapter 3 the effect of using multiple layered geometry of cylindrical nano-laser is studied. Variation of material gain in the active region is analysed and the effects to the modal gain is observed. Effects on multilayer core with respect to the dual core structure are compared with respect to the overall modal gain and the device length of the structure.

In chapter 4, the annular core (multilayer geometry) of cylindrical nano-laser discussed in chapter 3 is studied in detail for a nano-laser structure utilizing a more realistic, Gaussian gain profile. The effects on the variation of gain along the radius of the core are studied using cTMM and Finite Element Method (FEM). The results are evaluated for the overall modal gain and device length.

In chapter 5, the lasing performance of semiconductor nanowire lasers have been explored. Moreover the wave guiding and lasing characteristics of such structures are examined over a wide wavelength range: 330nm to 830nm. The modal gain and corresponding laser cavity length for the TE_{01} and TM_{01} modes is calculated for thin silver cladding thicknesses from 5nm to 20nm. Results obtained are compared with FEM analysis and a 3D FEM model is evaluated for the results obtained using the 2D cTMM.

In chapter 6, a study of the dynamical performance of nano-laser has also been carried out, where the focus is to determine the influence of Purcell spontaneous emission enhancement factor F, and the spontaneous emission coupling factor, β for direct current modulation in both the small signal and large signal regimes. Rate equation model of semiconductor nano-laser is used to study small and large signal modulation. Modulation bandwidths are evaluated using direct current modulation for range of values of β, F and bias current.

In chapter 7, conclusions are drawn based on the results obtained and recommendations for future work are made.

References

[1] T.H. Mainman, “Stimulated radiation in ruby,” *Nature*, vol. 187, pp. 493-494, Aug. 1960.

[2] M. I. Nathan, W. P. Dumke, G. Burns, F. H. Dill, and G. Lasher, “Stimulated emission of radiation from GaAs p-n junctions,” *Appl. Phys. Lett.,* vol. 1, no. 1, pp. 62-63, Nov. 1962.

[3] N. Holonyak, and S. F. Bevacqua, “Coherent (visible) light emission from Ga(As1-xpx) junctions,” *Appl. Phys. Lett.,* vol. 1, no. 82, pp. 82-83, Dec. 1962.

[4] R. N. Hall, G.E. Fenner, J. D. Kingsley and R. O. Carlson, “Coherent Light Emission from GaAs Junctions,” *Phys. Rev. Lett.,* vol. no. 9, pp. 366-368, Nov. 1962.

[5] M. T. Hill, Y. S. Oei, B. Smalbrugge, Y. Zhu, T. de Vries, P. J. van Veldhoven, F. W. M. van Otten, T. J. Eijkemans, J. P. Turkiewicz, H. de Waardt, E. Jan Geluk, S. H. Kwon, Y. H. Lee, R. Nötzel, and M. K. Smit, “Lasing in metallic-coated nanocavities,” *Nature Photonics*, vol. 1, pp. 589-594, Oct. 2007.

[6] R. F. Oulton, V. J. Sorger, T. Zentgraf, R. M. Ma, C. Gladden, L. Dai, G. Bartal and X. Zhang, “Plasmon lasers at deep subwavelength scale,” *Nature*, vol. 461, pp. 629-632, Oct. 2009.

[7] Q. Li, J. B. Wright, W.W. Chow, T. S. Luk, I. Brener, L. F. Lester, G. T. Wang, “Single-mode GaN nano-laser lasers,” *Opt. Exp.,* vol. 20, no. 16, pp. 17873-17879, 2012.

[8] M. A. Noginov, G. Zhu, A. M. Belgrave, R. Bakker, V. M.Shalaev, E. E. Narimanov, S. Stout, E. Herz, T. Suteewong and U. Wiesner, “Demonstration of a spaser-based nanolaser,” *Nature*, vol. 460, pp. 1110-1113, Aug. 2009.

[9] K. Yu, A. Lakhani, M. C. Wu, “Subwavelength metal-optic semiconductor nanopatch lasers,” *Opt. Exp*., vol.18, no. 9, pp. 8790-8799, Apr. 2010.

[10] Y.-J. Lu , J. S. Kim , H.-Y. Chen , C. H. Wu , N. Dabidian , C. E. Sanders , C.-Y. Wang , M.-Y. Lu , B.-H. Li , X. G. Qiu , W.-H. Chang , L.-J. Chen , G. Shvets , C.-K Shih and S. G. Gwo "Plasmonic nanolasers using epitaxially grown silver film", *Science*, vol. 337, no. 6093, pp.450 -453 2012

[11] S. J. Al-Bader and M. Imtaar, “Azimuthally Uniform Surface-Plasma Modes in Thin Metallic Cylindrical Shells” *IEEE J. Quantum Electron*., vol. 28, no. 2, pp. 525-533, Feb. 1992.

[12] A. V. Maslov and C. Z. Ning, "Size reduction of a semiconductor nanowire laser by using metal coating," Proc. *SPIE*., vol. 6468, pp. 646801-1–646801-7, 2007.

[13] V. Krishnamurthy and B. Klein, "Theoretical investigation of metal cladding for nanowire and cylindrical micropost lasers," *IEEE J. Quantum Electron*., vol. 44, no. 1, pp. 67-74, Jan. 2008.

[14] K. Ikeda, Y. Fainman, K. A.Shore and H. Kawaguchi, "Modified long range surface plasmon polariton modes for laser nano resonators." *J. Appl. Phys*., vol. 110, no. 6, pp. 063106-1–063106-6, Sep. 2011.

[15] P. R. West, S. Ishii, G. Naik, N. Emani, V. M. Shalaev, and A. Boltasseva, "Searching for Better Plasmonic Materials", Laser & Photonics Reviews, vol 4, no 6, pp 795-808, November 2010.

[16] A. V. Maslov and C. Z. Ning, "Modal gain in a Semiconductor nanowire laser with anisotropic bandstructure*," IEEE J. Quantum Electron*., vol. 40, no. 10 pp. 1389–1397, Oct. 2004.

[17] A. V. Maslov and C. Z. Ning, "Nitride Semiconductor Devices: Principles and Simulation" Wiley VCH Verlag GmbH & Co. KGaA, Weinheim, 2007, pp. 469-471.

[18] D. V. Thourhout, T. Spuesens, S. K. Selvaraja, L. Liu, G. Roelkens, R. Kumar, G. Morthier, P. Rojo-Romeo, F. Mandorlo, P. Regreny, O. Raz, C. Kopp, and L. Grenouillet, "Nanophotonic devices for optical interconnect," *IEEE J. Sel. Top. Quantum Electron.*, vol. 16, no. 5, pp. 1363–1375, Oct. 2010.

[19] E. M. Purcell, "Spontaneous emission probabilities at radio frequencies," *Phys. Rev.*, vol. 69, p. 681, 1946.

[20] T. Suhr, N. Gregerson, Y. Yvind, and J. Mork, "Modulation response of nanoLEDs and nanolasers exploiting Purcell enhanced spontaneous emission," *Opt. Exp.*, vol. 18, no. 11, pp. 11230-11241, May. 2010.

[21] H. Gao, A. Fu, S. C. Andrews and P. Yang, "Cleaved-coupled nanowire lasers," *Proc. Natl. Acad. Sci*., vol. 110, no. 3, pp. 865-869, Jan. 2013.

[22] K. Ding and C. Z. Ning, "Metallic sub-wavelength-cavity semiconductor nanolasers," *Light: Sci. Appl.,* vol. 1, no. 7, p. 20, Jul. 2012.

[23] X. M. Lv, L. X. Zou, Y. Z. Huang, Y. D. Yang, J. L. Xiao, Q. F. Yao and J. D. Lin, "Influence of Mode *Q* Factor and Absorption Loss on Dynamical Characteristics for semiconductor Microcavity Lasers by Rate Equation Analysis," *IEEE J. Quantum Electron.*, vol. 47, no. 12, pp. 1519-1525, Dec. 2011.

[24] E. K. Lau, A. Lakhani, R. S. Tucker, and M. C. Wu, "Enhanced modulation bandwidth of nanocavity light emitting devices," *Opt. Exp.*, vol. 17, no. 10, pp. 7790–7799, Apr. 2009.

[25] K. A. Shore, "Modulation bandwidth of metal-clad semiconductor nanolasers with cavity-enhanced spontaneous emission," *Electron. Lett.*, vol. 46, no. 25, pp. 1688-1689, Dec. 2010.

[26] P. Yeh, *Optical waves in layered media*. New York: John Wiley & Sons, Inc., 1988.

[27] P. Yeh, A. Yariv, and E. Marom, "Theory of Bragg fiber," *J. Opt. Soc. Am.*, vol. 68, no. 9, pp. 1196-1201, Sep. 1978.

Chapter 2

Analysis of Lasing in Dual Core Cylindrical Metal Clad Nano-Lasers

2.1 Introduction

The analysis of Metal-clad nano lasers have been explored in recent years [1-2]. Specific attention has been given to cylindrical metal clad nano-lasers to their operation based on the excitation and support of Surface Plasmon Polariton (SPP) waveguide modes [3-7]. The work carried out by Ikeda et al. gives insight to the gain properties of the structure [8], where it is assumed that the active core region could be modelled as a single layer (uniform core) of prescribed optical properties and, specifically, of defined optical gain.

In that context, the aim of this chapter is to analyse cylindrical metal-clad semiconductor lasers giving specific attention to the role of SPP modes. The approach adopted is to take into account spatial profiling of the optical gain using a dual core structure. The cylindrical transfer matrix method [9, 10], is used as a means for optimising lasing operation of such structures[1].

2.2 Dual Core Cylindrical Nano-Laser Structure

The structure under consideration is a cylindrical metal-clad nano-laser. In previous work such a structure has been studied assuming a uniform (single) core [7, 8]. In order to take into account spatial variations in gain in the active region of such a structure, a two-layer (dual) core model is utilized. The cross-section of such a structure is illustrated in Figure 2.1. The key elements of the structure are the core semiconductor region and the metal cladding. The analysis methodology adopted here is of general application but for the work presented in this chapter, it is assumed that the metal-clad structure is surrounded by air. In addition, for all results discussed, the operating wavelength of the laser is taken to be 1μm. It is straightforward to examine alternative configurations and notably the use of

[1] This chapter is based on the paper:

Z. A. Sattar and K. A. Shore, "Spatial profiling of optical gain for optimizing lasing in plasmonic nano-lasers." *J. Euro. Opt. Soc. Rapid. Publications*. vol. 8, pp. 13045-1–13045-6, July 2013.

alternative surrounding media. Following earlier work the core semiconductor material is assumed to be $In_{0.2}Ga_{0.8}As$ with a refractive index of 3.6 at the chosen operating wavelength λ = 1μm [11-12]. The metal cladding is taken to be gold with a complex refractive index of n_3 = 0.22 – j6.71 [13] and the thickness of metal clad is assumed to be 20nm [14]. These parameters are considered in order to analyse the uniform core structure [8] with the dual core structure as shown in Figure 2.1 surrounded by air with refractive index n_4. The use of 20nm metal thickness has been considered as reasonable finite thickness in metal clad nano-lasers in previous work [7]. Moreover, it has been reported that for metal thickness above 50nm, the losses in the structure become independent of the metal thickness and is therefore termed infinite thickness.

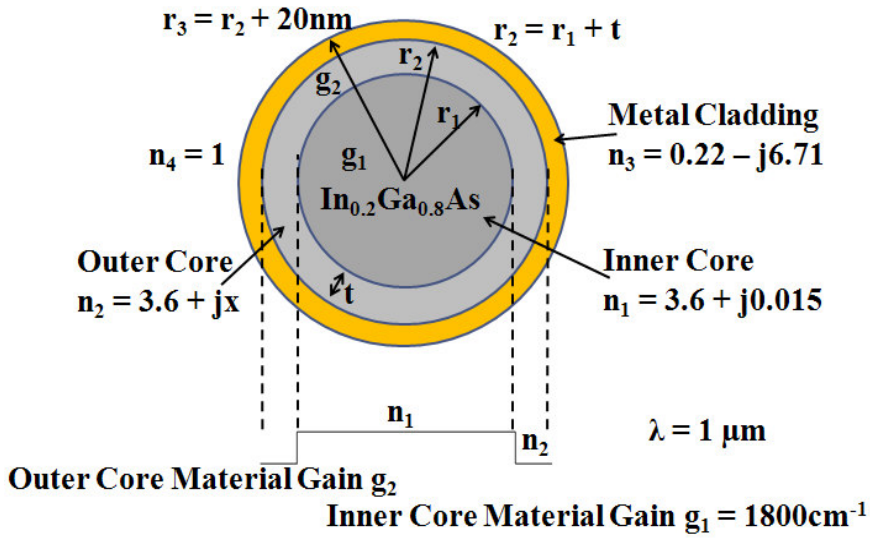

Figure 2.1 Cross-section of cylindrical semiconductor metal-clad nano-laser

The model which has been developed for this work allows for the definition of an arbitrary number of layers in the active core semiconductor region as well as in the cladding region. This utility has been developed in order to explore combinations of gain profiles and/or surrounding media.

However, for the specific calculations performed in this chapter, the core semiconductor is considered to be comprised of just two regions with differing material gains. In this case, the overall core radius r_2 is defined as the sum of the radius of the 'inner core', r_1, and the thickness of the 'outer core', *t*. r_3 is the overall radius of the structure including the metal cladding.

For the cases explored here the gain in the inner core, g_1 is taken to be greater than that of the outer core g_2. It is underlined that the relative values of such gains are dependent upon the precise electrical excitation scheme utilised in such lasers. The methodology allows exploration of such alternatives. For the sake of definiteness, the results obtained here have sought to make a comparison of the lasing conditions when allowance is made for a variation in the outer core material gain g_2 whilst the inner core material gain g_1 is held at a fixed value of 1800 cm^{-1}.

The material gain, g_1 in the inner core is introduced through the imaginary part of the refractive index of the active region, which is related to the gain coefficient by $\frac{4\pi}{\lambda} Im(n_{core} + jk_{core})$. Where n_{core} is real part of the refractive index of and k_{core} is the imaginary part of the refractive index of the inner and outer core n_1 and n_2. The real part of the inner core region is kept constant to 3.6 whereas the gain is introduced by varying the imaginary part from 0 to 0.015 as in [8]. This in turns provide a maximum material gain in the inner core which approximates to 1800cm^{-1} at the wavelength, λ = 1μm. In effect, when the outer core layer is introduced in the core region, the material gain g_1 is kept constant to 1800cm^{-1} and g_2 is varied from 0 to 1760cm^{-1} which is equivalent to a refractive index of the outer core 3.6 + j0.014.

Lasers constructed with such geometries may support several kinds of waveguide modes and notably bound modes which are largely confined to the active core and surface Plasmon Polariton (SPP) modes which derive from the dielectric-metal interface. In this chapter attention has been given to both kinds of modes and notably confined TE modes and low order TM SPP modes.

2.3 Transfer Matrix Method & Analysis Technique

Analysis of the structure has been performed using the well-known Transfer Matrix Method [9, 10] which, in principle, enables direct evaluation of structures where consideration is given to an arbitrary number of multilayers. The outline of the analysis technique presented here is specifically for the case under consideration i.e. with a two-layer (dual) active core; a metal cladding and the surrounding medium being air. It is noted that some algebraic manipulation needs to be undertaken when the number of layers utilised is changed.

In this chapter along with chapters 3, 4, and 5the nano-laser structure is analysed using the cylindrical Transfer Matrix Method, which is described in detail here. The model which has been developed here allows for the definition of arbitrary number of layers in the active layer core semiconductor region as well as in the cladding region. This utility has been developed in order to explore combinations of gain profiles and/or surrounding media. However, for the specific calculations performed here, the core semiconductor is considered to be comprised of an inner core and N annular outer core regions of radius r, with the index profile n in (2.1),

$$n(r) = \begin{cases} n_{inner\ core} & 0 \le r < r_1 \\ n_{outer\ core\ 1} & r_1 \le r < r_2 \\ \vdots & \\ n_{outer\ core\ N} & r_N \le r < r_{N+1} \\ n_{metal} & r_{N+1} \le r < r_{N+1} + t_m \\ n_{air} & r \ge r_{N+1} + t_m \end{cases} \tag{2.1}$$

Where, n_{metal} and n_{air} is the refractive index of metal and air respectively and t_m is the thickness of metal cladding. The refractive index profile of active core annuli includes a material gain profile such that,

$$g_{inner\ core} > g_{outer\ core\ 1} > g_{outer\ core\ 2} \dots\dots > g_{outer\ core\ N} \tag{2.2}$$

The method of pumping in lasers determines the gain in the core active region. In the analysis it is assumed that a certain value for the material gain is attained by some means, therefore for an active core with gain included (g_{core}) the index profile for N annuli becomes,

$$\begin{aligned} n_{inner\ core} &= n_{core} + j\frac{g_{inner\ core}}{2\gamma_o} \\ n_{outer\ core\ 1} &= n_{core} + j\frac{g_{outer\ core\ 1}}{2\gamma_o} \\ &\vdots \\ n_{outer\ core\ N} &= n_{core} + j\frac{g_{outer\ core\ N}}{2\gamma_o} \end{aligned} \tag{2.3}$$

Where, $\gamma_o$is the propagation constant in free space,

$$\gamma_o = \frac{2\pi}{\lambda_o} \tag{2.4}$$

Where, λ_o is the wavelength of propagation. The Transfer Matrix Method solves the Eigen modes for the structure. The direction of propagation is considered in the z axis and therefore, all field components within the cylindrical structure can be represented in the form,

$$f(r,\theta,z,t) = f(r,\theta)e^{i(\beta z-\omega t)} \tag{2.5}$$

Where f represents the field components in the structure, i.e., $E_z, E_r, E_\theta, H_z, H_r, H_\theta$. ω being the angular frequency and β is the mode propagation constant. The field propagates within the structure of radius r radially with angle θ along the direction of propagation z at time t.

$$E_r = \frac{1}{\gamma}\left(j\beta E_z{}'(r) + \frac{j\omega\mu}{r}H_z{}'(\theta)\right) \tag{2.6}$$

$$E_\theta = \frac{1}{\gamma}\left(\frac{j\beta}{r}E_z{}'(\theta) - j\omega\mu H_z{}'(r)\right) \tag{2.7}$$

$$H_r = \frac{1}{\gamma}\left(j\beta H_z{}'(r) - \frac{j\omega\epsilon}{r}E_z{}'(\theta)\right) \tag{2.8}$$

$$H_\theta = \frac{1}{\gamma}\left(\frac{j\beta}{r}H_z{}'(\theta) + j\omega\epsilon E_z{}'(r)\right) \tag{2.9}$$

Where $E_z(r,\theta)$ and $H_z(r,\theta)$ satisfy the wave equation,

$$\left[\frac{\partial^2}{\partial r^2} + \frac{1}{r}\frac{\partial}{\partial r} + \frac{1}{r^2}\frac{\partial^2}{\partial\theta^2}\right]\begin{Bmatrix}E_z\\H_z\end{Bmatrix} = 0 \tag{2.10}$$

And, μ, ϵ are the permeability and permittivity of the medium and γ is propagation constant in the medium as in equation (2.11),

$$\gamma = \sqrt{{\gamma_o}^2 n^2 - \beta^2} \tag{2.11}$$

Where, n is the refractive index defined by $n = \sqrt{\mu\epsilon}$, γ_0 is the propagation constant in free space. $\beta = \gamma_o n_{eff}$, n_{eff} is the effective refractive index of the mode. In the analysis $\mu = 1$ is considered therefore $n^2 = \epsilon$. For the analysis of the structure, the transverse field component for the TM and TE mode is expressed in terms of E_z and H_z respectively as,

$$E_{zi} = [U_i J_o(\gamma_i r_i) + V_i Y_o(\gamma_i r_i)] \tag{2.12}$$

$$H_{zi} = [W_i J_o(\gamma_i r_i) + Q_i Y_o(\gamma_i r_i)] \tag{2.13}$$

Where J_o and Y_o are the zero order Bessel functions of the first and second kind respectively. U_i, V_i, W_i, Q_i are field amplitudes, the indices *i = 1, 2, 3.....N, N+1, N+2* represents the appropriate region of the structure as in chapter 2, 3, 4 and 5 and γ_i is represented in the form of material and modal gain as in equation (2.14)

$$\gamma_i = \gamma_o \sqrt{\left(Re(n_i) \pm j\frac{g_i}{2\gamma_o}\right)^2 - \left(Re(n_{eff}) \pm j\frac{G}{2\gamma_o}\right)^2} \tag{2.14}$$

Where,

$\boldsymbol{Re(n_i)}$ is the real part of refractive index of each layer,

$\boldsymbol{G}$ is the modal gain/loss, which is evaluated using the cTMM,

$\boldsymbol{g_i}$ is the material gain for the semiconductor core and loss for the metal.

$\boldsymbol{Re(n_{eff})}$ is the real part of the effective refractive index of the mode.

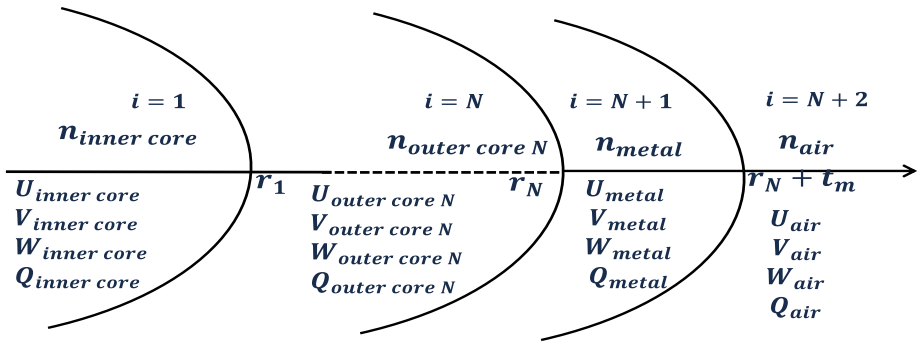

Figure 2.2: Layer interface for the annulus core structure. Where i defines the semiconductor core annuli, the metal layer and the outer most cladding i.e., air.

The boundary conditions at each interface are that E_z, E_θ, H_z and H_θ are continuous. In the analysis the boundary conditions are satisfied by using a matrix A_i and B_i in equation (2.15) and (2.16), which links the field amplitudes with adjacent layers i.e., U_i, V_i, W_i, Q_i to $U_{i+1}, V_{i+1}, W_{i+1}, Q_{i+1}$ as shown in Figure 2.2.

For TM mode, the field amplitudes at the boundary interface is given by equation (2.15)

$$\begin{pmatrix} U_{i+1} \\ V_{i+1} \end{pmatrix} = A_i \begin{pmatrix} U_i \\ V_i \end{pmatrix} \tag{2.15}$$

For TE mode, the field amplitudes at the boundary interface is given by equation (2.16)

$$\begin{pmatrix} W_{i+1} \\ Q_{i+1} \end{pmatrix} = B_i \begin{pmatrix} W_i \\ Q_i \end{pmatrix} \tag{2.16}$$

The matrices M and P for the TM and TE modes that links the field parameters from the first layer i.e., inner core to the outer most cladding i.e., air, can be represented as,

$$\begin{pmatrix} U_{air} \\ V_{air} \end{pmatrix} = M \begin{pmatrix} U_{inner\ core} \\ V_{inner\ core} \end{pmatrix} \tag{2.17}$$

$$\begin{pmatrix} W_{air} \\ Q_{air} \end{pmatrix} = P \begin{pmatrix} W_{inner\ core} \\ Q_{inner\ core} \end{pmatrix} \tag{2.18}$$

Where M and P are formed by the matrix multiplication of the matrices A_i & B_i for layers *i = 1, 2, 3…..N, N+1, N+2* such that,

$$M = A_1\, A_2\, A_3 \ldots \ldots A_{i-1} \tag{2.19}$$

$$P = B_1\, B_2\, B_3 \ldots \ldots B_{i-1} \tag{2.20}$$

Where the boundary interface $A_1\, A_2 \ldots A_{i-1}$ in (2.19) and $B_1\, B_2 \ldots B_{i-1}$ in (2.20) are calculated by

$$A_i = {m_{TM}}^{-1}(i+1, r_i) m_{TM}(i, r_i) \tag{2.21}$$

$$B_i = {m_{TE}}^{-1}(i+1, r_i) m_{TE}(i, r_i) \tag{2.22}$$

m_{TE} and m_{TM} in $(A.21)$ and $(A.22)$ are in the form,

$$m_{TE}(i, r_i) = \begin{bmatrix} J_o(\gamma_i r_i) & Y_o(\gamma_i r_i) \\ \frac{1}{\gamma_i} J_o'(\gamma_i r_i) & \frac{1}{\gamma_i} Y_o'(\gamma_i r_i) \end{bmatrix} \tag{2.23}$$

$$m_{TM}(i, r_i) = \begin{bmatrix} J_o(\gamma_i r_i) & Y_o(\gamma_i r_i) \\ \frac{{n_i}^2}{\gamma_i} J_o'(\gamma_i r_i) & \frac{{n_i}^2}{\gamma_i} Y_o'(\gamma_i r_i) \end{bmatrix} \tag{2.24}$$

The matrices of TE and TM mode in equations (2.23) and (2.24) are formed on the basis of the field components $E_z, E_\theta, H_z,$ and H_θ being continuous at their boundary interface.

For TM Mode

For TM mode matrix in equation (2.24) the field E_z using equation (2.12) the continuity of E_z at the boundary interface of the adjacent layers is given by equation (2.25)

$$(J_o(\gamma_{i+1} r_i) \quad Y_o(\gamma_{i+1} r_i)) \begin{pmatrix} U_{i+1} \\ V_{i+1} \end{pmatrix} = (J_o(\gamma_i r_i) \quad Y_o(\gamma_i r_i) \begin{pmatrix} U_i \\ V_i \end{pmatrix} \tag{2.25}$$

For the TM mode the field $H_z = 0$, and therefore for the field H_θ using equation (2.12) and (2.9) the continuity of H_θ is given in equation (2.26)

$$\begin{pmatrix} \frac{\omega {n_{i+1}}^2}{\gamma_{i+1}} J_o'(\gamma_{i+1} r_i) & \frac{\omega {n_{i+1}}^2}{\gamma_{i+1}} Y_o'(\gamma_{i+1} r_i) \end{pmatrix} \begin{pmatrix} U_{i+1} \\ V_{i+1} \end{pmatrix} = \begin{pmatrix} \frac{\omega {n_i}^2}{\gamma_i} J_o'(\gamma_i r_i) & \frac{\omega {n_i}^2}{\gamma_i} Y_o'(\gamma_i r_i) \end{pmatrix} \begin{pmatrix} U_i \\ V_i \end{pmatrix} \tag{2.26}$$

Where the primed quantities in equation (2.26) are the derivatives with respect to their own argument. Rearranging equations (2.25) and (2.26) is of the form,

$$\begin{pmatrix} J_o(\gamma_{i+1}r_i) & Y_o(\gamma_{i+1}r_i) \\ \frac{{n_{i+1}}^2}{\gamma_{i+1}} J_o'(\gamma_{i+1}r_i) & \frac{{n_{i+1}}^2}{\gamma_{i+1}} Y_o'(\gamma_{i+1}r_i) \end{pmatrix} \begin{pmatrix} U_{i+1} \\ V_{i+1} \end{pmatrix} = \begin{pmatrix} J_o(\gamma_i r_i) & Y_o(\gamma_i r_i) \\ \frac{{n_i}^2}{\gamma_i} J_o'(\gamma_i r_i) & \frac{{n_i}^2}{\gamma_i} Y_o'(\gamma_i r_i) \end{pmatrix} \begin{pmatrix} U_i \\ V_i \end{pmatrix} \quad (2.27)$$

Therefore for TM mode, equation (2.27) can be written as,

$$m_{TM}(i+1, r_i) \begin{pmatrix} U_{i+1} \\ V_{i+1} \end{pmatrix} = m_{TM}(i, r_i) \begin{pmatrix} U_i \\ V_i \end{pmatrix} \quad (2.28)$$

For TE mode

For TE mode matrix in equation (2.23) the field H_z using equation (2.13) the continuity of H_z at the boundary interface of the adjacent layers is given by equation (2.29),

$$(J_o(\gamma_{i+1}r_i) \quad Y_o(\gamma_{i+1}r_i)) \begin{pmatrix} W_{i+1} \\ Q_{i+1} \end{pmatrix} = (J_o(\gamma_i r_i) \quad Y_o(\gamma_i r_i)) \begin{pmatrix} W_i \\ Q_i \end{pmatrix} \quad (2.29)$$

For the TE mode the field $E_z = 0$, and therefore for the field E_θ using equation (2.13) and (2.7) the continuity of E_θ is given in equation (2.30)

$$\begin{pmatrix} -\frac{\omega}{\gamma_{i+1}} J_o'(\gamma_{i+1}r_i) & -\frac{\omega}{\gamma_{i+1}} Y_o'(\gamma_{i+1}r_i) \end{pmatrix} \begin{pmatrix} W_{i+1} \\ Q_{i+1} \end{pmatrix} = \begin{pmatrix} -\frac{\omega}{\gamma_i} J_o'(\gamma_i r_i) & -\frac{\omega}{\gamma_i} Y_o'(\gamma_i r_i) \end{pmatrix} \begin{pmatrix} W_i \\ Q_i \end{pmatrix} \quad (2.30)$$

Rearranging equations (2.29) and (2.30), is of the form,

$$\begin{pmatrix} J_o(\gamma_{i+1}r_i) & Y_o(\gamma_{i+1}r_i) \\ \frac{1}{\gamma_{i+1}}J_o{}'(\gamma_{i+1}r_i) & \frac{1}{\gamma_{i+1}}Y_o{}'(\gamma_{i+1}r_i) \end{pmatrix}\begin{pmatrix} W_{i+1} \\ Q_{i+1} \end{pmatrix} = \begin{pmatrix} J_o(\gamma_i r_i) & Y_o(\gamma_i r_i) \\ \frac{1}{\gamma_i}J_o{}'(\gamma_i r_i) & \frac{1}{\gamma_i}Y_o{}'(\gamma_i r_i) \end{pmatrix}\begin{pmatrix} W_i \\ Q_i \end{pmatrix} \quad (2.31)$$

Therefore for the TE mode, equation (2.31) can be written as,

$$m_{TE}(i+1, r_i)\begin{pmatrix} W_{i+1} \\ Q_{i+1} \end{pmatrix} = m_{TE}(i, r_i)\begin{pmatrix} W_i \\ Q_i \end{pmatrix} \quad (2.32)$$

Boundary Conditions for cTMM

In order to obtain a finite field at the centre of the inner core and a decaying field in the outer most dielectric, as shown in Figure 2.3, it is assumed that,

$$V_{inner\ core} = 0, Q_{inner\ core} = 0, V_{air} = jU_{air}\ \&\ Q_{air} = jW_{air} \quad (2.33)$$

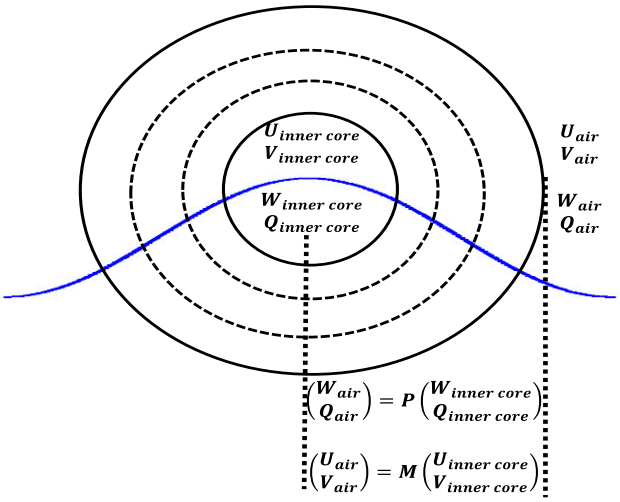

Figure 2.3 Representation for the boundary condition between the inner core and the outer most cladding.

Hence, after applying boundary conditions using (2.33) in (2.17) and (2.18), For TM mode

$$\begin{pmatrix} U_{air} \\ jU_{air} \end{pmatrix} = \begin{pmatrix} M_{11} & M_{12} \\ M_{21} & M_{22} \end{pmatrix}\begin{pmatrix} U_{inner\ core} \\ 0 \end{pmatrix} \quad (2.34)$$

For TE mode

$$\begin{pmatrix} W_{air} \\ jW_{air} \end{pmatrix} = \begin{pmatrix} P_{11} & P_{12} \\ P_{21} & P_{22} \end{pmatrix}\begin{pmatrix} W_{inner\ core} \\ 0 \end{pmatrix} \quad (2.35)$$

Re-arranging (2.34) and (2.35),

For TM mode

$$\left.\begin{matrix} U_{inner\ core}M_{11} - U_{air} = 0 \\ U_{inner\ core}M_{21} - jU_{air} = 0 \end{matrix}\right\} \quad (2.36)$$

For TE mode

$$\left.\begin{matrix} W_{inner\ core}P_{11} - W_{air} = 0 \\ W_{inner\ core}P_{21} - jW_{air} = 0 \end{matrix}\right\} \quad (2.37)$$

Writing (2.36) and (2.37) in matrix form,

$$\begin{pmatrix} M_{11} & -1 \\ M_{21} & -j \end{pmatrix}\begin{pmatrix} U_{inner\ core} \\ U_{air} \end{pmatrix} = 0 \quad (2.38)$$

$$\begin{pmatrix} P_{11} & -1 \\ P_{21} & -j \end{pmatrix}\begin{pmatrix} W_{inner\ core} \\ W_{air} \end{pmatrix} = 0 \quad (2.39)$$

The eigen-equations are obtained by taking the determinant of the matrix in (2.38) and (2.39) equal to zero as in equation (2.40) and (2.41)

$$\begin{vmatrix} M_{11} & -1 \\ M_{21} & -j \end{vmatrix} = 0 \quad (2.40)$$

$$\begin{vmatrix} P_{11} & -1 \\ P_{21} & -j \end{vmatrix} = 0 \quad (2.41)$$

Therefore the Eigen equation for the TM and TE mode becomes;

For TM mode;

$$M_{21} - jM_{11} = 0 \quad (2.42)$$

For TE mode;

$$P_{21} - jP_{11} = 0 \quad (2.43)$$

The eigenvalue equations in (2.42) and (2.43) were then used to evaluate the optical gain of the TE and TM modes and hence the lasing condition for the structure is determined. Simulations were performed using MATLAB. These eigen equations were

used to evaluate the effective refractive index (n_{eff}) of the TE_{01} and TM_{01} modes. In this way the modal gain, G, is found using equation (2.44).

$$G = \frac{4\pi}{\lambda} Im(n_{eff}) \tag{2.44}$$

Where, $Im(n_{eff})$ is the imaginary part of the effective refractive index of the mode. For conventional laser diodes with an optical cavity of length L, mirrors with identical reflectivities R and, based on the weak wave-guiding and internal losses α, at target wavelengths, the threshold condition for the gain coefficient g is given as $g = \alpha + \frac{1}{L}\ln\left(\frac{1}{R}\right)$. It has been identified and discussed in chapter 4, that due to the strong wave-guiding and optical confinement because of the metal cladding, the length of the device is independent of the internal losses and hence internal losses may be neglected. Therefore in this thesis lasing condition is defined by the length of the device L as in equation (2.45)

$$L = \frac{1}{G} ln\left(\frac{1}{R}\right) \tag{2.45}$$

Where R is the reflectivity calculated using equation (2.46).

$$R = \left(\frac{n_{core} - 1}{n_{core} + 1}\right)^2 \tag{2.46}$$

For a conventional laser diode, the reflectivity from its facets is given by the Fresnel formula as in equation (2.46). This formula is not strictly applicable for nano-lasers as the diameter of the core is smaller than the lasing wavelength and due to diffraction at the edges calculation of the modal reflectivity is quite challenging [15]. Exact calculation of the facet reflectivities of such structures requires careful account to be taken of the precise structure and notably the presence or otherwise of surrounding metallic layers. In the present case, it is simply assumed that the facet reflectivity is determined by the change in dielectric constant between the semiconductor material and the surrounding medium assumed to be air. For the analysis carried out, the reflectivity R is assumed 0.32.

2.4 Modal Gain & Device Length Calculation

The principal aim of this chapter is to evaluate the optical gain and lasing condition for the TE and TM mode which has the potential to lase in the chosen structure. Initial analysis is carried out in order to evaluate the effect of metal cladding in the structure.

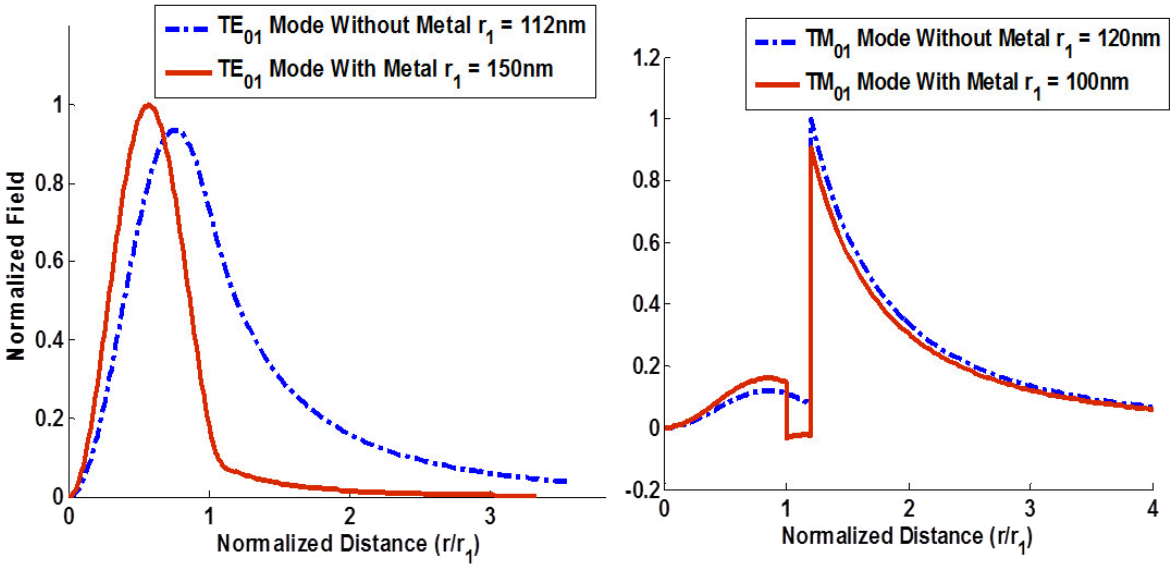

Figure 2.4 TE_{01} and TM_{01} mode profiles for structures with and without metal cladding.

Figure 2.4 shows the TE_{01} and TM_{01} mode profiles for structures with and without metal cladding, i.e. at t = 20 nm and t = 0nm respectively. Two important features are observed when metal cladding is used. 1) The mode is better confined in the core and the field intensity is greater as compared to that of the case when no metal cladding is considered, showing that confinement of the mode offers better performance when metal cladding is utilised. 2) For TE mode structure with 20nm metal cladding the cut off core radius is increased to 150nm while without metal it is 112nm. For the TM mode structure with metal of 20nm, the cut off radius is reduced to 100 nm, while for structure without metal cladding the core radius is 120 nm. Further analysis on modal gain and device length is carried out in later sections.

2.4.1 TE mode analysis

In the analysis the dimensions of the device were fixed in the following way. The overall core radius (r_2) was held constant at 200nm whilst the inner core radius (r_1) and outer core thickness (t) were varied. The analysis is performed for different inner core radius and outer core thickness and a comparison is drawn with respect to the modal gain.

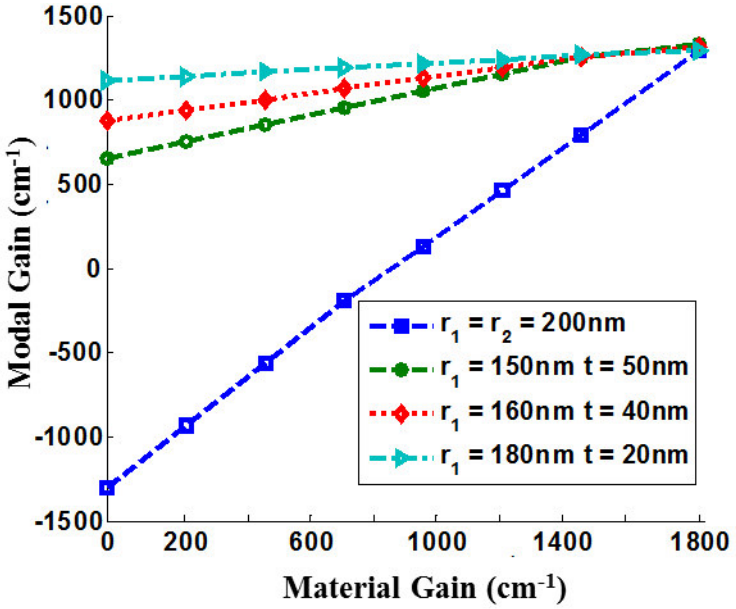

Figure 2.5 TE_{01} Modal Gain vs Material Gain for different inner core radii for fixed overall core radius

Calculations are therefore done for the structure without outer core, i.e. $r_1 = r_2 = 200nm$, and with outer core, as summarized in Table 2.1. Outcomes of representative calculations where the inner core and outer core material gain is varied are shown in Figure 2.5. It is observed that the modal gain linearly increases as the material gain is increased. However for the dual core structure, due to the spatial gain distribution the transverse profile of the gain is better guided inside the active region allowing more modal gain to develop. This is known as gain guiding. Therefore higher modal gain is observed in Figure 2.5 when spatial profiling of the optical gain is considered. For the dual core structure with the inner core material gain of 1800cm^{-1} and variation in the outer core material gain a shift in the modal gain towards the positive at zero material gain for the dual core structure is observed. Furthermore, an increase in the inner core radius the modal gain shifts towards the more positive end. The shift in modal gain also depends on the thickness of the outer core.

Table 2.1 Specifications for the TE_{01} Mode Analysis

Inner Core radius $r_1(nm)$	*Outer Core thickness* t (nm)	g_1 (cm^{-1})	g_2 (cm^{-1})	*Length* (μm)
200	-	0-1800	-	9-80
150	50	1800	0-1760	9-18
160	40	1800	0-1760	9-15
180	20	1800	0-1760	9-10

Having obtained the appropriate modal gain it is possible to utilise the lasing condition as in equation (2.45) to determine the length of device required to achieve lasing. Outcomes of such calculations are given in Figure 2.6. It is noted that devices supporting TE_{01} modes having cavity lengths of order 10 μm appear to have the potential to support lasing action.

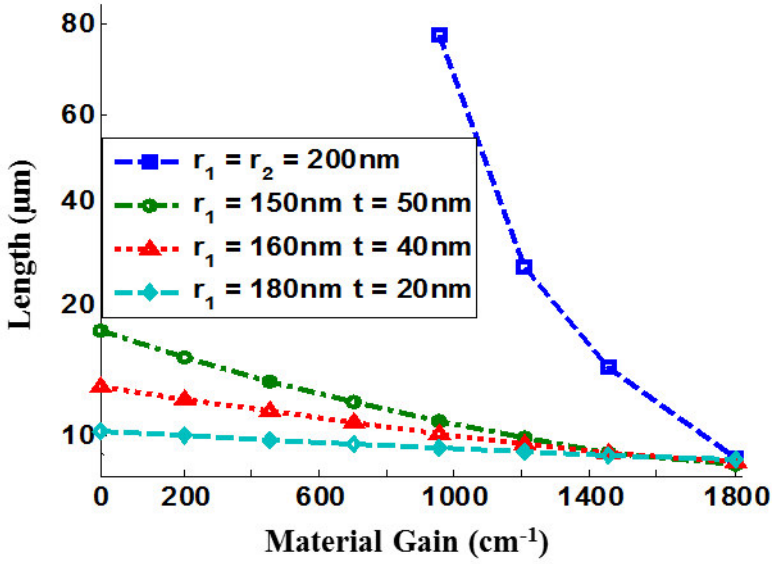

Figure 2.6 Device Length vs Material Gain for TE_{01} Mode

2.4.2 TM SPP Mode Analysis

Attention is now turned to the modal gain and lasing conditions for the TM_{01} SPP modes of the defined structure. In this respect the capability of the present model to examine profiled optical gain will be exploited to identify conditions under which lasing action may be achieved. There are two kinds of SPP modes: core–metal surface guided modes and air–metal surface guided modes [5].

As discussed in chapter 1, the modes guided at the air-metal interface are of much practical interest in cylindrical devices that incorporate small core radius. On the other hand, core-metal surface guided modes experience high losses and may have reduced applications potential [7].

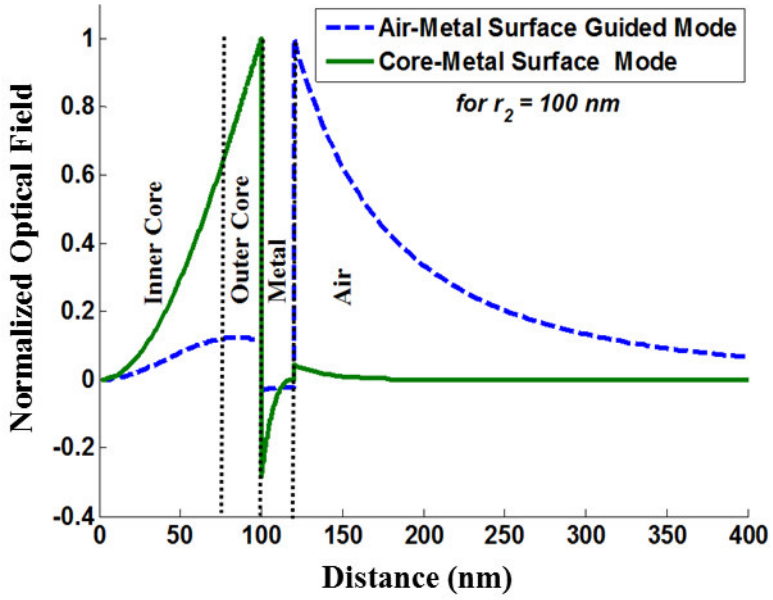

Figure 2.7 Optical Field of the TM_{01} Air-Metal and Core-Metal surface guided modes

Figure 2.7 shows the optical field of these two types of SPP modes in the device having an overall core radius of 100nm and a metal cladding thickness of 20nm. The TM_{01} air metal surface guided mode is transformed to core guided mode when the overall core radius increases from 100nm to $r_2 \geq 220$nm. It has been observed that at cut off the TM_{01} air-metal surface guided mode, has gain and can support lasing. However the mode profile in Figure 2.7 shows that the field is guided outside the core and has no field maximum at the centre, therefore coupling of such modes to dielectric waveguides and on chip optical fibres is an issue.

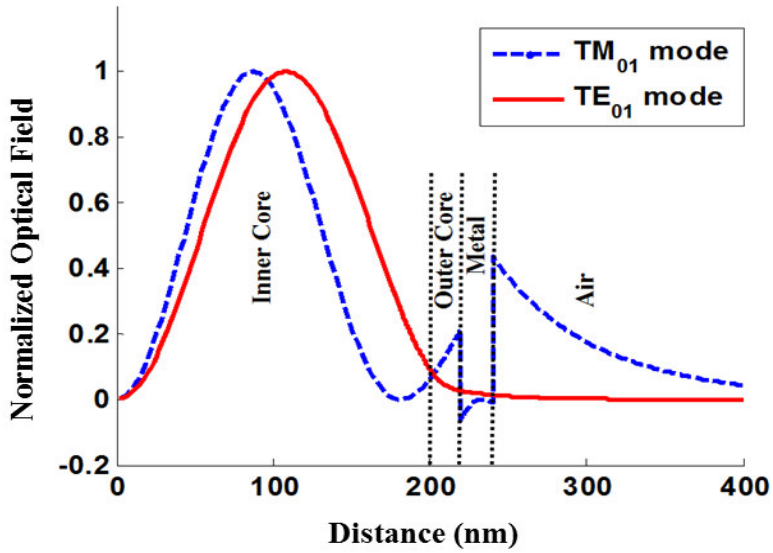

Figure 2.8 Optical Field of the TM_{01} Core-Guided mode and TE_{01} mode at Core radius 220nm.

Figure 2.8 shows the optical field of the TE and TM (core guided) modes formed in metal-clad cylindrical structures of radii 220nm. Representations of the intensity profiles of the optical modes are shown in Figure 2.9(a-c) for the TM_{01} air-metal, core-metal surface guided and core guided modes and 2.9(d) TE_{01} mode, which corresponds to Figure 2.7 and 2.8. In the figures the locations of the metal cladding is denoted by a double white circles.

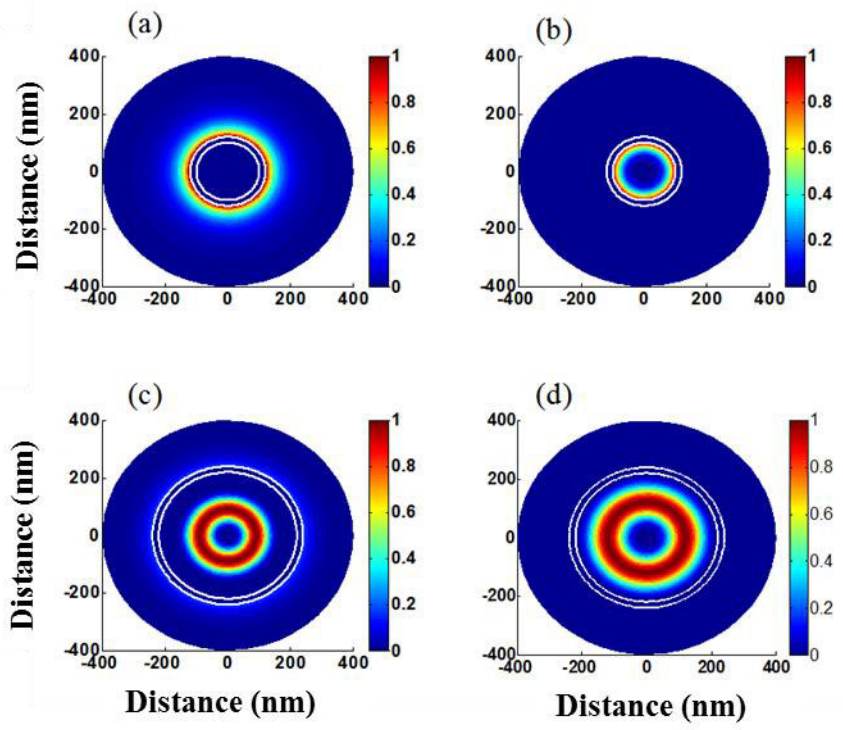

Figure 2.9 Intensity profile of the (a) TM_{01} Air-Metal surface guided mode (b) TM_{01} Core-Metal surface guided mode (c) TM_{01} Core guided mode (d) TE_{01} mode

As already indicated the focus of these investigations is on the opportunities offered by local gain profiling to obtain lasing action and thence to make a comparison with that obtained in the case of the TE mode analysed in the previous sub-section. As exemplars of this approach the inner core gain is held constant at 1800cm^{-1} and variations allowed in the outer core material gain. Attention is also given to variations in the radius of the inner core and thickness of outer core as summarized in Table 2.2.

Table 2.2 Specifications for the TM_{01} Mode

Inner Core radius $r_1(nm)$	*Outer Core thickness* t (nm)	g_1 (cm^{-1})	g_2 (cm^{-1})	*Length* (μm)
100	-	0-1800	-	100-1100
50	50	1800	0-1760	100-250
60	40	1800	0-1760	90-150
80	20	1800	0-1760	90-100

Figure 2.10(a) shows that for a device with an inner core radius of 80nm the opportunity exists to achieve a positive modal gain over a quite wide range of outer-core material gain. Figure 2.10(b) through to 2.10(d) show that when the inner-core radius is increased the accessible modal gain drops quite significantly such that when the inner core radius is 100nm the metal losses are high, such that positive modal gain cannot be obtained even for large values of outer-core material gain.

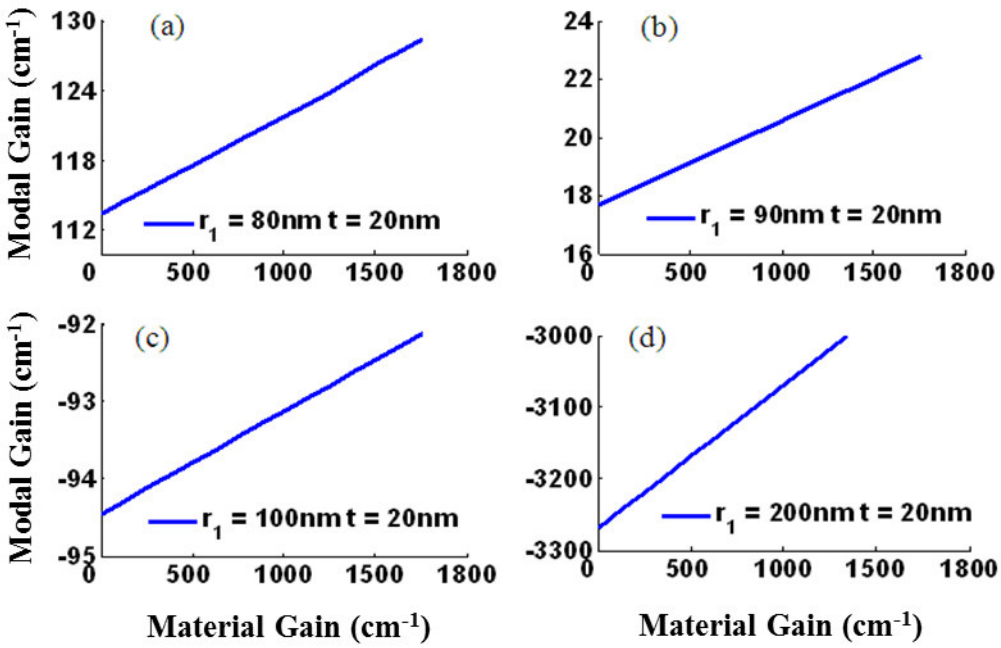

Figure 2.10 (a-d) TM_{01} Modal Gain vs Material Gain for different active region radii

It is pointed out that for the case of an inner core radius of 220nm shown in Figure 2.10(d) the mode is transformed into a core guided mode. Nevertheless due to the dominance of the metal losses the modal loss becomes exceedingly large. Having established the propensity of small radius structures to deliver positive modal gain, attention is given to the influence of varying the gain profile via changes in the inner and outer core radii. In the calculations illustrated in Figure 2.11, the overall active core radius is set at 100nm whilst the values of the inner and outer core dimensions are changed.

Determination of the modal gain is again effected for a fixed inner core gain of 1800cm^{-1} and variations in the outer core material gain allowed in comparison to a structure without outer core. As may be anticipated, when the mode is enabled to access an increased active volume of higher gain the modal gain is increased. It is

noted that in all cases it is possible to achieve positive modal gain.

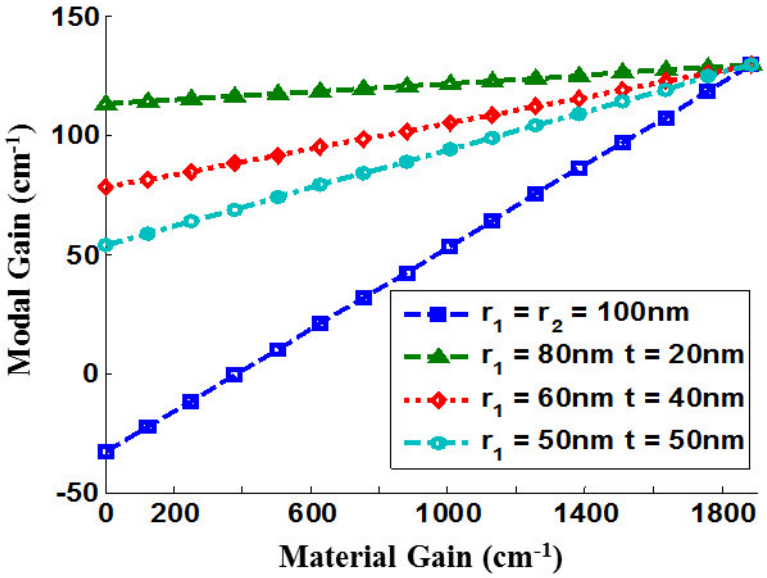

Figure 2.11 TM_{01} Modal Gain vs Material Gain for different inner core radius where the overall core radius is kept constant.

Guided by the results displayed in Figure 2.11, attention is now given to the determination of the cavity lengths required to sustain lasing. Outcomes of such calculations are shown in Figure 2.12. It is seen that for the TM mode significantly greater cavity lengths – here of order 100 μm - are required relative to those obtained in the TE case as shown in Figure 2.6.

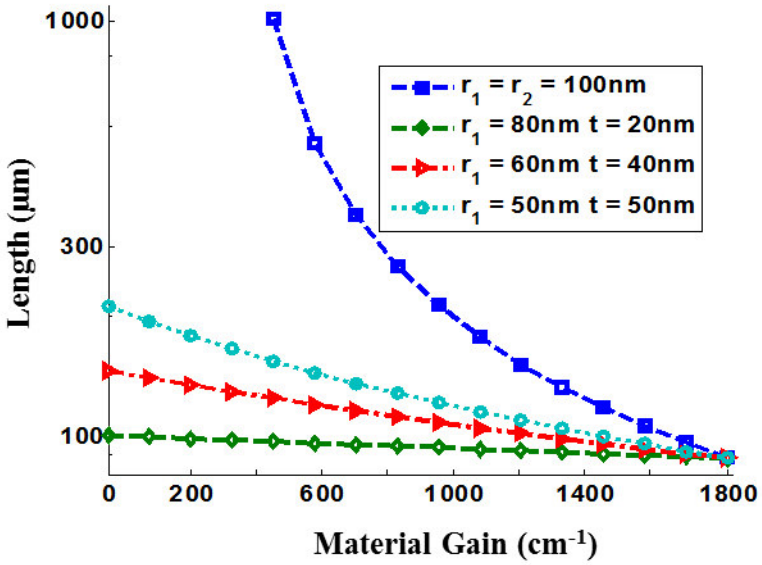

Figure 2.12 Device Length vs Material Gain for TM_{01} mode.

2.5 Conclusion

An analysis has been performed of the wave-guiding at lasing conditions in a cylindrical nano-laser structure. The model which has been utilized for this purpose allows for variations in the material gain of the active core to be taken into account. The model has been applied to the specific case of a two-layer (dual) active core and a comparison has been made of the requirements for achieving lasing via the excitation of either TE_{01} or TM_{01} modes. In the former case it is found that structures of length of order 10 μm have the potential to lase whereas in the latter case device lengths of order 100 μm are needed to achieve lasing. The model developed here provides the basis for more detailed nano-laser design and specifically is capable of extension to provide a self-consistent analysis of the wave-guiding and lasing properties of such metal-clad cylindrical nano-lasers.

References

[1] M. T. Hill, M. Marell, E. S. P. Leong, B. Smalbrugge, Y. Zhu, M. Sun, P. J. van Veldhoven, E. Jan Geluk, F. Karouta, Y. S. Oei, R. Nötzel, C. Z. Ning, and M. K. Smit, "Lasing in metal-insulator-metal sub- wavelength plasmonics waveguides," *Opt. Exp*., vol. 17, no. 13, pp. 11107-11112, Jun. 2009.

[2] M. A. Noginov, G. Zhu, A. M. Belgrave, R. Bakker, V. M.Shalaev, E. E. Narimanov, S. Stout, E. Herz, T. Suteewong and U. Wiesner, "Demonstration of a spaser-based nanolaser," *Nature*, vol. 460, pp. 1110-1113, Aug. 2009.

[3] R. F. Oulton, V. J. Sorger, T. Zentgraf, R. M. Ma, C. Gladden, L. Dai, G. Bartal and X. Zhang, "Plasmon lasers at deep subwavelength scale," *Nature*, vol. 461, pp. 629-632, Oct. 2009.

[4] K. Yu, A. Lakhani, M. C. Wu, "Subwavelength metal-optic semiconductor nanopatch lasers," *Opt. Exp*., vol.18, no. 9, pp. 8790-8799, Apr. 2010.

[5] S. J. Al-Bader and M. Imtaar, "Azimuthally Uniform Surface-Plasma Modes in Thin Metallic Cylindrical Shells" *IEEE J. Quantum Electron*., vol. 28, no. 2, pp. 525-533, Feb. 1992.

[6] A. V. Maslov and C. Z. Ning, "Size reduction of a semiconductor nanowire laser by using metal coating," Proc. *SPIE*., vol. 6468, pp. 646801-1–646801-7, 2007.

[7] V. Krishnamurthy and B. Klein, “Theoretical investigation of metal cladding for nanowire and cylindrical micropost lasers,” *IEEE J. Quantum Electron*., vol. 44, no. 1, pp. 67-74, Jan. 2008.

[8] K. Ikeda, Y. Fainman, K. A.Shore and H. Kawaguchi, “Modified long range surface plasmon polariton modes for laser nano resonators.” *J. Appl. Phys*., vol. 110, no. 6, pp. 063106-1–063106-6, Sep. 2011.

[9] P. Yeh, *Optical waves in layered media*. New York: John Wiley & Sons, Inc., 1988.

[10] P. Yeh, A. Yariv, and E. Marom, “Theory of Bragg fiber,” *J. Opt. Soc. Am*., vol. 68, no. 9, pp. 1196-1201, Sep. 1978.

[11] J. Noborosika, J. Motohisa, J. Takeda, M. Inari, Y. Miyoshi, N. Ooike, and T. Fukui, “Growth of GaAs and InGaAs nanowires by utilizing selective area MOVPE,” inProc. 2004 Int. Conf. Indium Phospide and Related Materials, Kagoshima, Japan, May-Jun. 2004, pp. 647–650.

[12] Kim, H. J. Joyce, Q. Gao, H. H. Tan, C. Jagadish, M. Paladugu, J.Zou, and A. A. Suvorova, “Influence of nanowire density on the shape and optical properties of ternary InGaAs nanowires,”Nanoletters, vol. 6, no. 4, pp. 599–604, 2006.

[13] M. A. Ordal, L. L. Long, R. J. Bell, S. E. Bell, R. R. Bell, R. W. Alexander Jr., and C. A. Ward, “Optical properties of metals Al, Co, Cu, Au, Fe, Pb, Ni, Pd, Pt, Ag, Ti and W in infrared and far infrared,” Appl. Opt., vol. 22, no. 7, pp. 1099–1119, 1983.

[14] G. Winter, S. Wedge, and W. L. Barnes, “Can lasing at visible wavelengths be achieved using low-loss long-range surface plasmon-polariton mode?,” *New J. Phys*., vol. 8, no. 125, pp. 1–14, 2006.

[15] A. V. Maslov and C. Z. Ning, “Reflection of guided modes in semiconductor nanowire lasers*,” Appl. Phys. Lett*., vol. 83, no. 6, pp. 1237-1–1237-3, 2003.

Chapter 3

Annular Core Geometry Analysis of Lasing in Cylindrical Metal-Clad Nano-Lasers

3.1 Introduction

Advances in semiconductor laser technology have been pursued with a view to the implementation of integrated photonic components. In this context a specific challenge is to design and fabricate ultra-compact semiconductor lasers amenable to high-density photonic integration. Crucial issues in this regard are the identification of structures which enable effective light confinement and thereby enable lasing in nano-scale cavities [1-8].

In the previous chapter a dual active core model of a cylindrical metal clad nano-laser has been analysed, where the inner core material gain is kept constant and variation in the outer core material gain is considered. A shift in the modal gain towards the positive is observed. In this chapter a more detailed analysis is presented in which an arbitrary number of annular layers may be utilised in order to model the optical properties of the laser active core. Using this approach the modal gain and lasing condition are determined for cylindrical metal clad nano-lasers.

3.2 Annular Core Cylindrical Nano-Laser Structure

The structure under consideration is a cylindrical annular core metal-clad nano-laser. In previous work such a structure has been studied assuming either a uniform core [9, 10] or a dual core [11]. In order to take into account spatial gain variations in the active region of such a structure an annular core structure is utilized. The cross-section of such a structure is illustrated in Figure 3.1.

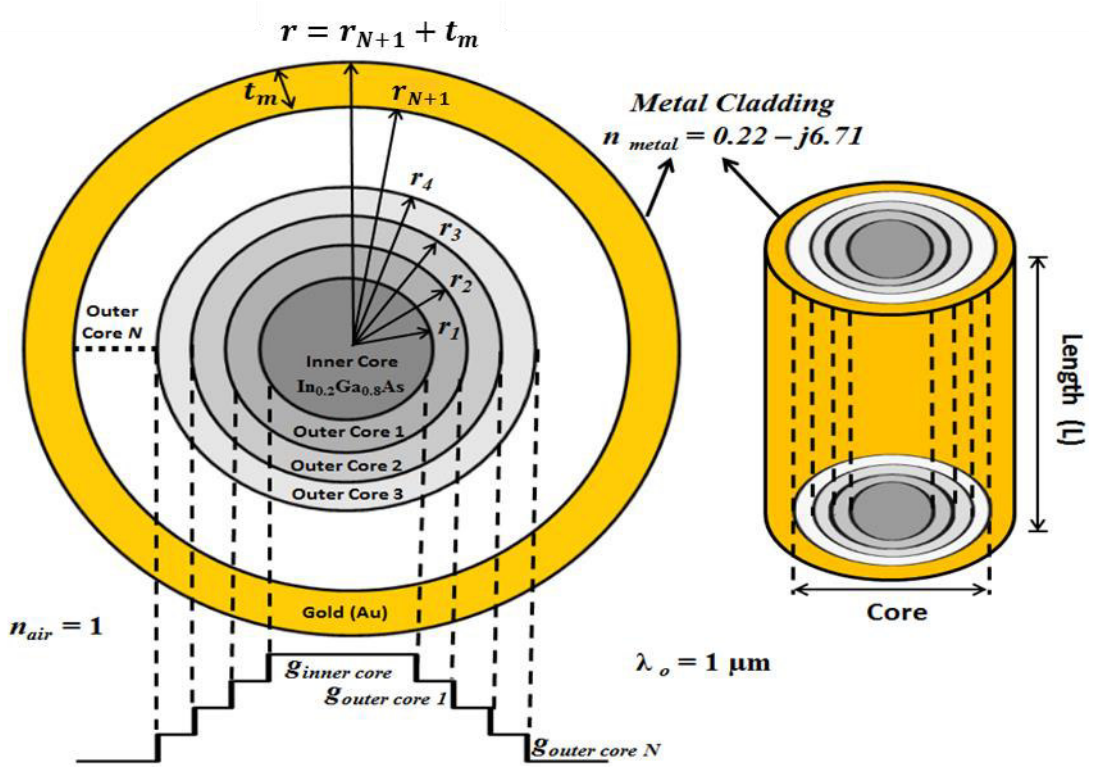

Figure 3.1 Cross-section & Schematic of the cylindrical semiconductor annular core metal-clad nano-laser.

The key elements of the structure are similar to that discussed in chapter 2 i.e. the refractive index of $In_{0.2}Ga_{0.8}As$ core semiconductor and 20nm thick gold metal cladding are 3.6 and *0.22 – j6.71* respectively surrounded by air with refractive index n_{air} at the operating wavelength $\lambda_o = 1\mu m$.

For the specific calculations performed here, the core semiconductor is considered to be comprised of an inner core and N annular outer core regions, with the index profile n in equation (3.1),

$$n(r) = \begin{cases} n_{inner\ core} & 0 \le r < r_1 \\ n_{outer\ core\ 1} & r_1 \le r < r_2 \\ \quad . & \\ \quad . & \\ n_{outer\ core\ N} & r_N \le r < r_{N+1} \\ n_{metal} & r_{N+1} \le r < r_{N+1} + t_m \\ n_{air} & r \ge r_{N+1} + t_m \end{cases} \tag{3.1}$$

Where, r is the radius of the structure, $n_{inner\ core}$ to $n_{outer\ core\ N}$ is the refractive index of the core, n_{metal} and n_{air} is the refractive index of gold and air respectively and t_m is the thickness of metal. The index profile of active core annuli is varied with a difference in the material gain such that,

$$g_{inner\ core} > g_{outer\ core\ 1} > g_{outer\ core\ 2} \ldots\ldots > g_{outer\ core\ N} \tag{3.2}$$

It is noted that the method of pumping determines the gain in the core active region. Experimental studies of nano-lasers have been performed using both optical pumping and electrical pumping [5-8]. It is challenging to achieve highly doped p-n junctions in nanowires that can offer electrical excitation [12]. The work carried out here does not rely on any particular pumping method. For the analysis carried out no particular assumptions are made about the laser pumping method which is required to provide the gain profile defined in equation (3.2). Therefore, for an $In_{0.2}Ga_{0.8}As$ core the index profile for N annuli can be defined as in equation (3.3),

$$\begin{aligned} n_{inner\ core} &= 3.6 + j\frac{g_{inner\ core}}{2\gamma_o} \\ n_{outer\ core\ 1} &= 3.6 + j\frac{g_{outer\ core\ 1}}{2\gamma_o} \\ &\vdots \\ n_{outer\ core\ N} &= 3.6 + j\frac{g_{outer\ core\ N}}{2\gamma_o} \end{aligned} \tag{3.3}$$

Where, $\boldsymbol{\gamma_o}$is the propagation constant in free space, $\boldsymbol{n_{inner\ core} \ldots . to\ n_{outer\ core\ N}}$ and $\boldsymbol{g_{inner\ core} \ldots . to\ g_{outer\ core\ N}}$ are the refractive index and material gain of the active core region.

3.3 Modal Gain & Device Length Calculation

Following the cylindrical Transfer Matrix Method, discussed in appendix A, the annular core structure in Figure 3.1 is analysed and the optical gain and lasing condition is evaluated. In order to bench mark the laser performance the operating conditions for the TE_{01} and TM_{01} mode which has the potential to lase are examined. For the analysis carried out, the dimensions of the device were held fixed such that the overall core radius r_{N+1} was kept constant by keeping the inner core radius r_1 at a constant value with variation in the thickness of the outer core layers. The thickness of each outer core annulus is therefore,

$$t_{outer\ core\ 1} = r_2 - r_1$$

$$t_{outer\ core\ 2} = r_3 - r_2$$

.

$$t_{outer\ core\ N} = r_{N+1} - r_N$$

The inner core material gain for the structure is kept at 1885cm^{-1} which is equivalent to a refractive index 3.6 + j0.015, whilst the respective material gains in the outer core(s) are varied and analysed to evaluate the device length for the structure.

3.3.1 TE and TM Mode Analysis

For the TE_{01} mode analysis the dimensions of the device were fixed such that $\boldsymbol{r_{N+1} = 200nm}$ with inner core radius $\boldsymbol{r_1 = 100nm}$. The analysis is performed for different outer core thickness and comparison is drawn with respect to the modal gain. Calculations are therefore done for the structure without outer core, i.e. $\boldsymbol{r_1 = r_{N+1} = 200nm}$, and with outer core layers 1, 2 and 5. Table 3.1 summarizes the distribution of the structure layers along with the respective material gain, i.e. g_1 for the inner core, g_2 for outer core 1, so on and so forth.

Table 3.1 Specifications for the TE mode analysis.

N	r_1 (nm)	t_1 (nm)	t_2 (nm)	t_3 (nm)	t_4 (nm)	t_5 (nm)
Without Outer Core	200	-	-	-	-	-
1	100	100	-	-	-	-
2	100	50	50	-	-	-
5	100	20	20	20	20	20

N	g_1 (cm^{-1})	g_2 (cm^{-1})	g_3 (cm^{-1})	g_4 (cm^{-1})	g_5 (cm^{-1})	g_6 (cm^{-1})
Without Outer Core	0-1885	-	-	-	-	-
1	1885	0-1760	-	-	-	-
2	1885	1760	0-1635	-	-	-
5	1885	1760	1635	1510	1385	0-1260

As shown in Table 3.1 the material gain within the outer cores are distributed in descending order in accordance to the number of layers. Figure 3.2 shows that for an overall radius of 200nm the TE_{01} mode suffer losses when no material gain is considered, and an effective increase in the modal gain is observed at material gain of 1885cm^{-1}. When the number of outer core layers N is increased, an effective shift towards the positive in the modal gain is observed when the number of layers is ≥ 2.

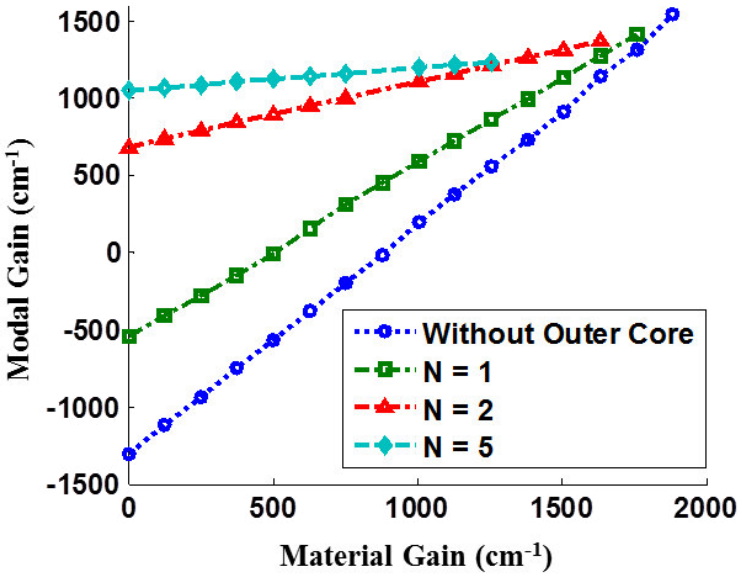

Figure 3.2 Modal Gain vs Material Gain for the TE_{01} mode at different number of outer core annuli and without outer core.

The shift in modal gain also depends on the thickness of the outer core layers. Outcomes of representative calculations are shown in Figure 3.2. Having obtained the appropriate modal gain it is possible to utilize the lasing condition to determine the length of device required to achieve lasing. Outcomes of such calculations are given in Figure 3.3. It is noted that devices supporting TE_{01} modes having cavity lengths of order 10 μm appear to have the potential to support lasing action. Figure 3.3 also depicts that the length of the device becomes constant when the number of outer core layers are 5, which shows that any further increase in the number of outer core layers would not further reduce the effective length of the device.

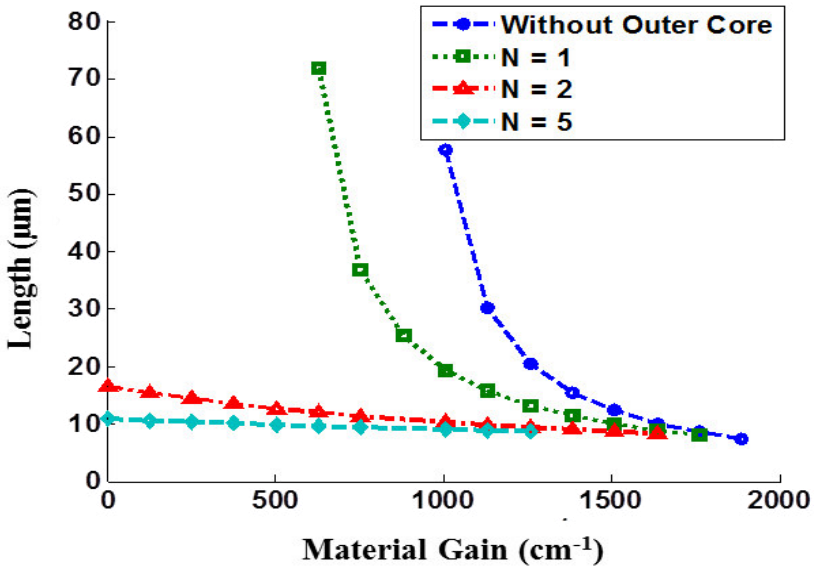

Figure 3.3 Length vs Material Gain for the TE_{01} mode at different number of outer core annuli and without outer core.

The TM modes are Surface Plasmon Polariton (SPP) modes as discussed in chapter 2 in section 2.4.2. TM modal gain and lasing conditions for the annular core structure is evaluated. It has been noted that at the cut-off radius of a metal coated nano-laser it is possible to achieve lasing in the TM_{01} mode [13]. Therefore for TM_{01} mode, analysis is performed for an overall core radius $r_{N+1} = 100nm$, which is the cut off radius for the considered structure. Calculations are done for the structure without outer core, i.e. $r_1 = r_{N+1} = 100nm$, and with outer core layers 1, 2 and 4.

Table 3.2 Specifications for the TM mode analysis.

N	r_1 (nm)	t_1 (nm)	t_2 (nm)	t_3 (nm)	t_4 (nm)
Without Outer Core	100	-	-	-	-
1	60	40	-	-	-
2	60	20	20	-	-
4	60	10	10	10	10

N	g_1 (cm^{-1})	g_2 (cm^{-1})	g_3 (cm^{-1})	g_4 (cm^{-1})	g_5 (cm^{-1})
Without Outer Core	0-1885	-	-	-	-
1	1885	0-1760	-	-	-
2	1885	1760	0-1635	-	-
4	1885	1760	1635	1510	0-1385

Table 3.2 summarizes the distribution of the structure layers along with the respective material gain. For an overall radius of 100nm the TM_{01} mode suffer losses when no material gain is considered, and an effective increase in the modal gain is observed at material gain of $1885cm^{-1}$. In comparison to the TE_{01} mode, a similar trend towards the effect of increased number of layers to the TM_{01} modal gain is observed, whilst the overall modal gain of the TM_{01} mode is predominantly lower than that of the TE_{01} mode.

Figure 3.4 shows the effect of layers to the modal gain of the TM_{01} mode. Determination of the modal gain is again effected for a fixed inner core gain of $1885cm^{-1}$ and variations in the outer core material gain allowed. As may be anticipated, when the mode is enabled to access an increased active volume of higher gain the modal gain is increased. It is noted that in all cases it is possible to achieve positive modal gain.

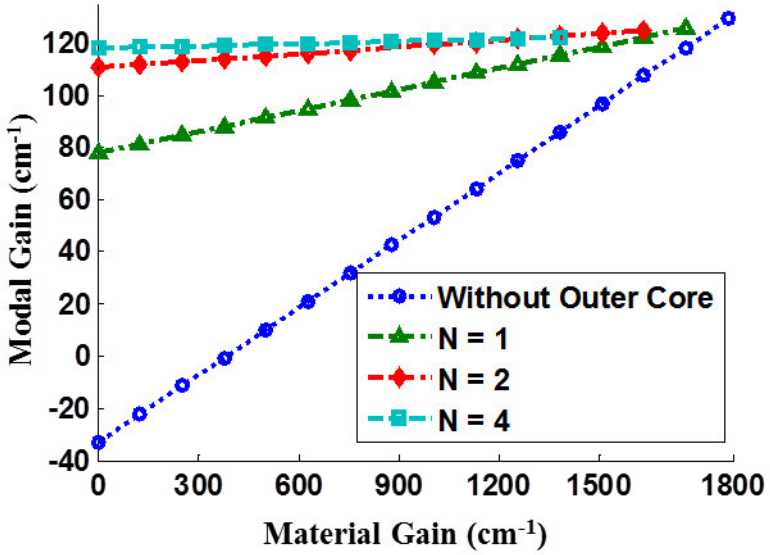

Figure 3.4 Modal Gain vs Material Gain for the TM_{01} mode at different number of outer core annuli and without outer core.

Guided by the results displayed in Figure 3.4, attention is now given to the determination of the cavity lengths required to sustain lasing. Outcomes of such calculations are shown in Figure 3.5. It is seen that for the TM mode significantly greater cavity lengths – here of order 100μm - are required relative to those obtained in the TE case as shown in Figure 3.3.

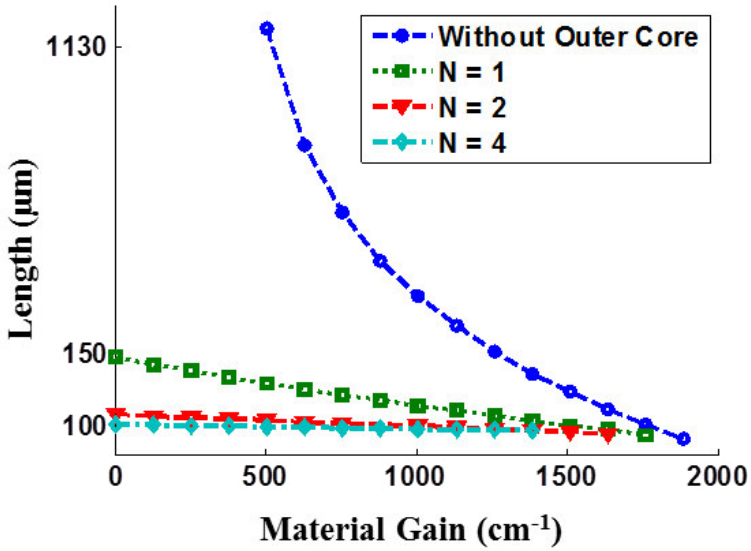

Figure 3.5 Length vs Material Gain for the TM_{01} mode at different number of outer core annuli and without outer core.

3.4 Conclusion

Analysis on the lasing characteristics of cylindrical metal-clad nano-laser is investigated along with the effect of increased number of outer core annuli to the modal gain and the device length for the TE_{01} and TM_{01} mode of propagation. The model which has been utilized for this purpose allows for variations in the material gain of the active core to be taken into account. The results highlight that increased number of outer core layers tends to shift the modal gain to the positive while after a specific range the overall modal gain becomes constant. It is found that structures of length of order 10 μm have the potential to lase for the TE_{01} mode whereas device lengths of order 100 μm are needed to achieve lasing for the TM_{01} mode.

References

[1] S. J. Al-Bader and M. Imtaar, "Azimuthally Uniform Surface-Plasma Modes in Thin Metallic Cylindrical Shells" *IEEE J. Quantum Electron*., vol. 28, no. 2, pp. 525-533, Feb. 1992.

[2] T. Baba, "Photonic crystals and microdisk cavities based on GaInAsP-InP system," *IEEE J. Sel. Top. Quantum Electron.,* vol. 3, no. 3, pp. 808-830, Jun. 1997.

[3] H. Altug, D. Englund, and J. Vučković, "Ultrafast photonic crystal nanocavity laser," *Nat. Phys.,* vol. 2, pp. 484-488, Jul. 2006.

[4] M. T. Hill, Y. S. Oei, B. Smalbrugge, Y. Zhu, T. de Vries, P. J. van Veldhoven, F. W. M. van Otten, T. J. Eijkemans, J. P. Turkiewicz, H. de Waardt, E. Jan Geluk, S. H. Kwon, Y. H. Lee, R. Nötzel, and M. K. Smit, "Lasing in metallic-coated nanocavities," *Nature Photonics*, vol. 1, pp. 589-594, Oct. 2007.

[5] M. T. Hill, M. Marell, E. S. P. Leong, B. Smalbrugge, Y. Zhu, M. Sun, P. J. van Veldhoven, E. Jan Geluk, F. Karouta, Y. S. Oei, R. Nötzel, C. Z. Ning, and M. K. Smit, "Lasing in metal-insulator-metal sub- wavelength plasmonics waveguides," *Opt. Exp*., vol. 17, no. 13, pp. 11107-11112, Jun. 2009.

[6] R. F. Oulton, V. J. Sorger, T. Zentgraf, R. M. Ma, C. Gladden, L. Dai, G. Bartal and X. Zhang, "Plasmon lasers at deep subwavelength scale," *Nature*, vol. 461, pp. 629-632, Oct. 2009.

[7] M. A. Noginov, G. Zhu, A. M. Belgrave, R. Bakker, V. M.Shalaev, E. E. Narimanov, S. Stout, E. Herz, T. Suteewong and U. Wiesner, "Demonstration of a spaser-based nanolaser," *Nature*, vol. 460, pp. 1110-1113, Aug. 2009.

[8] K. Yu, A. Lakhani, M. C. Wu, "Subwavelength metal-optic semiconductor nanopatch lasers," *Opt. Exp*., vol.18, no. 9, pp. 8790-8799, Apr. 2010.

[9] V. Krishnamurthy and B. Klein, “Theoretical investigation of metal cladding for nanowire and cylindrical micropost lasers,” *IEEE J. Quantum Electron*., vol. 44, no. 1, pp. 67-74, Jan. 2008.

[10] K. Ikeda, Y. Fainman, K. A.Shore and H. Kawaguchi, “Modified long range surface plasmon polariton modes for laser nano resonators.” *J. Appl. Phys*., vol. 110, no. 6, pp. 063106-1–063106-6, Sep. 2011.

[11] Z. A. Sattar and K. A. Shore, “Spatial profiling of optical gain for optimizing lasing in plasmonic nano-lasers.” *J. Euro. Opt. Soc. Rap. Public*., vol. 8, pp. 13045-1–13045-6, July 2013.

[12] A. V. Maslov and C. Z. Ning, “Nitride Semiconductor Devices: Principles and Simulation” Wiley VCH Verlag GmbH & Co. KGaA, Weinheim, 2007, pp. 469-471.

[13] A. V. Maslov and C. Z. Ning, “Size reduction of a semiconductor nanowire laser by using metal coating,” Proc.SPIE., vol.6468,pp. 646801–(1)–(7), 2007.

Chapter 4

Spatial Profiling of Optical Gain for Optimizing Lasing in Cylindrical Metal Clad Nano-Lasers

4.1 Introduction

The design process for advanced laser structures is reliant on accurate modeling of the physical processes underpinning the operational characteristics of candidate semiconductor nano-laser designs [1-4]. Moreover the drive towards miniaturization relies on the utilization of novel structural features. In general the modeling of such aspects requires the adoption of numerical techniques in order to provide accurate predictions of the behaviour of proposed nano-lasers.

Cylindrical semiconductor metal-clad nano-lasers offer an improvement to the confinement and modal gain. Some improvements can be made through the optimization of the geometry and materials and by reducing structural imperfections. In chapter 2 and 3 the lasing condition for a dual and multilayer active core model of $In_{0.2}Ga_{0.8}As$ metal clad nano-laser respectively is determined. In this chapter a more realistic model is considered with material gain variation in the core[2].

In comparison to chapter 2 and 3, in this chapter $In_{0.53}Ga_{0.47}As$ is utilised, as the core active region due to its high achieveable material gain than $In_{0.2}Ga_{0.8}As$ [5]. The analysis to determine the modal gain and device length is carried out using the cylindrical transfer matrix method (cTMM) discussed in Appendix A and the Finite Element Method (FEM).

4.2 Nano-Laser Structure

The structure under consideration is a cylindrical annular core metal-clad nano-laser. In chapter 3, such a multilayer structure has been studied assuming gain variation only in the outer core region, where the material gain in the inner core is kept

[2] This chapter is based on the paper:

Z. A. Sattar, Z. Wang and K. A. Shore, "Wave-Guiding Analysis of Annular Core Geometry Metal-Clad Semiconductor Nano-Lasers" *IEEE J. Quantum Electron*., vol. 50, no. 1,pp. 15-22, Jan. 2014.

constant.

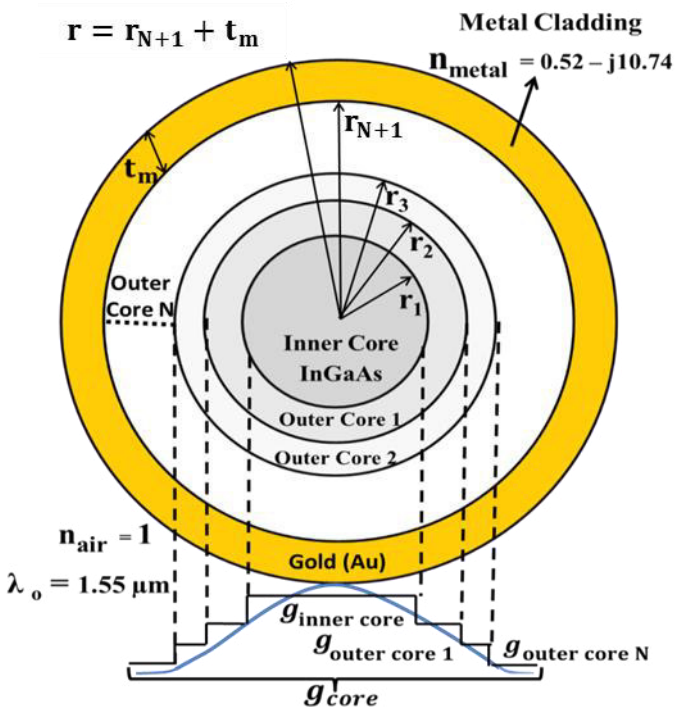

Figure 4.1 Cross-section of the cylindrical semiconductor annular core metal-clad nano-laser

In this chapter more realistic material gain variations in the active region is utilised. The core semiconductor material is assumed to be $In_{0.53}Ga_{0.47}As$ at the operating wavelength λ_o = 1.55μm [6]. The metal cladding is taken to be gold with a refractive index of $n_{metal} = 0.52 - j10.74$ [7] and the thickness of metal-clad is assumed to be $t_m = 20nm$ [8]. The cross-section of such a structure is illustrated in Figure 4.1. For $In_{0.53}Ga_{0.47}As$ core with refractive index 3.53 and material gain included (g_{core}), the index profile for inner core and N outer core annuli is defined as in equation (3.3) in chapter 3. The overall structure is surrounded by air with refractive index n_{air}.

4.3 Gain Profile

In order to take into account a more realistic gain profile in the active core region, the material gain profile in the core is represented using equation (4.1). It is assumed that a gain profile arises due to the diffusion of the carriers [9].

$$g_{core} = g_p e^{(-r^2/2\sigma^2)} \tag{4.1}$$

Where, g_p is the peak material gain, and g_{core} varies along the radius of the core $0 \leq r \leq r_{N+1}$ and σ is the carrier diffusion length.

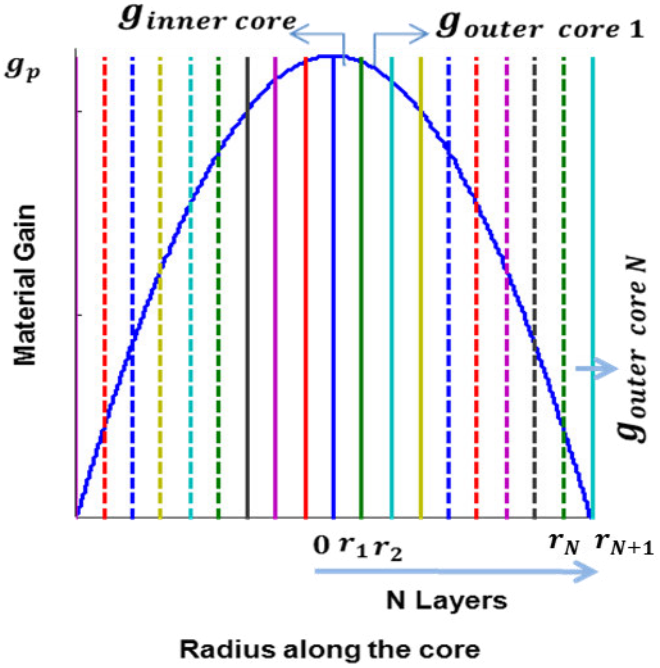

Figure 4.2 Schematic of the Material Gain Profile for N Layers in the Core

As shown in Figure 4.2, the material gain varies along the radius of the core. For spatial profiling of the material gain, the core is divided into inner core and *N* outer core layers. The gain in each layer is evaluated as an average of the values of the material gain at their respective boundaries, such that using equation (4.1) the gain in each layer is,

$$g_{inner\ core} = \frac{g_p}{2}\left(e^{-\left(\frac{r_0^2}{2\sigma^2}\right)} + e^{-\left(\frac{r_1^2}{2\sigma^2}\right)}\right)$$

$$g_{outer\ core\ 1} = \frac{g_p}{2}\left(e^{-\left(\frac{r_1^2}{2\sigma^2}\right)} + e^{-\left(\frac{r_2^2}{2\sigma^2}\right)}\right)$$

$$\vdots$$

$$g_{outer\ core\ N} = \frac{g_p}{2}\left(e^{-\left(\frac{r_N^2}{2\sigma^2}\right)} + e^{-\left(\frac{r_{N+1}^2}{2\sigma^2}\right)}\right)$$

The overall modal gain *G* and length *L* is calculated using equation (2.44) and (2.45) in chapter 2 respectively. The optical confinement factor was also calculated to observe confinement in TE and TM mode. For conventional lasers, the confinement factor of the laser is determined by the mode overlap. It is a ratio of the optical mode

profile within the core to the overall mode of the structure. The confinement of such lasers were approximately <=1. Which can also be related to the ratio of the modal gain to the material gain of the laser, given by,

$$Confinement\ Factor = Modal\ Gain/Material\ Gain$$

It should be borne in mind that due to the strong wave-guiding and confinement the modal gain of nano-lasers is dependent on the cavity design and therefore confinement factor for such nano-laser is defined by [3], as in equation (4.2),

$$\Gamma = \frac{G_{with\ gain} - G_{w/o\ gain}}{G_{material}} \tag{4.2}$$

Where, $G_{with\ gain}$ is the calculated modal gain of the structure including material gain, $G_{w/o\ gain}$ is the calculated modal gain of the structure without material gain and $G_{material}$ is the material gain in the structure.

The analysis undertaken in this chapter is considered to be applicable to the pumping method which results, due to carrier diffusion, in the material gain having a Gaussian profile as discussed.

4.4 TE and TM mode Analysis

To evaluate the effect of spatial profiling of the material gain in the core to the overall modal gain of the structure, cTMM is used. It has been noted that for the TM_{01} mode the maximum gain is achieved at cut off radius [4]. On the other hand for the TE modes the gain will increase with device radius [10]. As such a comparison is made between the lower order TE and TM modes at their respective cut-off radii. For the analysis carried out here the overall radius r_{N+1} of the core for the TE_{01} and TM_{01} mode is therefore assumed to be 250nm and 180nm respectively.

For the gain profile in equation (4.1) a peak material gain g_p = 2000cm^{-1}, a diffusion length σ = 400nm [11] is used. The effect of increasing the number of outer core layers (N) on the modal gain is examined for the gain profile as shown in Figure 4.2. The overall modal gain is evaluated using equation (2.7) in chapter 2.

Figure 4.3 shows the effect of the increasing number of layers on the evaluation of modal gain using cTMM. For a uniform core, the material gain in the core will be the average of the peak value g_p to the minimum value of the material gain at r_{N+1} for the gain profile defined in equation (4.1). The evaluated modal gain for a uniform core is 50cm^{-1} for the TE_{01} mode and 8cm^{-1} for the TM_{01} mode as shown in Figure 4.3. The lower value of the modal gain for TM_{01} mode reflecting its lossy nature as discussed in chapter 1 and 2.

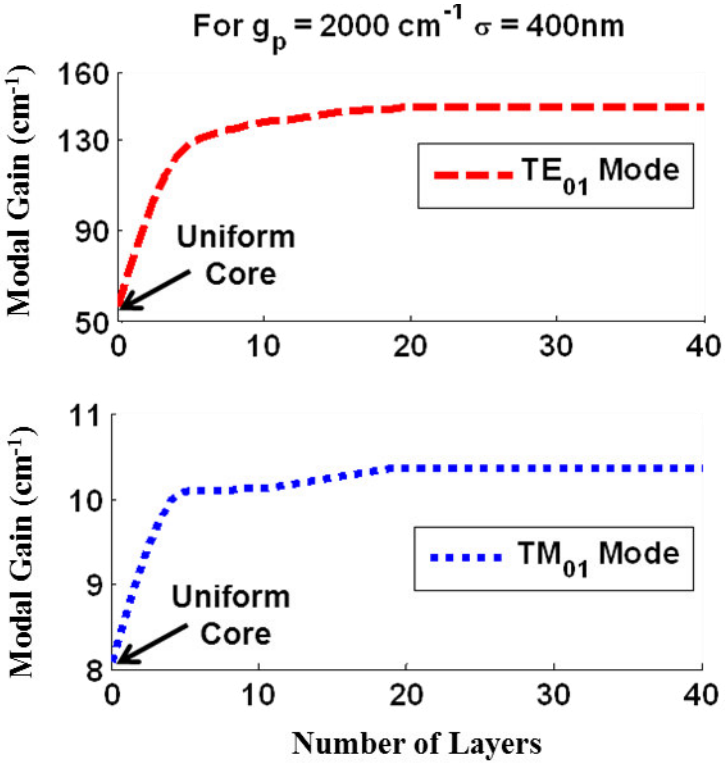

Figure 4.3 Effect of increased number of layers in the core to the Modal Gain

When additional layers are introduced to obtain a better approximation of the gain profile the overall modal gain increases because values of the local gain intermediate between the maximum and minimum are taken into account. As can be seen that due to gain guiding effects, as more layers are introduced, the modal gain is increased until it saturates after N = 20. For $N \geq 20$ the gain remains constant as shown in Figure 4.3.

For further analysis the results obtained here are therefore carried out using $N = 20$. Attention is now turned to the effect of variation of diffusion length σ on the modal

gain. The diffusion length of the considered semiconductor material is therefore varied from 400nm–2000nm as in [11-13] and the modal gain is evaluated for a peak material gain g_p= 2000cm^{-1}. For the material gain distribution considered here, an increase in the diffusion length reduces the gain variation in the core.

For diffusion lengths of order 1μm, an essentially uniform material gain is obtained across the active core. As shown in Figure 4.4, the greater variation in the gain profile for smaller diffusion lengths naturally results in a reduced modal gain, for both the TE_{01} and the TM_{01} mode. For the considered structure, values of diffusion length (σ) less than 1μm, material gain (carrier density) variation is taken into account. The modal gain variation becomes insignificant for σ greater than 1μm. Figure 4.4 also shows that there is an increase in the modal gain for the TE_{01} mode compared to that of the TM_{01} mode, as TM_{01} is less confined to the core.

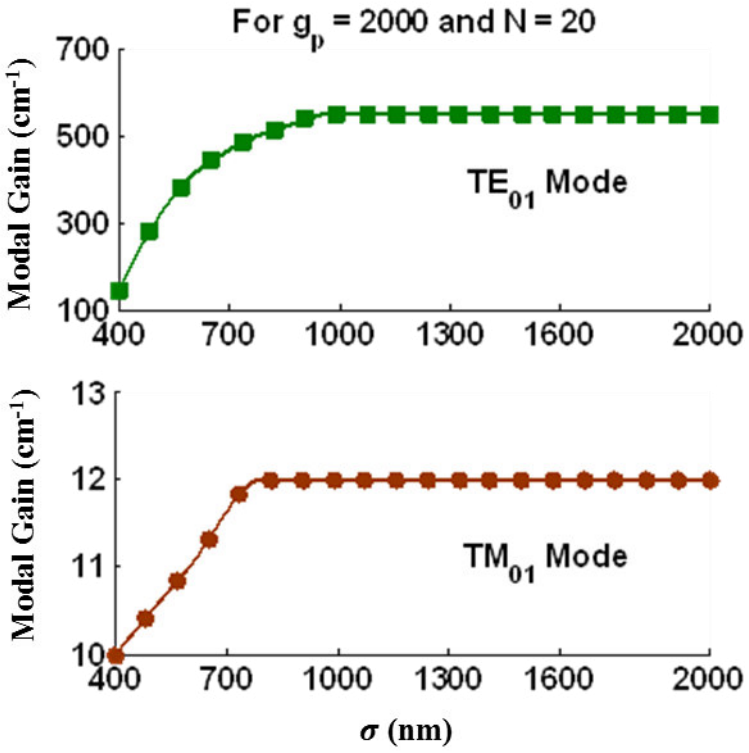

Figure 4.4 Modal Gain dependence on increased diffusion length (σ)

Table 4.1: Device Specifications for the TE_{01} Mode for $r_{N+1} = 250\ nm$ and TM_{01} Mode for $r_{N+1} = 180\ nm$ at N = 20

$g_p(cm^{-1})$ / σ	Overall Modal Gain (cm^{-1})						Device Length (µm)					
	400nm		600nm		1000nm		400nm		600nm		1000nm	
	TE mode	TM mode	TE mode	TM mode	TE mode	TM mode	TE mode	TM mode	TE mode	TM mode	TE mode	TM mode
2000	144	10	408	11	550	12	81	1126	29	1015	21	965
3000	3108	53	3504	54	3716	55	4	222	3	215	3	212
4000	6068	94	6595	97	6877	98	2	123	2	121	2	119
5000	9017	136	9671	139	10021	140	1	86	1	84	1	83
6000	11946	177	12724	180	13139	182	1	66	1	65	1	64

Table 4.1 summarizes the modal gain and lasing lengths for the device parameters in the cases of diffusion lengths of 400nm, 600nm and 1000nm and for a peak material gain of 2000cm^{-1}. Using both cTMM and the Finite Element Method (FEM) calculations have been performed of the modal gain of the TE_{01} and TM_{01} modes. In comparison to the cTMM method, Finite Element Method creates a mesh (many boundaries) within a structure that needs to be analysed. The analysis is carried out by evaluating the fields at individual boundaries. The overall field is then calculated as the sum of the fields contributed by individual boundaries. For structures including complex geometries, Finite Element Method is limited due to number of meshes required for proper convergence to occur which requires a lot of simulation time and storage.

Here use has been made of peak material gains in the range 2000cm^{-1} to 6000cm^{-1} as in[5, 6] and a diffusion length of 400nm. Figure 4.5 shows that for an overall device radius of 250nm the TE_{01} mode has a lower modal gain at peak material gain of 2000cm^{-1} and for the values of the peak material gain $g_p \geq 3000cm^{-1}$ higher modal gain than that of the peak material gain is observed. It is seen from Figure 4.5 that similar predictions are obtained using both the cTMM approach alter the Finite Element Method.

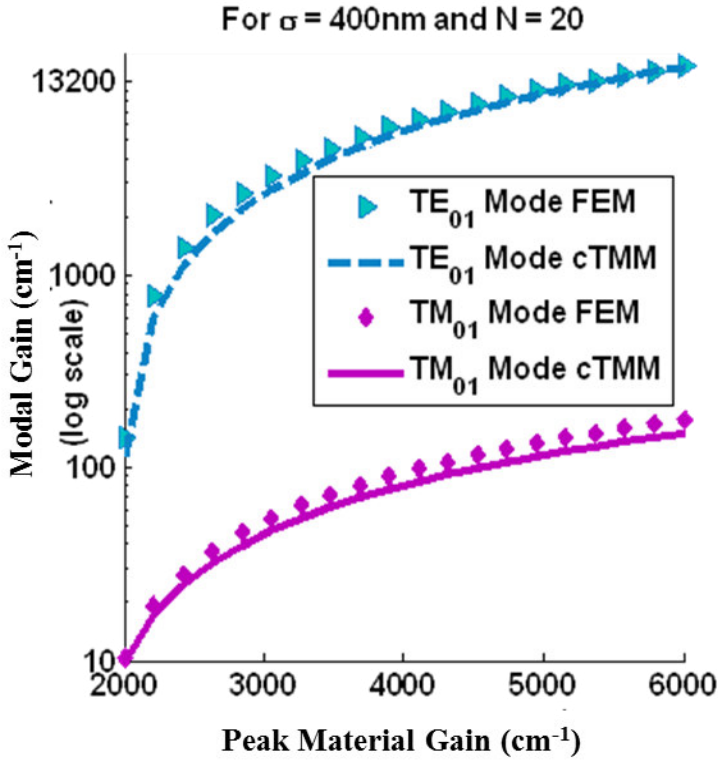

Figure 4.5: Modal Gain vs Peak Material Gain for TE_{01} and TM_{01} mode evaluated using the Finite Element Method (FEM) and Cylindrical Transfer Matrix Method (cTMM).

The mode confinement factor has been evaluated using equation (4.2). It is observed that increasing the number of layers in the core has little effect on the calculated confinement factor which is in the range 3.1 to 3.15 for the TE_{01} mode and 0.041 to 0.042 for TM_{01} mode as shown in Figure 4.6.

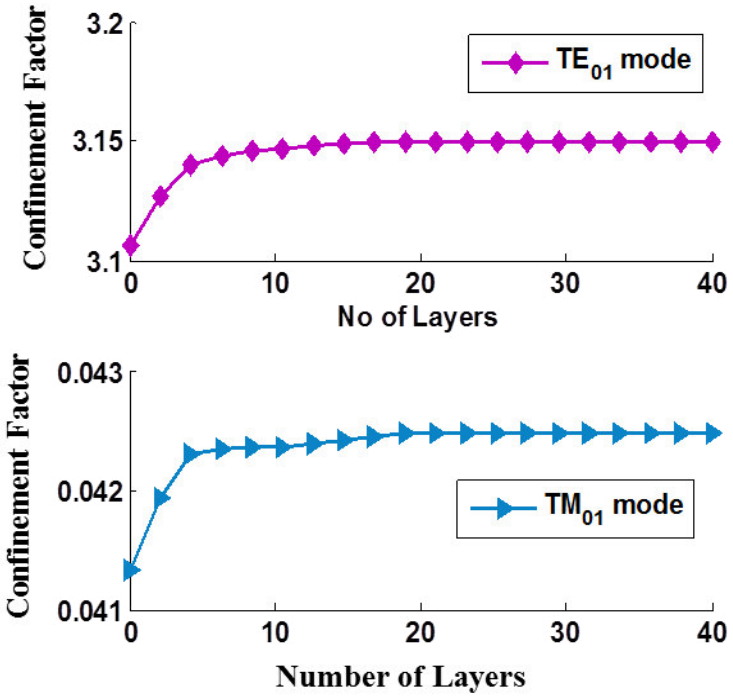

Figure 4.6: Confinement Factor vs Number of Layers for peak material gain 6000cm^{-1}

High confinement factor which can exceed unity has been reported resulting in high modal gain [14-15]. It is pointed out that the TM_{01} mode resides mostly in air rather in the core [16] as shown by the optical field of TM_{01} and TE_{01} mode in Figure 4.7.

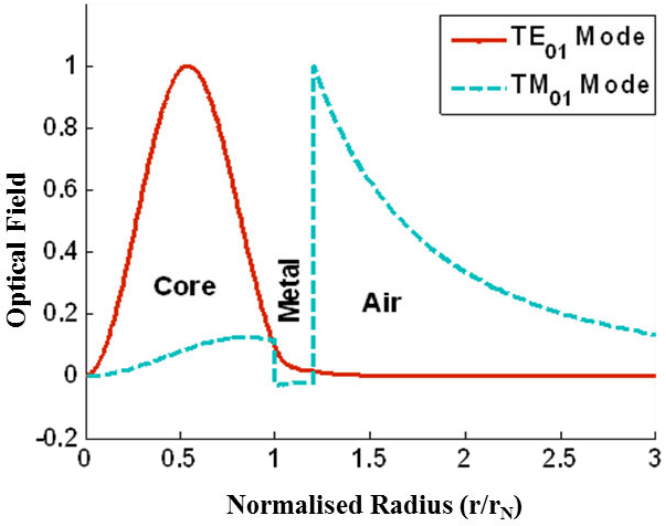

Figure 4.7: Optical field for the TE_{01} and TM_{01} modes

4.5 Lasing Cavity Length Calculations

Guided by the results shown in Figure 4.5, attention is now given to the determination of the cavity lengths required to sustain lasing. The lasing condition depends on the modal gain, loss and the reflectivity of the laser facet. For the case examined here the facet reflectivity is $R \simeq 0.31$.

The effect of additional losses (α) on predicted device lengths for TE_{01} and TM_{01} modes for the case of a peak material gain of $6000cm^{-1}$ is estimated as shown in Figure 4.8. As would be anticipated, due to the smaller gain achieved by the TM_{01} mode, the relevant cavity lengths are very sensitive to losses. In contrast the predicted cavity lengths for the TE_{01} mode are not greatly changed even when significantly higher waveguide losses are taken into account. In the absence of accurate estimates of the loss, use is made of a simplified form of the lasing condition to determine the device length L, as in equation (2.45) there by obtaining a best-case estimate of the device length.

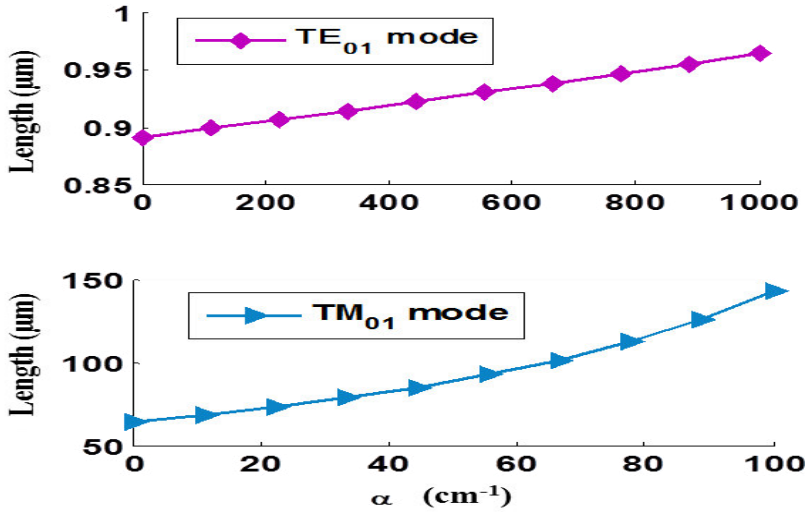

Figure 4.8: Effect of additional losses (α) on predicted device lengths for TE_{01} and TM_{01} modes – for the case of a peak material gain of 6000cm^{-1}

Figure 4.9 shows the device length for structures operating at TE_{01} mode and TM_{01} mode. It is observed that as the peak material gain increases the length of the device decreases. Furthermore as the mode becomes more confined inside the core the modal gain is enhanced thus reducing the device length required to achieve lasing. Recent experimental results show that in InGaAs-based nano-lasers TE mode lasing can be achieved for a device length of 0.9μm [17]. Figure 4.9 shows that devices supporting TE_{01} and TM_{01} modes having cavity lengths of order 1μm and 60μm respectively appear to have the potential to support lasing action as summarised in Table 4.1.

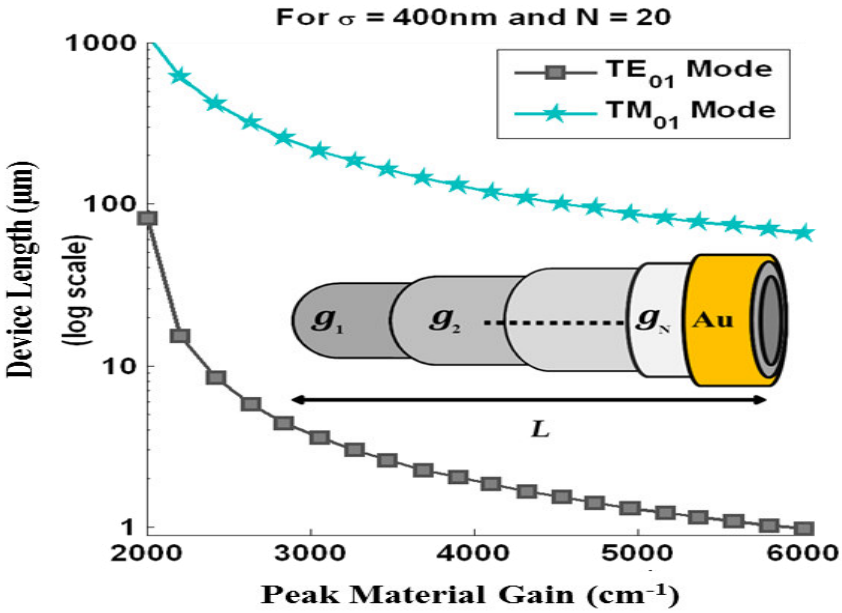

Figure 4.9: Device Length Vs Peak Material Gain for TE_{01} and TM_{01} mode

4.6 Conclusion

In this chapter a description has been given of an investigation of the lasing characteristics of cylindrical metal-clad nano-lasers using numerical technique. The model which has been utilized for this purpose allows for variations of the material gain in the active core to be taken into account. Analysis is performed for TE and TM modes at their respective cut-off radii. It is found that due to high modal gain for the TE_{01} mode devices of lengths of order 1 μm have the potential to lase whereas for the TM_{01} mode device lengths of order 60 μm are needed to achieve lasing.

References

[1] K. Yu, A. Lakhani, M. C. Wu, "Sub-wavelength metal-optic semiconductor nano-patch lasers," *Opt. Exp*., vol.18, no. 9, pp. 8790-8799, Apr. 2010.

[2] M. A. Noginov, G. Zhu, A. M. Belgrave, R. Bakker, V. M.Shalaev, E. E. Narimanov, S. Stout, E. Herz, T. Suteewong and U. Wiesner, "Demonstration of a spaser-based nanolaser," *Nature*, vol. 460, pp. 1110-1113, Aug. 2009.

[3] V. Krishnamurthy and B. Klein, "Theoretical investigation of metal cladding for nanowire and cylindrical micropost lasers," *IEEE J. Quantum Electron*., vol. 44, no. 1, pp. 67-74, Jan. 2008.

[4] A. V. Maslov and C. Z. Ning, "Size reduction of a semiconductor nanowire laser by using metal coating," Proc. *SPIE*., vol. 6468, pp. 646801-1–646801-7, 2007.

[5] L. A. Coldren and S. W. Corzine*, Diode Lasers and Photonic Integrated Circuits*, 1st ed. New York: Wiley, 1995.

[6] V.E. Babicheva, I. V. Kulkova, R. Malureanu, K. Yvind, and A.V. Lavrinenko, "Plasmonic modulator based on gain-assisted metal-semiconductor-metal waveguide" *Semicond. Sci. Technol*., vol. 7, pp. 858-860, May. 2012.

[7] P. B. Johnson, and R. W. Christy, "Optical Constants of the Noble Metals," *Phys. Rev. B*, vol. 6, pp. 4370-4379, 1972

[8] G. Winter, S. Wedge, and W. L. Barnes, "Can lasing at visible wavelengths be achieved using low-loss long-range surface plasmon-polariton mode?," *New J. Phys*., vol. 8, no. 125, pp. 1–14, 2006.

[9] P. Bhattacharya*, Semiconductor Optoelectronic Devices*, 2nd ed. New Jersey: Prentice-Hall, 1997.

[10] K. Ikeda, Y. Fainman, K. A.Shore and H. Kawaguchi, "Modified long range surface plasmon polariton modes for laser nano resonators." *J. Appl. Phys*., vol. 110, no. 6, pp. 063106-1–063106-6, Sep. 2011.

[11] D. Cui, S.M Hubbard, D. Pavlidis, A. Eisenbach, and C. Chelli, "Impact of doping and MOCVD conditions on minority carrier lifetime of zinc-and carbon-doped InGaAs and its applications to zinc- and carbon-doped InP/InGaAs heterostructure bipolar transistor" *Semicond. Sci. Technol*., vol. 17, pp. 503-509, May. 2002.

[12] P. Ambree, B. Gruska, and K. Wandel, "Dependence of the electron diffusion length in p-InGaAs layers on the acceptor diffusion process" *Semicond. Sci. Technol*., vol. 7, pp. 858-860, April. 1992.

[13] R.B. Lee, K. J. Vahala, C. Zah, and R. Bhat, "Direct determination of the ambipolar diffusion length in strained $In_xGa_{1-x}As$/InP quantum wells by cathodoluminescence" *Appl. Phys. Lett*., vol. 62, no. 19, pp. 2411-2412, May. 1993.

[14] A. V. Maslov and C. Z. Ning, "Modal gain in a Semiconductor nanowire laser with anisotropic bandstructure*," IEEE J. Quantum Electron*., vol. 40, no. 10 pp. 1389–1397, Oct. 2004.

[15] D.B. Li, and C. Z. Ning, "Giant Modal gain, amplified surface plasmon-polariton propagation, and slowing down of energy velocity in a metal-semiconductor-metal structure," *Phy. Rev. B*., vol.80, pp. 153304-1–153304-4, Oct. 2009.

[16] S. J. Al-Bader and M. Imtaar, "Azimuthally Uniform Surface-Plasma Modes in Thin Metallic Cylindrical Shells" *IEEE J. Quantum Electron*., vol. 28, no. 2, pp. 525-533, Feb. 1992.

[17] K. Ding and C.Z. Ning, "Metallic sub-wavelength-cavity semiconductor nano-lasers" *Light: Sci. & Appl.,* vol. 1, p. 20, Jul. 2012.

Chapter 5

Device Length Calculation of Visible Emitting Nano-Lasers

5.1 Introduction

An ever-present motif of semiconductor laser design has been the miniaturization of laser structures [1-6]. In the previous chapters analysis is carried out using a 2D model of cylindrical nano-lasers where InGaAs core has been used surrounded by metal clad thickness of 20nm at 1μm wavelength [7-8]. In this chapter an exploration has been undertaken of the lasing properties for device length calculation of visible emitting nano-lasers in which GaN and silver are used as the core active region and metal cladding respectively. The modal gain for the TE_{01} and TM_{01} modes is calculated for thin silver cladding thicknesses from 5nm to 20nm, over a rather wide wavelength range: 330nm to 830nm for optimizing device length of the nano-laser. Calculations have been performed for 2D model using the Cylindrical Transfer Matrix Method (cTMM) in appendix A and Finite Element Method (FEM). 3D model has been developed using FEM and analysis using insulating layer between core and the metal cladding has also been performed[3].

5.2 Device Length Optimisation

A 2D cylindrical metal-clad nano-laser structure in Figure 5.1 is used to analyse the optimum device length. The key elements of the structure are the core semiconductor (GaN) region and the metal cladding (Ag). The analysis methodology adopted here is of general application but for the work presented here it is assumed that the metal-clad structure is surrounded by air. In addition, for all results discussed in this chapter the operating wavelength of the laser is taken in a range from 330nm to

[3] This chapter is based on conference and journal paper:

Z. A. Sattar, and K. A. Shore, "Design Analysis of Ultra-Short Cavity Silver-Clad Semiconductor Nano-Lasers," published in the 10th Int. Conf. *CLEO-PR&OECC/PS,* Kyoto, Japan, Jul, 2013.

Z. A. Sattar, Z. Wang and K. A. Shore, "Design Optimization of Metallic Sub-Wavelength Nanowire Lasers," IET Optoelectronics, vol. 8, no. 2, pp. 129 – 136, April 2014.

830nm. The core semiconductor material is assumed to be of radius r_{core} surrounded by silver of thickness t.

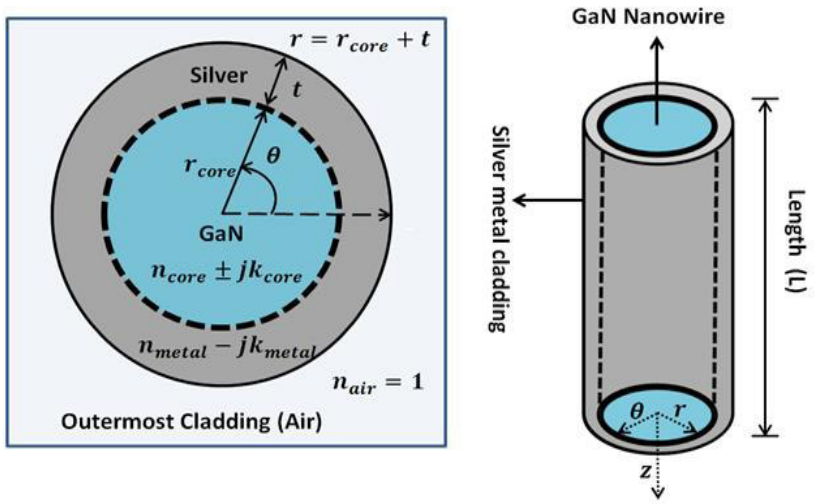

(a) **(b)**

Figure 5.1: Cylindrical semiconductor metal-clad GaN nano-laser (a) Cross-sectional view (b) Schematic diagram

The structure is evaluated at different operating wavelengths taking into account the wavelength dependence of the complex refractive index of the semiconductor $n_{core} \pm jk_{core}$ and the metal $n_{metal} - jk_{metal}$ (where '+' represents gain and '–' represents loss). The thickness of the metal cladding used, ranges from 5 nm to 20 nm as in [9-10]. The overall radius of the structure r comprise of the core radius r_{core} and thickness t of the metal.

Recent experimental investigation on GaN nano-laser under optical pumping shows that for a 4.7μm long GaN nano-lasers a material gain of 5.8 x10^3 cm^{-1} is required to achieve lasing [11]. Other research by Zhang et al established that material gains of order 4x$10^3$$cm^{-1}$ can be maintained for GaN nano-lasers [12]. Moreover, experimental results confirm that modal gain about 4.8x$10^3$$cm^{-1}$ can be achieved for a material gain in the range of 5x$10^3$$cm^{-1}$ to 10x$10^3$$cm^{-1}$ [13].

On this basis, for the specific calculations performed in this chapter the core semiconductor is considered to provide a material gain of 5x$10^3$$cm^{-1}$ over all wavelengths of interest. In order to access the wavelength range considered here use may be made of InGaN quantum wells in nano-laser [14]. While the structure would

change, the technique applied would largely remain the same. Other material platforms may also be considered to access the wide spectral range considered here.

5.2.1 Analysis Technique

Analysis of the generic 2D structure has been performed using cTMM as discussed in previous chapters. The outline of the analysis technique presented here is specifically for the case under consideration i.e. with a dielectric (semiconductor) core; a metal (Silver) cladding and the surrounding medium being air. All calculations are done over a range of wavelength 330-830nm for TE and TM modes.

In the simulations, it is assumed that a certain value for the material gain is attained by some means as discussed in chapter 2 section 2.2 and chapter 3 section 3.2. For the specific calculations, here it is taken that for the active region (GaN) a gain of $5x10^3$ cm^{-1} is achieved. In order to evaluate the gain properties for the cylindrical metal clad nano-laser structure in Figure 5.1, the relevant optical modes needs to be obtained.

The eigenvalue equations in appendix A were used to evaluate the complex effective refractive index ($\boldsymbol{n_{eff}} \pm \boldsymbol{k_{eff}}$) of the relevant modes. In this way the optical gain $\boldsymbol{G}$ and device length $\boldsymbol{L}$ is found using equation (2.44) and (2.45) in chapter 2 respectively for the TE and TM modes. The modal gain and length is calculated over a wide range of wavelengths λ for TE and TM modes at their cut off radius using metal cladding thickness in the range 5nm to 20nm. For wavelength 330nm – 830nm the cases examined here the facet reflectivity is calculated using equation (2.46) in chapter 2, which is in the range $0.15 \leq R \leq 0.2$.

5.2.2 GaN and Silver Index Profile

The lasing properties of a cylindrical GaN nano-laser structure with silver cladding layer of different thicknesses is analysed. The intention is to identify an optimum thickness of silver for GaN nano-laser structure to achieve lasing over a range of wavelengths. The calculations utilize the refractive index data of bulk GaN [15] and Ag [16] for wavelengths between 330nm and 830nm as shown in Figure 5.2 (a) and 5.2 (b). The index profile of GaN shows that it suffers higher losses at the wavelengths from 330nm to 370nm.

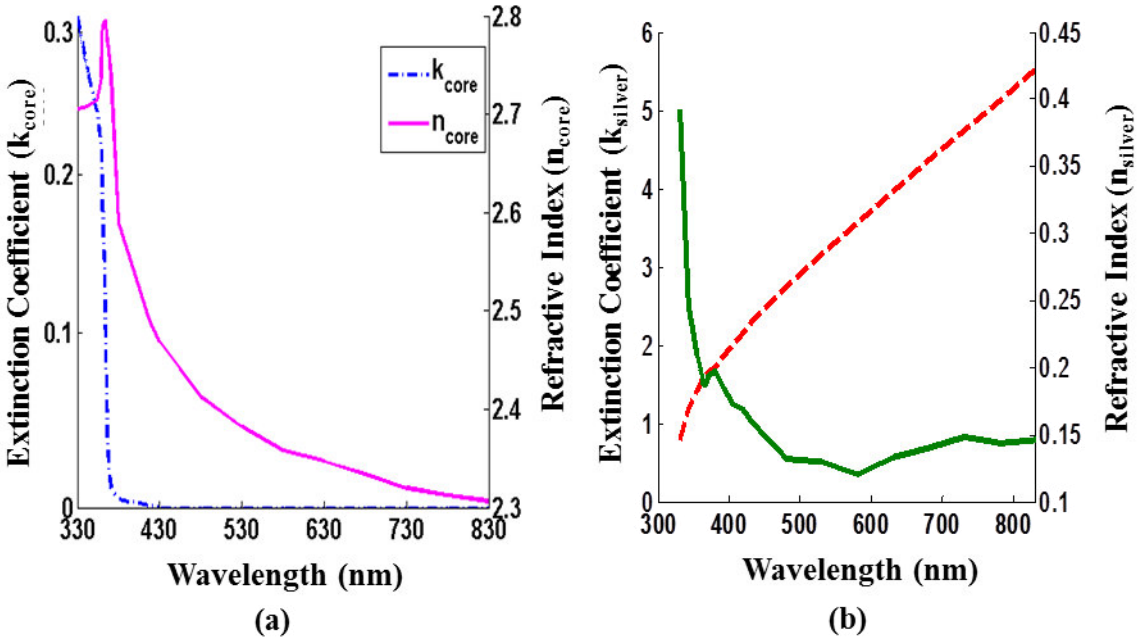

Figure 5.2: (a) GaN Index Profile [15] (b) Index profile of Silver [16]. The dotted line shows the extinction coefficient that determines loss and the solid line shows the real part of the complex refractive index.

The addition of a metal layer to the structures will generally result in an increase in the losses. However it should be borne in mind that the loss experienced by the relevant optical mode depends upon the penetration of the optical mode into the metal [17-18].

5.3 TE and TM Mode Analysis for Device Length Optimisation

5.3.1 Cut-Off Radius vs Wavelength

It has been noted that at the cut-off radius of a metal-coated nano-laser it is possible to achieve lasing in the TM_{01} mode [5]. For radius of the core greater than the cut off radius, the modal gain of TM_{01} mode in such nano-lasers reduces, whilst the modal gain of TE_{01} mode increases [18]. In order to draw a comparison between the lower order TE and TM modes analysis is therefore performed at their respective cut-off radii for the range of wavelengths. Figure 5.3 shows the cut off radius for λ= 330nm to 830nm of the TE_{01} and TM_{01} modes with silver thicknesses 't' (5nm, 10nm, 15nm and 20nm) and t = 0nm represents structure without silver layer.

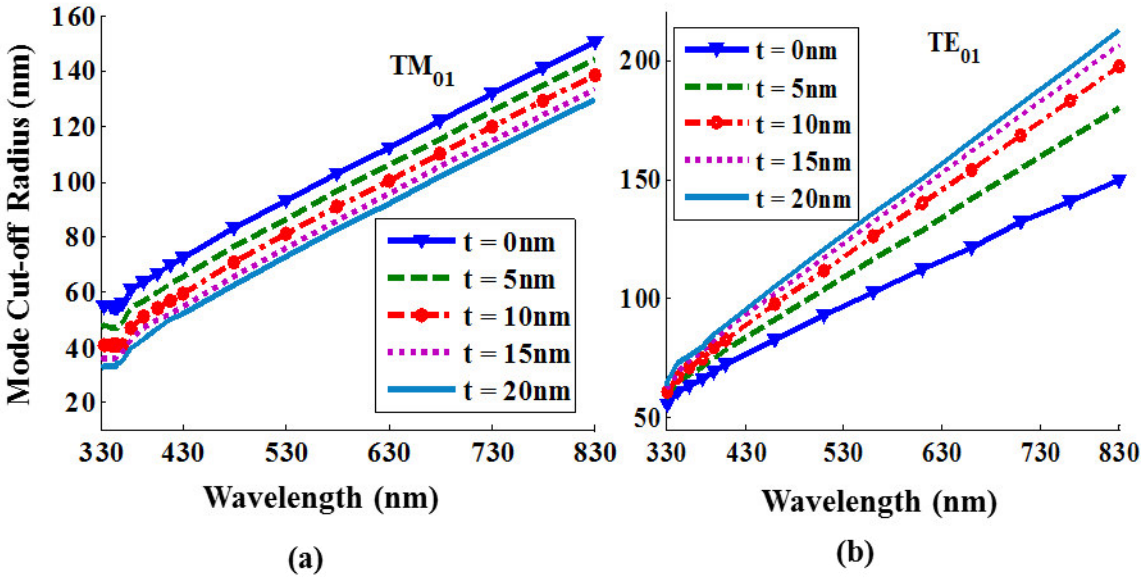

Figure 5.3: Cut-Off Radius at λ = 330nm to 830nm (a) TM_{01} Mode (b) TE_{01} Mode

5.3.2 Modal Gain at Wavelength 330nm – 370nm

With a material gain of $5x10^3$ cm^{-1} for the GaN nano-laser, it was found that lasing does not occur for the wavelengths 330nm to 370nm at their cut off radii however a small gain is observed when the wavelength for the structure is greater than 370nm. Figure 5.4 shows the loss profile for the TE_{01} and TM_{01} modes for a GaN nano-laser structure without a silver layer.

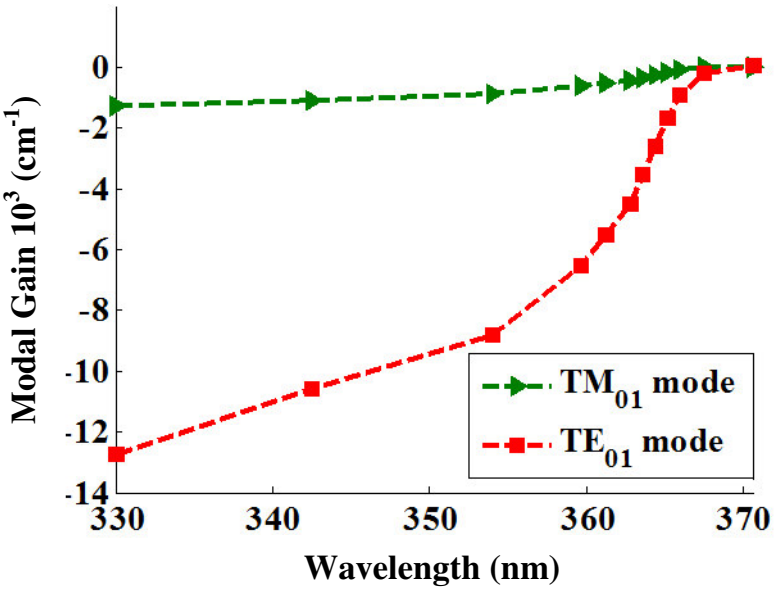

Figure 5.4: Modal Gain for TE_{01} and TM_{01} Mode at Cut-Off Radius at λ = 330nm – 370nm

It is noted that the structure exhibits loss even when the material gain of $5x10^3$ cm^{-1} is included and that including a metal layer will increase the overall loss. It is concluded that the achievement of lasing in the wavelength range 330nm to 370nm will be extremely challenging and hence this range is not considered further in this chapter.

5.3.3 Modal Gain at Wavelength 370nm – 830nm

i) Wavelength 370nm – 430nm

The calculation of the modal gain for the TE_{01} and TM_{01} mode is carried out over a range of wavelengths from 370nm to 830nm with and without silver cladding. As the thickness of silver is increased it is observed that for the range of wavelengths from 370nm to 430nm, the modal gain is decreased and the loss is increased at the respective cut off radius. Results shown in Figure 5.5 illustrate this point. Figure 5.5(a) shows the modal gain for TE_{01} mode and Figure 5.5(b) shows the modal gain for TM_{01} mode for wavelengths from 370nm to 430nm.

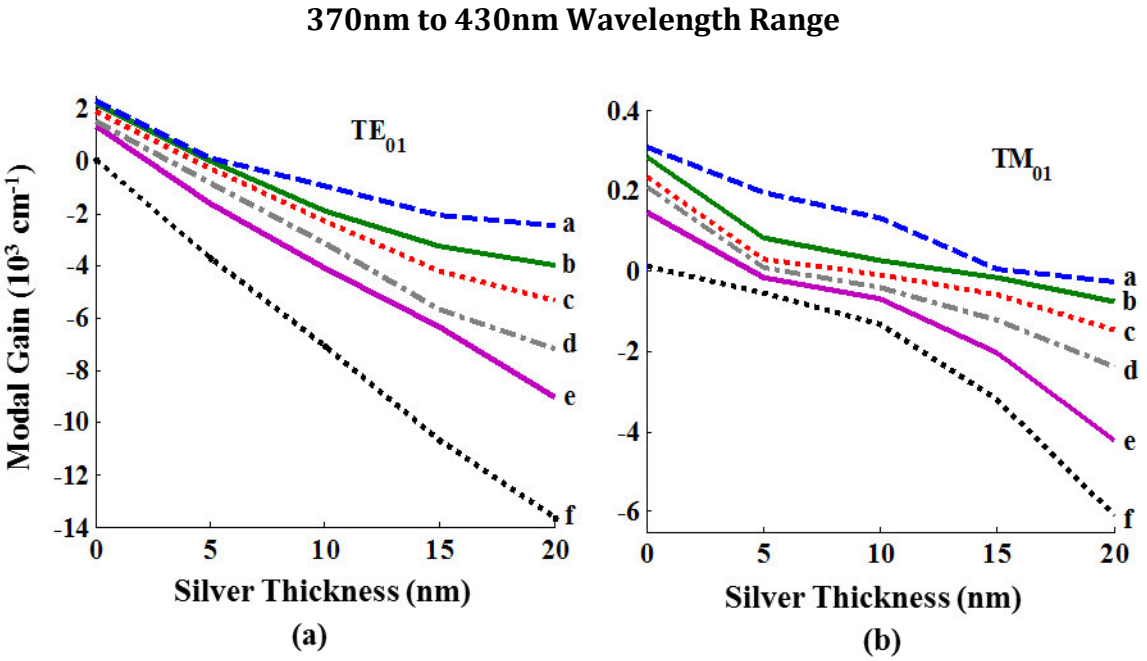

Figure 5.5: Modal Gain Vs Silver Thickness at λ (a =370.625nm, b=380nm, c =392.5nm, d =405nm, e =417.5nm, f = 430nm). (a) TE_{01} Mode (b) TM_{01} Mode

ii) Wavelength 480nm – 830nm

In comparison to the modal gain observed in Figure 5.5 for the TE and TM modes of GaN nano-laser, introducing the silver layer leads to an increase in the modal gain over the wavelength of 480nm to 830nm at their cut off radius as shown in Figure 5.6. At 830nm an InGaN quantum well is required rather than GaN and will therefore require index data of InGaN to be used; however at the wavelength of 830nm $In_{0.7}Ga_{0.3}N$ has the same refractive index as that of GaN as in [19-20]. Therefore the refractive index of GaN at 830nm can be used to model a laser of a different material e.g. $In_{0.7}Ga_{0.3}N$. Figure 5.6 (a) and 5.6 (b) shows the modal gain for the TE_{01} and TM_{01} mode respectively. The modal gain rapidly increases as the wavelength increase since the mode becomes more confined inside the core for structures that have a silver layer of thickness 10nm, 15nm and 20nm as shown in Figure 5.6.

480nm to 830nm Wavelength Range

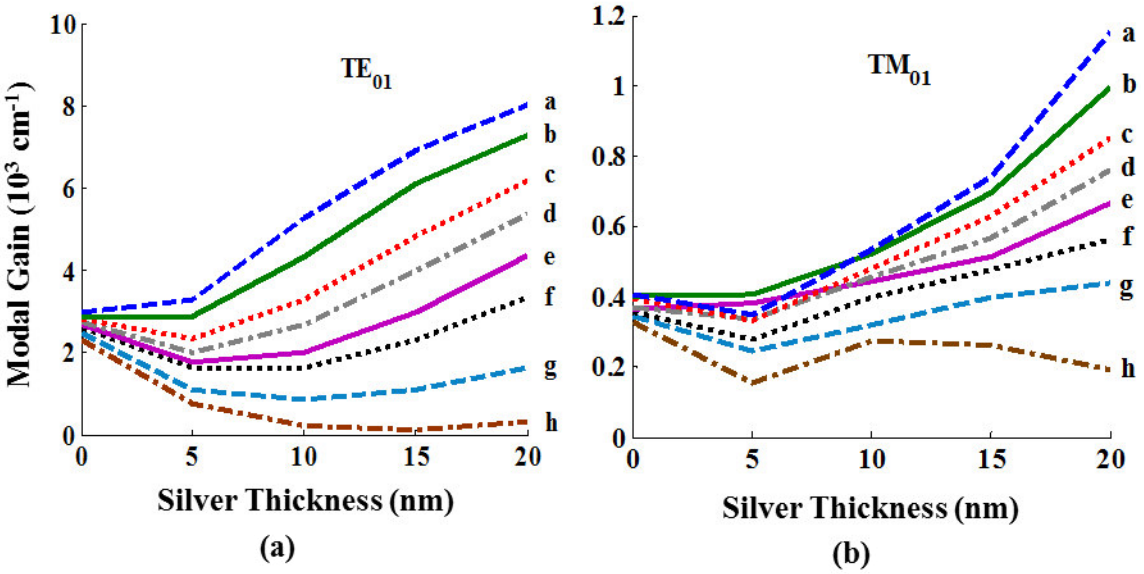

Figure 5.6: Modal Gain Vs Silver Thickness at λ (a =830nm, b=780nm, c =730nm, d =680nm, e =630nm, f = 580nm, g = 530nm, h = 480nm) using cTMM (a) TE_{01} Mode (b) TM_{01} Mode

The lower modal gain at wavelengths 480nm to 580nm is due in part to the increased silver losses at these operating wavelengths. It has been reported that strong wave-guiding in nano-lasers leads to very large values of the modal gain that can exceed the bulk gain [14]. It is observed from the Figure 5.6 (a) that the gain increases as the wavelength and silver thickness increase and at 830nm wavelength for a 20nm silver thickness the modal gain is $8x10^3$ cm^{-1} for TE_{01} mode. The TM_{01} mode is a Surface

Plasmon Polariton (SPP) mode which is a lossy mode [21-23] and therefore the modal gain of $1.15x10^{3}cm^{-1}$ for the TM_{01} mode is lower than the TE_{01} mode as shown in Figure 5.6 (b).

5.3.4 FEM Analysis at Wavelength 480nm – 830nm

Results for the TE_{01} and TM_{01} mode at their cut off radius were also analysed using the Finite Element Method (FEM). Figure 5.7 shows these results for the modal gain over the wavelength range of 480nm to 830nm. Similar patterns to the effect of silver thickness on the modal gain in the nano-laser as compared to the results obtained through cTMM in Figure 5.6 were observed. The FEM results have small difference from the calculated results obtained from cTMM which is due to the computational space boundary provided by FEM [18].

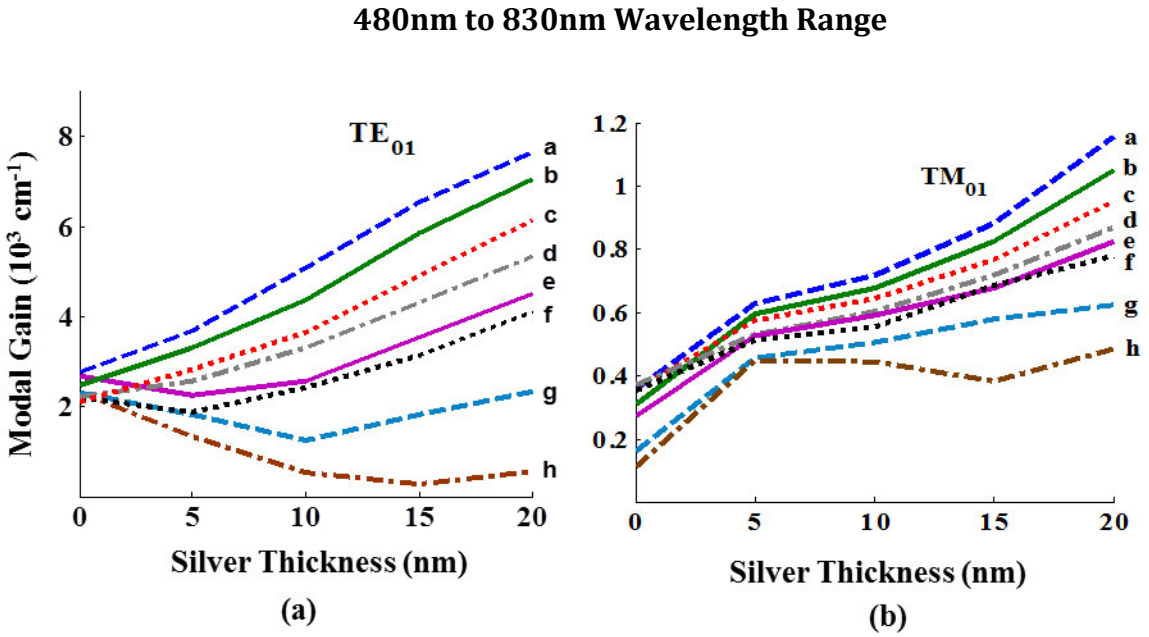

Figure 5.7: Modal Gain Vs Silver Thickness at λ (a = 830nm, b = 780nm, c = 730nm, d = 680nm, e = 630nm, f = 580nm, g = 530nm, h = 480nm) using FEM (a) TE_{01} Mode (b) TM_{01} Mode

5.3.5 Effect of Insulating Layer on Modal Gain at Wavelength 480nm – 830nm

For the cases explored above no account had been taken into consideration that an insulating layer between the metal and the core semiconductor may be required to prevent charge transfer from active region to metal layer. In order to deposit the

metal layer on the insulating layer, annealing of metal is required, which softens the material so that it can be cut and shaped accordingly.

In order to explore the impact of such a requirement, the analysis on the effect of a 20nm thick Si_3N_4 insulating layer as in [21] on the modal gain over a range of wavelengths, 480-830nm for structures having a 20nm thick silver cladding at their mode cut off radii is carried out. The refractive index of the insulating layer is generally lower than that of the core material and will thus enhance the wave-guiding properties and push the optical field away from the metal cladding and towards the device core. In this way confinement to the core and the overall modal gain will both increase [9]. The enhancement of the modal gain is shown in Figure 5.8 where a comparison is made between structures having an insulating layer and those without an insulating layer. However in the wavelength range 780nm -830nm there is a smaller difference between the refractive index of the core and the insulating layer. This tends to reduce the optical field confinement and hence the modal gain. This effect is captured in Figure 5.8.

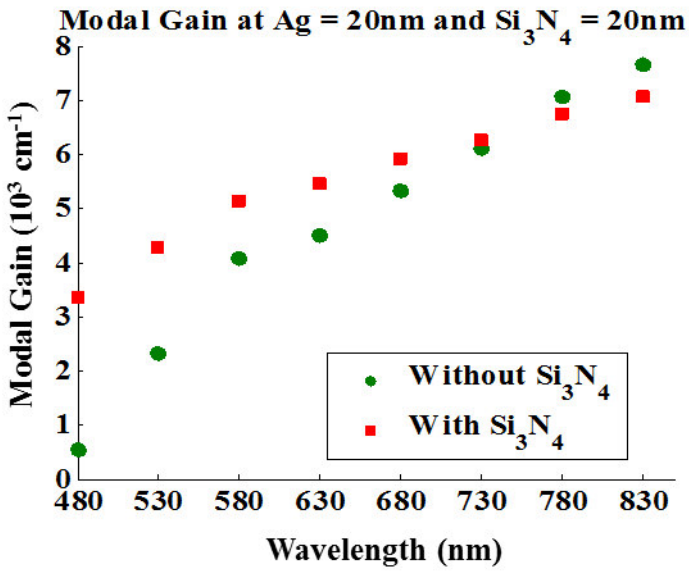

Figure 5.8: Effect of a 20nm insulating (Si_3N_4) layer on the modal gain for TE_{01} mode at cut off radii at λ = 330nm – 370nm

5.3.6 Confinement Factor at Wavelength 480nm – 830nm

From the modal gain, the mode confinement factor is evaluated using equation (4.2) in chapter 4. The confinement factor for the TE_{01} and TM_{01} mode with and without

silver layer is shown in Figure 5.9. Figure 5.9 (a) shows that at the cut-off radius for the TE_{01} mode high confinement for a 20nm silver thickness is achieved. High confinement greater than unity has been reported in [4, 14]. The strong wave-guiding due to the high refractive index contrast and highly reflective metal cladding, the optical mode is better confined inside the cavity. This confinement of the mode is greater than unity and can therefore increase the modal gain. The modes become better confined as the thickness of the metal increases. Figure 5.9 (b) shows the confinement factor of the TM_{01} modes for the structure. The lower confinement factor of TM_{01} mode as compared to TE_{01} mode is due to the fact that the TM_{01} mode is an SPP mode which resides mostly in air rather in the core at cut off radius [7].

480nm to 830nm Wavelength Range

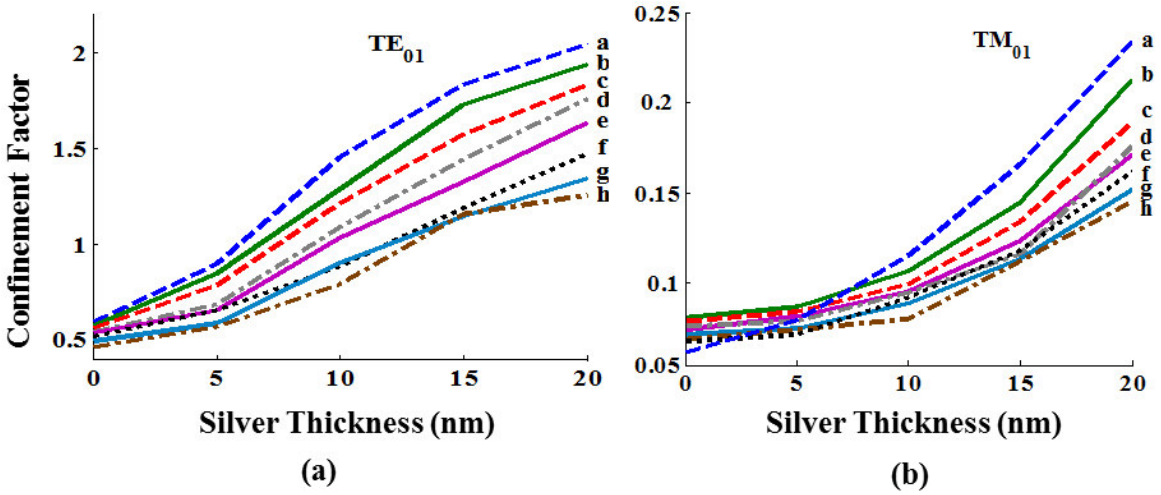

Figure 5.9: Confinement Factor vs Silver Thickness at λ (a = 830nm, b =780nm, c =730nm, d =680nm, e = 630nm, f = 580nm, g = 530nm, h = 480nm) (a) TE_{01} Mode (b) TM_{01} Mode

5.3.7 Device Length Estimation at Wavelength 480nm – 830nm

Now, estimation of the device length is undertaken using equation (2.45) in chapter 2. Figure 5.10 shows the device length for a GaN silver clad nano-laser structure. As shown in Figure 5.10 (a), as the thickness of the silver is increased the device length is decreased since the mode becomes more confined inside the core, as the loss is compensated by more modal gain which in turn reduces the length of the structure. Due to the higher modal gain of the TE_{01} mode it is possible to have device lengths for GaN nano-laser structures around 2μm, at the cut-off radius for λ = 830nm. The device length for the TM_{01} mode reduces as the modal gain increase and at the

wavelength of 830nm for silver thickness of 20nm the minimum device length around 18μm as shown in Figure 5.10 (b) can be achieved.

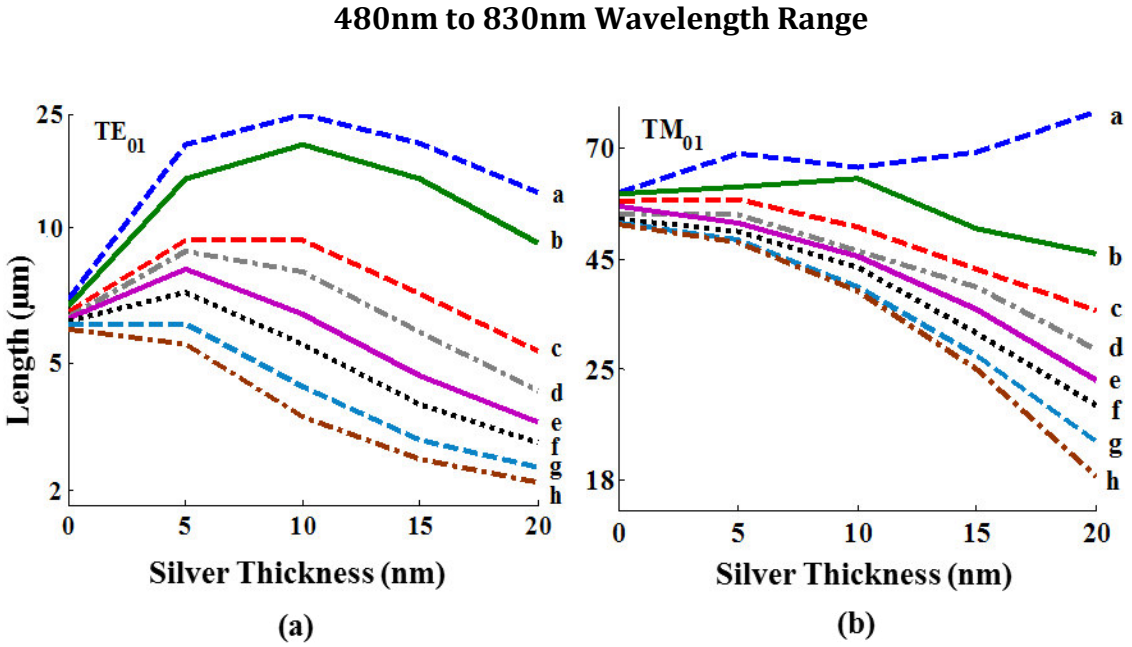

Figure 5.10: Device Length for the structure at λ (a = 480nm, b = 530nm, c = 580nm, d = 630nm, e = 680nm, f = 730nm, g = 780nm, h = 830nm) (a) TE_{01} Mode (b) TM_{01} Mode

5.3.8 3D FEM Simulation of 2μm Device

The analysis in this chapter has been performed on the 2D nano-laser model over the wavelength range 330-830nm. 3D FEM analysis has also been performed for the evaluated short device length of 2μm in Figure 5.10 for TE mode, with: 213nm-radius GaN core, 20nm-thick Si_3N_4 insulating layer, together with a silver metal cladding layer of 20nm thickness surrounded by air at wavelength 830nm.

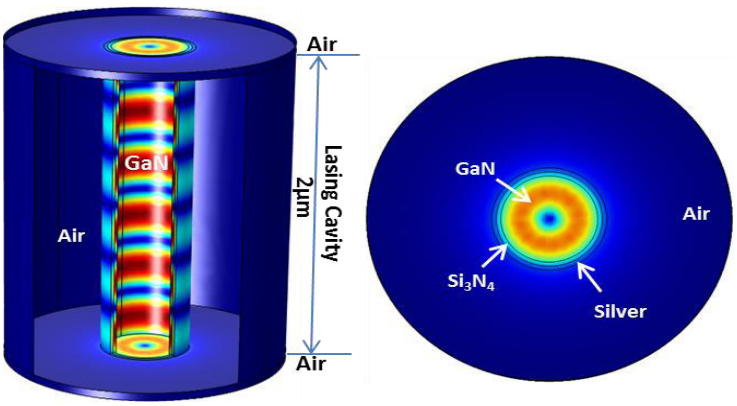

Figure 5.11: 3D and 2D view of TE_{01} mode for the Device Length of 2μm of core radius 213nm, with 20nm thick Si_3N_4, and a metal cladding of 20nm surrounded by air.

Figure 5.11 shows the calculated TE lasing mode inside the GaN nano-laser cavity at 830 nm wavelength. The colour patterns define the intensity of the mode in each region of the laser, i.e. the core, metal and air, where 'red' is the maximum and 'blue' is the minimum intensity. The intensity along the length (z direction) of the laser has a wavelength of 830nm, along a 2μm laser. Standing wave intensities are observed as shown in the Figure 5.12 (a) and (b).

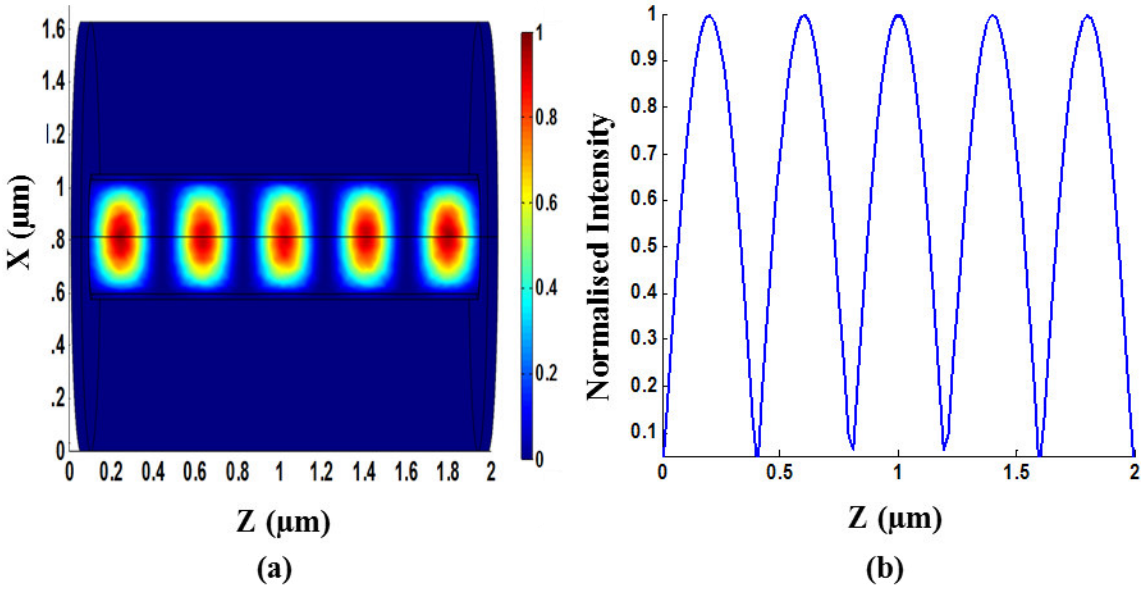

Figure 5.12: (a) and (b) Standing waves patterns for TE_{01} mode in the 'xz' plane

5.4 Conclusion

The lasing properties of a cylindrical GaN visible emitting nano-laser structure with silver cladding layer of different thicknesses is analysed. The optimum thickness of silver for GaN nano-laser structure to achieve lasing over a range of wavelengths is evaluated. For the TE_{01} mode it is found that structures of length of order 2 μm have the potential to lase with core radius 213nm whereas for the TM_{01} mode with core radius 130nm device lengths of order 18 μm are needed to achieve lasing at λ = 830nm using 20nm silver metal cladding.

References

[1] H. Gao, A. Fu, S. C. Andrews and P. Yang, "Cleaved-coupled nanowire lasers," *Proc. Natl. Acad. Sci.,* vol. 110, no. 3, pp. 865-869, Jan. 2013.

[2] V.E. Babicheva, I. V. Kulkova, R. Malureanu, K. Yvind, and A.V. Lavrinenko, "Plasmonic modulator based on gain-assisted metal-semiconductor-metal waveguide" *Semicond. Sci. Technol*., vol. 7, pp. 858-860, May. 2012.

[3] G. Winter, S. Wedge, and W. L. Barnes, "Can lasing at visible wavelengths be achieved using low-loss long-range surface plasmon-polariton mode?," *New J. Phys*., vol. 8, no. 125, pp. 1–14, 2006.

[4] A. V. Maslov and C. Z. Ning, "Modal gain in a Semiconductor nanowire laser with anisotropic bandstructure*," IEEE J. Quantum Electron*., vol. 40, no. 10 pp. 1389–1397, Oct. 2004.

[5] A. V. Maslov and C. Z. Ning, "Size reduction of a semiconductor nanowire laser by using metal coating," Proc. *SPIE*., vol. 6468, pp. 646801-1–646801-7, 2007.

[6] D. Bour, C. Chua, Z. Yang, M. Teepe, and N. Johnson, "Silver-clad nitride semiconductor laser diode," *Appl. Phys. Lett.,* vol. 94, no. 4, pp.041124–1–3,2009.

[7] Z. A. Sattar and K. A. Shore, "Spatial profiling of optical gain for optimizing lasing in plasmonic nano-lasers." *J. Euro. Opt. Soc. Rap. Public*., vol. 8, pp. 13045-1–13045-6, July 2013.

[8] Z. A. Sattar, Z. Wang and K. A. Shore, "Wave-Guiding Analysis of Annular Core Geometry Metal-Clad Semiconductor Nano-Lasers" *IEEE J. Quantum Electron*., vol. 50, no. 1,pp. 15-22, Jan. 2014.

[9] D. B. Li, and C. Z. Ning, "Interplay of various loss mechanisms and ultimate size limit of a surface plasmon polariton semiconductor nanolasers," *Optics Express.,* vol. 20, no. 1516, pp. 16349-16357, 2012.

[10] V. E. Babicheva, R. Malureanu, and A. V. Lavrinenko, "Finite-thickness metal-semiconductor-metal waveguide as plasmonic modulator," *AIP Conf. Proc.,* vol. 41, no. 1475, pp. 41-43, 2012.

[11] Q. Li, J. B. Wright, W.W. Chow, T. S. Luk, I. Brener, L. F. Lester, G. T. Wang, "Single-mode GaN nano-laser lasers," *Opt. Exp.,* vol. 20, no. 16, pp. 17873-17879, 2012.

[12] J. Zhang and N. Tansu, "Engineering of AlGaN-Delta-GaN Quantum-Well Gain Media for Mid- and Deep-Ultraviolet Lasers," *IEEE J. Phot. Soc.,* vol. 5, no. 2, pp. 2600209-1-2600209-10, 2013.

[13] J. P. Richters, M. Grundmann, H. V. Wenckstern, C. P. Dietrich, C. Ronning, M. Gnauck, J. Kalden, J. Gutowski, and T. Voss, "Modal gain and its diameter dependence in single-ZnO micro-and nano-lasers," *Semicond. Sci. Technol.,* vol. 27, no. 1, pp. 015005-1-015005-5, 2012.

[14] J. Piprek*, Nitride Semiconductor Devices: Principles and Simulation*. Berlin, Germany: Springer-Verlag, 2007.

[15] T. Yang, S. Goto, M. Kawata, K. Uchida, A. Niwa, and J. Gotoh, "Optical properties of GaN thin films on sapphire substrates characterized by variable – angle spectroscopic ellipsometry," *Jpn, J. Appl. Phys.,* vol. 37, no. 10A, pp. L1105-L1108, 1998.

[16] P. B. Johnson, and R.W. Christy, "Optical constants of the noble metals," *Phys. Rev.,* vol. B6, no. 12, pp. 4370–4379, 1972.

[17] V. Krishnamurthy, and B. Klein, "Theoretical investigation of metal cladding for nano-laser and cylindrical micropost lasers," *IEEE J. Quantum Electron.,* vol. 44, no. 1, pp. 67-74, 2008.

[18] K. Ikeda, Y. Fainman, K. A.Shore and H. Kawaguchi, "Modified long range surface plasmon polariton modes for laser nano resonators." *J. Appl. Phys*., vol. 110, no. 6, pp. 063106-1–063106-6, Sep. 2011.

[19] M. Anani, H. Abid, Z. Chama, C. Mathieu, A. Sayede, and B. Khelifa, "$In_xGa_{1-x}N$ refractive index calculations," *Microelectron. J.,* vol. 38, pp. 262-266, 2007.

[20] J. Piprek, and S. Nakamura, "Physics of high-power InGaN/GaN lasers," *IEE Proc. Optoelectron.,* vol. 149, no. 4, pp. 145-151, 2002.

[21] M. T. Hill, M. Marell, E. S. P. Leong, B. Smalbrugge, Y. Zhu, M. Sun, P. J. Van Veldhoven, E. Jan Geluk, F. Karouta, Y. S. Oei, R. Notzel, C. Z. Ning, and M. K. Smit, "Lasing in metal-insulator-metal subwavelength plasmonics waveguides,"*Opt. Exp.,* vol. 17, no. 13, pp.11107-11112, Jun. 2009.

[22] R. F. Oulton, V. J. Sorger, T. Zentgraf, R. M. Ma, C. Gladden, L. Dai, G. Bartal, and X. Zhang, "Plasmon lasers at deep sub wavelength scale", *Nature,* vol. 461, no. 7264, pp. 629-632, 2009.

[23] A. M. Lakhani, M. K. Kim, E. K. Lau and M. C. Wu, "Plasmonic crystal defect nanolaser," *Opt. Exp.*, vol. 19, no. 19, pp. 18237–18245, Sep. 2011.

Chapter 6

Analysis of the Direct Modulation Response of Nano-Lasers

6.1 Introduction

In previous chapters, analysis has been carried out where specific attention was given to determining the lasing condition of nano-lasers [1-4]. The aim of this chapter is to explore the dynamical performance of the nano-laser using direct current modulation. Direct current modulation of nano-lasers offers a cost-effective option as an efficient light source for on chip interconnection [5]. As discussed in chapter 1, such nano-lasers are anticipated to exhibit enhanced dynamical performance [6-13], which may arise from a combination of physical factors including Purcell spontaneous emission enhancement factor F, spontaneous emission coupling factor, β. In that context the aim is to determine the influence of F and β for direct current modulation response in both the small signal and large signal regimes. For simplicity sinusoidal modulation is adopted.

6.2 Nano-Laser Dynamics

To analyse the dynamical performance of a nano-laser, the parameters used are shown in Table 6.1. Using these parameters and the rate equations (6.1) and (6.2) as in [14], the influence of F and β, on the small and large signal modulation of nano-laser is explored.

$$\frac{dN}{dt} = \frac{I}{eV} - \frac{N}{\tau_s}\big(F\beta + (1-\beta)\big) - g_o(N-N_t)S \tag{6.1}$$

$$\frac{dS}{dt} = C_o\beta F\frac{N}{\tau_s} + C_o g_o(N-N_t)S - \frac{S}{\tau_p} \tag{6.2}$$

Where, I is the injection current; τ_s is the carrier lifetime; g_o is the differential gain coefficient; N_t is the transparency carrier density; C_o is the confinement factor; τ_p is the photon lifetime; N and S are the carrier and photon densities. When

consideration is given to the dynamics of nano-lasers attention needs to be given to the stronger damping which will result from enhanced spontaneous emission. Such damping gives rise to the broadening of the resonance from which the maximum modulation frequency of the laser is deduced [14].

Table 6.1 GaN Nano-laser Device Parameters

Transparency Carrier Density	N_t	5.77 x 10^{18} cm^{-3} [15]
Differential Gain	g_o	1.5 x 10^{-6} cm^3 /s [15]
Carrier Lifetime	τ_s	1ns [16]
Photon Lifetime	τ_p	0.2ps [11]
radius of the Core	r	213nm [4]
Length of Active Region	L	2µm [4]
Volume of Active Region	V	2.85 x 10^{-13} cm^3
Electron Charge	q	1.6 x 10^{-19} C
Confinement Factor	C_o	2 [3-4]
Spontaneous Emission Coupling Factor	β	0.004 [12]
Purcell Spontaneous Emission Enhancement Factor	F	30 [12]

6.3 Small and Large Signal Analysis

For direct current sinusoidal modulation of nano-laser, the injection current I, in equation (6.1) is taken to be of the form:

$$I(t) = I_{dc} + I_m sin(2\pi f_m t) \tag{6.3}$$

Where, I_{dc} is the dc bias current, I_m is the modulating current defined as $I_m = mI_{dc}$, m is the modulation depth of the sinusoidal signal with modulation frequency f_m at time t. For small signal modulation, the modulation depth is taken to be $m = 0.1$ and for large signal modulation, the modulation depth is taken to be $m = 0.8$. An important measure for the performance of laser is the modulation bandwidth which can be estimated analytically for small signal modulation using the rate equations

(6.1) and (6.2). In general an analytical expression for the direct-current modulation bandwidth can be obtained in the form, as in equation (6.4) [6, 17]:

$$f_{3dB} = \frac{1}{2\pi}\left[\sqrt{{\omega_d}^2 + \sqrt{{\omega_d}^4 + {\omega_R}^2}}\right] \tag{6.4}$$

Where, ${\omega_d}^2 = {\omega_R}^2 - \frac{{\gamma_R}^2}{2}$ with ω_R and γ_R being the resonance frequency, and the damping factor, as defined in equations, (6.5) and (6.6):

$${\omega_R}^2 = \frac{1}{\tau_p}\left(g_o S_0 + \frac{F\beta}{\tau_s}\right) + C_o\beta(1-\beta)\frac{FN_0}{S_0{\tau_s}^2} \tag{6.5}$$

$$\gamma_R = g_o S_0 + \frac{(1-\beta)}{\tau_s} + \frac{F\beta}{\tau_s}\left(1 + C_o\frac{N_0}{S_0}\right) \tag{6.6}$$

Where, N_0 and S_0 are the carrier and photon densities at the dc bias current I_{dc}. The dynamics of nano-laser is evaluated using the analytical form of small signal modulation response function $H(\omega)$ as in equation (6.7) [17]:

$$H(\omega) = \frac{{\omega_R}^2}{{\omega_R}^2 - \omega^2 + i\omega\gamma_R} \tag{6.7}$$

For numerical analysis on the performance of small and large signal modulation of nano-laser, a modulation index η is used. It is assumed that, due to the direct current modulation, the photon density makes excursions between the maximum and minimum photon density values, S_{max} and S_{min}. Therefore the modulation response index, η can be defined as in equation (6.8):

$$\eta = \frac{(S_{max} - S_{min})}{S_o} \tag{6.8}$$

The threshold current of a laser defines the minimum amount of current required to achieve lasing. Using the parameters in Table 6.1, the threshold current is found to be I_{th} = 0.265mA. To analyse the effects on modulation response in the small and large signal regimes, the analysis is performed for a dc bias current at 5-10 times the threshold current ($I_{dc} \geq 5I_{th}$) as in [13]. The modulation characteristics for small and large signal are calculated by solving the rate equations (6.1) and (6.2) numerically in MATLAB. The obtained S_{max} and S_{min} results were used in equation (6.8) to evaluate the modulation index η to determine the modulation response.

Analytical results were evaluated using equation (6.7). Figure 6.1 shows the analytical and numerical analysis using equations (6.7) and (6.8), of the small signal modulation response for a bias current $I_{dc} = 5I_{th}$, β = 0.004 and F = 10. It is shown that the analytical results and numerical results are in excellent agreement.

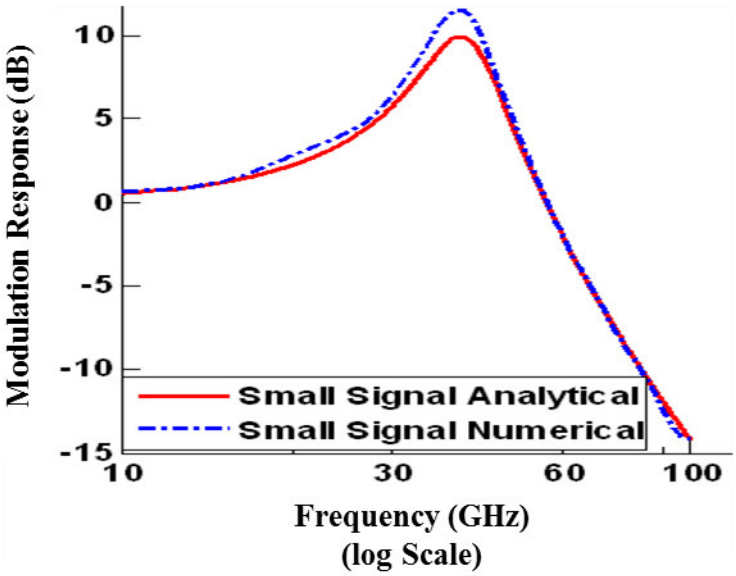

Figure 6.1: Numerical and Analytical Small Signal Modulation Response

Detailed analyses is carried out using numerical analysis in section 6.4 to determine the influence of varying the bias current, F and β for direct current modulation response in both the small and large signal regimes.

6.4 Numerical Analysis of Direct Current Modulation

In this chapter direct current modulation response of nano-lasers has been studied giving particular attention to the roles of the dc bias current, the Purcell spontaneous

emission enhancement factor *F* and the spontaneous emission coupling factor β in determining the modulation characteristics of nano-lasers.

Firstly, attention is given to the influence of *F*. Using fixed parameters β = 0.004 [12] and bias current $I_{dc} = 5I_{th,}$ variation in *F* in the range 10-40 is taken into account. Figure 6.2 (a) and 6.2 (b) shows the calculated modulation response for small and large signal respectively. It has been studied that the Purcell enhanced spontaneous emission reduces the device 3dB modulation bandwidth [14]. The small and large signal responses in Figure 6.2 (a) and 6.2 (b) show that the 3dB bandwidth decreases from 62 GHz to 50 GHz as the cavity Purcell factor increases from 10 to 40, representing a decline of about 20% in the 3dB bandwidth due to stronger damping.

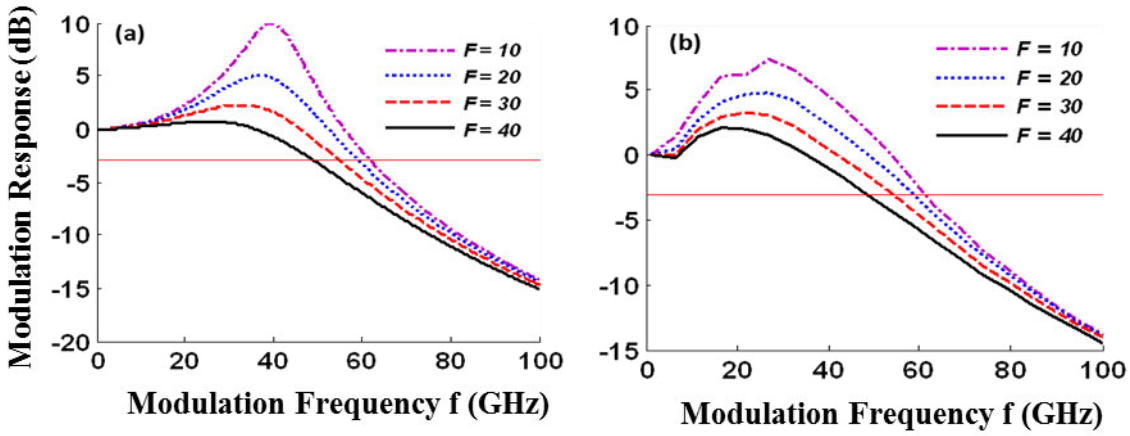

Figure 6.2: Modulation Response at β = 0.004 and $I_{dc} = 5I_{th}$ for (a) Small Signal (b) Large Signal Modulation. The solid red line indicates the -3dB level.

Moreover this enhancement of the Purcell factor suppresses the resonance peak from 10dB to 0.3dB for small signal and from 7dB to 2dB for large signal. Increasing *F*, results in the decrease of the 3dB bandwidth for small and large signal. The modulation response for small signal shows that the peak modulation frequency is greater than that of the large signal however the bandwidths are approximately the same with increased *F*.

Secondly attention is turned to the impact of the spontaneous emission factor β. Using parameters *F* = 30 at a bias current $I_{dc} = 5I_{th,}$ β is varied in the range 0.001 to 0.008. It is observed that when β increases in this range the 3dB bandwidth decreases from 62GHz to 36GHz as shown in Figure 6.3 (a) and 6.3 (b), representing a decline of approximately 40% for both small and large signal modulation. Also enhancement of

β tends to suppress the resonance peak from 12dB to 0dB for small signal modulation and from 8dB to 0.6dB for large signal modulation. Due to stronger damping effects, the peak response for small signal modulation rapidly degrades for β ≥ 0.008 relative to that in the large signal case. However, the 3dB bandwidth is approximately the same for both small and large signal modulation.

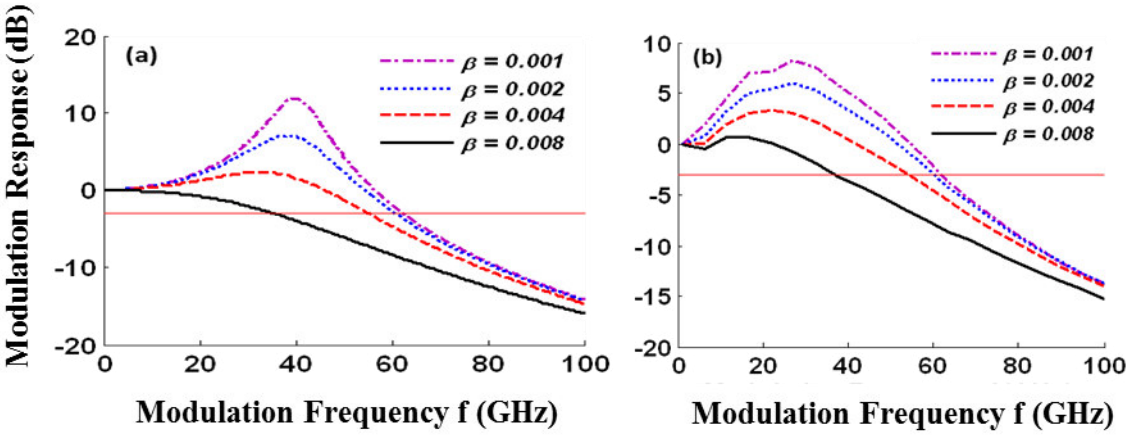

Figure 6.3: Modulation Response at F = 30 and I_{dc} = 5I_{th} for (a) Small Signal (b) Large Signal Modulation. The solid red line indicates the -3dB level

Now attention is given to the effect of varying the bias current. Using parameters F = 30, β = 0.004, variation in the dc bias current in the range 4I_{th} to 10I_{th} is considered. Enhancement of nano-laser dynamics have been studied where modulation bandwidths in excess of 100GHz can be achieved [7-10]. As expected, it is seen in Figure 6.4 (a) and 6.4 (b) that the 3dB bandwidth increases with bias current from 38GHz to 95 GHz, both for small and large signal modulation.

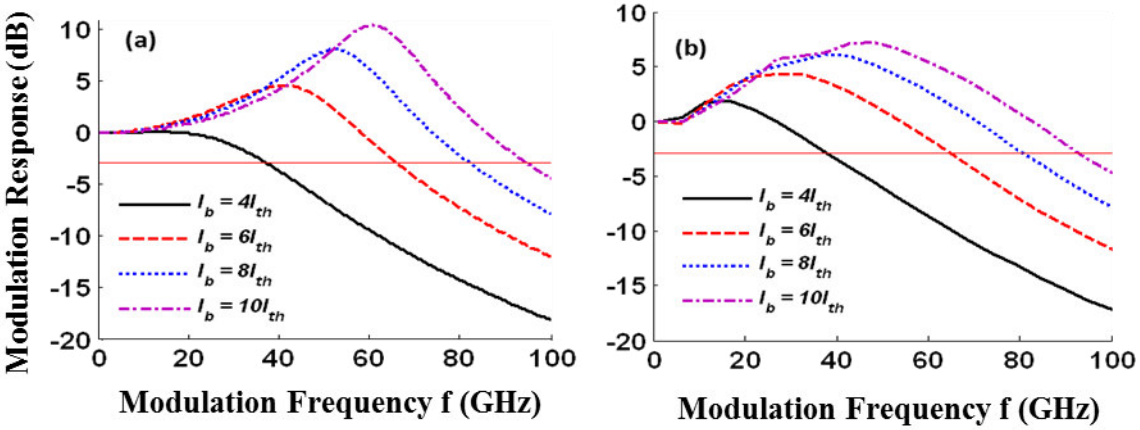

Figure 6.4: Modulation Response at β = 0.004 and F = 30 for (a) Small Signal (b) Large Signal Modulation. The solid red line indicates the -3dB level

Considering the effect of *F* and β for small and large signal modulations, it is observed that the peak modulation frequency for large signal is less than that of the small signal presumably due to the increased nonlinearity in the large signal regime. Figure 6.5 (a) and 6.5 (b) show the peak modulation frequency obtained by varying β and *F* for small signal modulation and large signal modulation respectively. It is observed that by selecting β and *F* values the peak of the modulation frequencies may be maximised. For the case considered here this is achieved at modulation frequencies of 38GHz and 28GHz for small and large signal cases respectively.

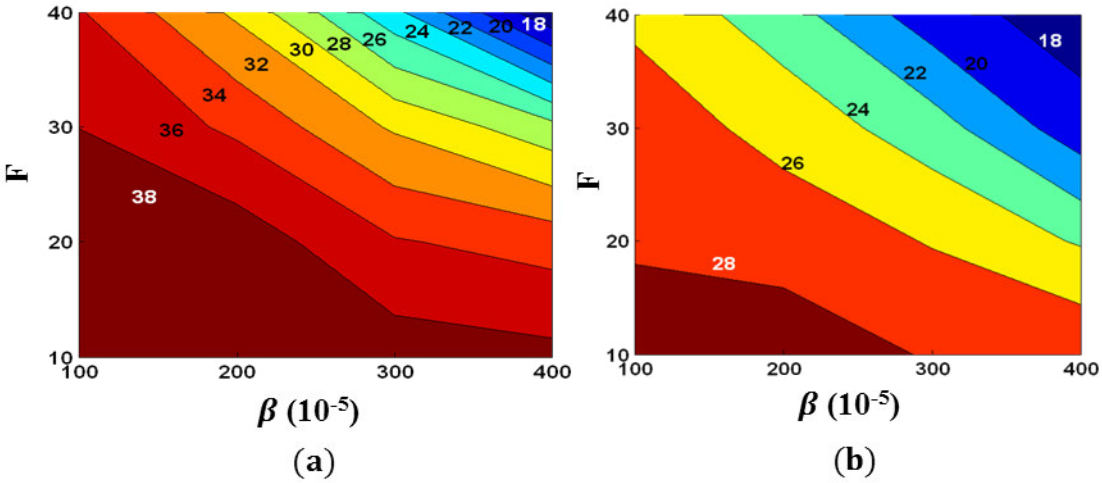

Figure 6.5: Peak modulation response frequency dependence on β and F for (a) Small Signal (b) Large Signal Modulation. The figure represents frequencies at which the signal has the peak modulation response. For small signal colour ranges from dark red to dark blue indicate frequencies in the range of 38GHz to 18 GHz. For large signal colour ranges from dark red to dark blue indicate frequencies in the range of 28GHz to 18 GHz.

Next a comparison is made of the magnitude of the modulation response for small and large signal modulation. Using β = 0.001, *F* = 10 and $I_{dc} = 5I_{th}$, small and large signal modulation response is compared in Figure 6.6. It is shown in Figure 6.6 that in both small and large signals regimes the peak modulation response occurs at frequencies 40GHz and 30GHz respectively. Figure 6.6 also shows that in the frequency range 1GHz to 36GHz large signal modulation produces a large modulation response than for the small signal case.

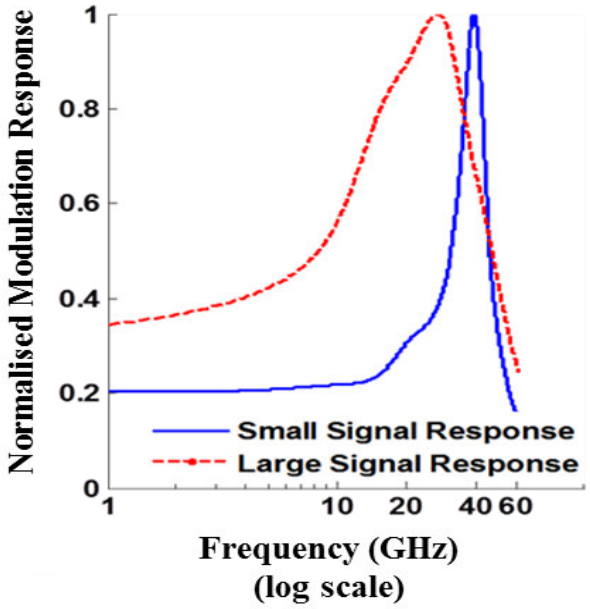

Figure 6.6: Modulation response for small and large signal

6.5 Conclusion

Direct modulation characteristics of nano-lasers have been determined in both the small signal and large signal regimes. Peak modulation response at frequencies of 40GHz and 30GHz can be achieved by careful selection of the parameters F and β. It is observed that Purcell enhanced spontaneous emission and spontaneous emission coupling factor reduces the 3dB modulation bandwidth due to strong damping of the laser. For small and large signal analysis, very high modulation bandwidth of approximately 60GHz may be achieved. Over the frequency range from 1GHz to 36GHz the large signal modulation response is greater than that for small signal case.

References

[1] Z. A. Sattar and K. A. Shore, "Spatial profiling of optical gain for optimizing lasing in plasmonic nano-lasers." *J. Euro. Opt. Soc. Rap. Public.*, vol. 8, pp. 13045-1–13045-6, Jul. 2013.

[2] Z. A. Sattar, Z. Wang and K. A. Shore, "Wave-Guiding Analysis of Annular Core Geometry Metal-Clad Semiconductor Nano-Lasers" *IEEE J. Quantum Electron.*, vol. 50, no. 1,pp. 15-22, Jan. 2014.

[3] Z. A. Sattar, and K. A. Shore, "Design Analysis of Ultra-Short Cavity Silver-Clad Semiconductor Nano-Lasers," Presented at the 10th Int. Conf. *CLEO-PR&OECC/PS,* Kyoto, Japan, Jul., 2013.

[4] Z. A. Sattar, Z. Wang and K. A. Shore, “Design Optimization of Metallic Sub-Wavelength Nanowire Lasers,” IET Optoelectronics, vol. 8, no. 2, pp. 129 – 136, April 2014..

[5] D. V. Thourhout, T. Spuesens, S. K. Selvaraja, L. Liu, G. Roelkens, R. Kumar, G. Morthier, P. Rojo-Romeo, F. Mandorlo, P. Regreny, O. Raz, C. Kopp, and L. Grenouillet, “Nanophotonic devices for optical interconnect,” *IEEE J. Sel. Top. Quantum Electron.*, vol. 16, no. 5, pp. 1363–1375, Oct. 2010.

[6] T. Suhr, N. Gregerson, Y. Yvind, and J. Mork, “Modulation response of nanoLEDs and nanolasers exploiting Purcell enhanced spontaneous emission,” *Opt. Exp.*, vol. 18, no. 11, pp. 11230-11241, May. 2010.

[7] T. Baba, “Photonic crystals and microdisk cavities based on GaInAsP-InP system,” *IEEE J. Sel. Top. Quantum Electron.,* vol. 3, no. 3, pp. 808-830, Jun. 1997.

[8] G. Björk and Y. Yamamoto, “Analysis of semiconductor microcavity lasers using rate equations," *IEEE J. Quantum Electron*., vol. 27, pp. 2386-396, Nov. 1991.

[9] H. Yokoyama and S. D. Brorson, “Rate equation analysis of microcavity lasers,” *J. Appl. Phys*., vol. 66, pp. 4801-4805, Dec. 1989.

[10] H. Altug, D. Englund, and J. Vučković, “Ultrafast photonic crystal nanocavity laser,” *Nat. Phys.,* vol. 2, pp. 484-488, Jul. 2006.

[11] H. Gao, A. Fu, S. C. Andrews and P. Yang, “Cleaved-coupled nanowire lasers,” *Proc. Natl. Acad. Sci.,* vol. 110, no. 3, pp. 865-869, Jan. 2013.

[12] K. Ding and C. Z. Ning, “Metallic sub-wavelength-cavity semiconductor nanolasers,” *Light: Sci. Appl.,* vol. 1, no. 7, p. 20, Jul. 2012.

[13] X. M. Lv, L. X. Zou, Y. Z. Huang, Y. D. Yang, J. L. Xiao, Q. F. Yao and J. D. Lin, “Influence of Mode *Q* Factor and Absorption Loss on Dynamical Characteristics for semiconductor Microcavity Lasers by Rate Equation Analysis,” *IEEE J. Quantum Electron.*, vol. 47, no. 12, pp. 1519-1525, Dec. 2011.

[14] K. A. Shore, “Modulation bandwidth of metal-clad semiconductor nanolasers with cavity-enhanced spontaneous emission,” *Electron. Lett*., vol. 46, no. 25, pp. 1688-1689, Dec. 2010.

[15] H. Morkoc, *Handbook of Nitride Semiconductors and Devices*, New York: Wiley, 2008.

[16] J. B. Schlager, K. A. Bertness, P. T. Blanchard, L. H. Robins, A. Roshko, and N. A. Sanford, “Steady state and time resolved photoluminescence from relaxed and strained GaN nanowires grown by catalyst-free molecular-beam epitaxy,” *J. Appl. Phys.,* vol. 103, no. 12, pp. 124309, Jun. 2008.

[17] L. A. Coldren and S. W. Corzine*, Diode Lasers and Photonic Integrated Circuits*, 1st ed. New York: Wiley, 1995.

Chapter 7

Summary & Future Work

7.1 Summary

Extensive research over the last 50 years has resulted in the development of an extremely wide variety of semiconductor lasers having attractive operating characteristics including high-speed and high-power devices. In recent years considerable attention has been given to semiconductor metal clad nano-lasers due to their potential applications in photonic integrated circuits, optical information processing and system-on-a-chip technologies.

This thesis has outlined the opportunities and challenges that arise in the design of metal-clad semiconductor nano-lasers. The approach adopted here takes account of spatial profiling of the optical gain as a means both for optimizing lasing operation and as a step towards a fully self-consistent theoretical model of such structures. A numerical model of cylindrical metal-clad nano-laser using cTMM (cylindrical transfer matrix method) has been used in this thesis, that utilizes material gain variation in the core, of prescribed optical properties and of specifically defined optical gain. Significant attention has been given to determining the modal gain and optical confinement factor to effect reduction in size of such lasers.

Firstly the effect of using 2D dual core and multiple layered geometry of cylindrical nano-laser has been analysed to provide insight into the effect of material gain variation in the active region to the modal gain. cTMM is used to solve the modal properties of TE_{01} and TM_{01} mode in the structure, with metal clad thickness of 20 nm at wavelength 1 μm. Effects on multilayer core and the dual core structure are compared with respect to the overall modal gain and the device length of the structure. It is found that structures of length of order 10 μm have the potential to lase for the TE_{01} mode whereas device lengths of order 100 μm are needed to achieve lasing for the TM_{01} mode

Additionally a more realistic, Gaussian gain profile is analysed for multilayer geometry of cylindrical nano-lasers. The effects on the variation of gain along the

radius of the core are evaluated using cTMM and Finite Element Method (FEM). Device lengths of order 1 μm and 60 μm have been obtained for the lasing of TE_{01} and TM_{01} mode respectively.

Moreover the wave guiding and lasing characteristic of metal-clad nanowire structure has been examined over a wide wavelength range: 330nm to 830nm. The modal gain and corresponding laser cavity length for the TE_{01} and TM_{01} modes is calculated for metal cladding thicknesses from 5nm to 20nm. Results obtained are compared with FEM analysis and a 3D FEM model is evaluated for the results obtained using the 2D cTMM. For the TE_{01} mode it is found that device length of 2 μm have the potential to lase whereas for the TM_{01} mode device lengths of order 18 μm are needed to achieve lasing at λ = 830nm for a 20nm metal cladding.

Finally an analysis of the dynamical performance of nano-laser has been carried out, where the focus is to determine the influence of Purcell spontaneous emission enhancement factor F, and the spontaneous emission coupling factor, β for direct current modulation in both the small signal and large signal regimes. It is observed that F and β, reduces the 3dB modulation bandwidth due to strong damping of the laser. For small and large signal analysis, very high modulation bandwidth of approximately 60GHz may be achieved.

7.2 Future Work

The analysis for advanced laser structures is reliant on accurate modelling of the physical processes underpinning the operational characteristics of candidate semiconductor nano-lasers. In general the modelling of such lasers requires the adoption of numerical techniques in order to provide accurate predictions of the behaviour of proposed nano-lasers. The numerical model utilized in this thesis using spatial profiling of material gain variation in the active region may be used to analyse candidate semiconductor lasers.

The method adopted here takes in account a wide range of wavelength and metal clad thickness. This approach can be used to optimize lasing operation in determining the optimum wavelength of operation and metal cladding thickness for designing nano-laser structures. It has been discussed that in order to access the wide wavelength range for a constant material gain, quantum wells may be used in nanowires.

Therefore, analysis of quantum wells (e.g. InGaAs/GaAs or InGaN/GaN, etc.) in nanowire needs to take place for better optimization of wavelength and metal clad thickness in such structures.

The numerical analysis carried out in this thesis provides the basis for more detailed nano-lasers design and specifically is capable of extension to provide a self-consistent analysis of metal clad cylindrical nano-lasers. With a view to practical utilisation, specific effort is needed on the operability of such lasers under electrical injection.

Due to the flexibility available via 3D FEM design using 3D modal analysis, it will be possible to consider more nano-laser structures, such as hexagonal structures and nanowire arrays.